Gold Nanocarriers To Deliver Oligonucleotides Into The CNS

Thesis

Faculty of Science, Technology, Engineering and Mathematics;

Department of Life, Health and Chemical Sciences;

Walton Hall, Milton Keynes, United Kingdom

Gold nanocarriers to deliver oligonucleotides into the CNS

A thesis submission to The Open University for the degree of Doctor in Philosophy

By Nayab Fatima (BSc, MSc)

Supervisors:

Professor David Male,

Dr Jane Loughlin,

Dr Radka Gromnicova

DECLARATION

I hereby declare that the work presented in this thesis “Gold nanocarriers to deliver oligonucleotides into the CNS” is a result of my own academic and experimental investigation; contributions made by other researchers are fully acknowledged in relevant parts of the text. Moreover, this work does not contain any material submitted for award of any other degree.

Nayab Fatima

May 2020

ABSTRACT

Delivery of therapeutical oligonucleotides to the central nervous system is challenging due to their inability to cross the blood-brain barrier. Current approaches to overcome this problem disturb the blood-brain barrier, administer too low dose for therapeutic purposes or have serious side effects. Therefore, nanocarriers, that are able to penetrate the blood-brain barrier, can be used to deliver them. Hence, the aim of this study was to investigate the potential of ~2 nm galactose-coated gold nanoparticles (NP-Gal) as a delivery system of oligonucleotides into the brain.

DNA oligonucleotides were attached to the NP-Gal via place exchange reaction. Several nanoparticle formulations were created, such as 20nt single-stranded versus double stranded versions of DNA-coated gold nanoparticles (NP-DNA-20^{ss}, NP-DNA-20^{ds}) and 40nt long double stranded versions of DNA-coated gold nanoparticles (NP-DNA-40^{ds}). These were analysed by (1) electrophoresis mobility shift assay (for detection of nanoparticles with different numbers of DNA molecules), and (2) fast protein liquid chromatography (for isolation of NP-DNA-40^{ds}) forming two fractionated formulations - low-density 40nt DNA nanoparticle formulation (NP-DNA-40^{LO}) and high-density 40nt DNA nanoparticle formulation (NP-DNA-40^{HI}). The rate and route of transport across brain endothelial cells (hCMEC/D3) was assessed by transmission electron microscopy. A 3D co-culture model of the blood brain barrier was used to detect nanoparticle uptake into astrocytes once they passed through brain endothelial cells. Next, we performed *in vivo* examination of tissue distribution of the nanoparticles following intracarotid and intravascular infusion (using ICP mass spectroscopy along with light and electron microscopy). Lastly, qPCR was used to quantify transport rate and efficiency of DNA cargo across brain endothelial cells.

DNA oligonucleotides attached to NP-Gal by place exchange reaction produced six different nanoparticle formulations. The cell uptake efficiency of NP-DNA-20^{ss}, NP-DNA-20^{ds} and NP-DNA-40^{ds} was compared; the more negatively-charged DNA bound nanoparticles had increased cellular uptake in human brain endothelial cells compared with the NP-Gal. This investigation pointed out the possibility that attaching more DNA onto each nanoparticle may increase the uptake efficiency of NP-Gal by brain endothelium. The transport rate of DNA nanoparticles free of unreacted DNA and nanoparticles - NP-DNA-40^{LO} and NP-DNA-40^{HI} was compared to the NP-Gal using a 3D co-culture model of blood-brain barrier. Both the NP-DNA-40^{LO} and NP-DNA-40^{HI} were more effective in crossing the brain endothelial cells and entering astrocytes compared to NP-Gal. Moreover, we found our nanoparticles to be not cytotoxic for hCMEC/D3 at the dose used in our studies (8µg/mL). Next, we investigated tissue localization of NP-Gal, NP-DNA-40^{LO} and NP-DNA-40^{HI} 10 minutes after intravascular infusion in rats. All three nanoparticles formulations localised in the brain endothelial cells and glial cells of the cortex. While NP-Gal were mainly found in the kidney, DNA-coated nanoparticles were found in the cytoplasm of liver hepatocytes and macrophages of the red pulp in the spleen. Lastly, we found that DNA cargo can be successfully delivered across brain endothelial cells. NP-DNA-40^{LO} and NP-DNA-40^{HI} carried over half of the DNA applied (apical side) across the brain endothelium. In conclusion, our study demonstrated the possibility to deliver 40nt DNA oligonucleotide across the blood-brain barrier using a 2nm gold nanocarrier. There was improvement in the bioavailability of oligonucleotides across the brain endothelial cells carried by NP-DNA-40^{LO} and NP-DNA-40^{HI} compared to naked DNA in vitro. In vivo, we found similar brain penetration of NP-Gal, NP-DNA-40^{LO} and NP-DNA-40^{HI} so further studies may be needed.

ACKNOWLEDGEMENTS

I was very fortunate to have David Male, Jane Loughlin and Radka Gromnicova as my supervisors. They all have provided me great supervision and support throughout my PhD research project and it was a pleasure to work them. I would also like to thank to Basil Sharrack for funding the project to get life-changing experience of PhD research.

I would like to thank all the collaborators that I met during my PhD journey, without them this work would not have been possible: Phil Williams and the rest of the team from Midatech Pharma UK, Ibon Perera from Midatech Pharma Spain, Mehmet Kaya and his team from Istanbul University, Igor Kraev, manager of the EM Suite at the Open University and the academics, administrators, lab support and peers from the Open University were very supportive during my journey.

I would also like to thank my mum and my siblings for their continuous moral support and belief in me on starting my career as a research scientist.

TABLE OF CONTENT

LIST OF FIGURES

LIST OF TABLES

Abbreviations

ABC transporter	ATP-binding cassette transporter
BBB	Blood Brain Barrier
BRCP	Breast Cancer Resistance Protein
CECs	cerebral micro-vessel endothelial cells
CNS	Central nervous system
Da	Dalton
DNA	Deoxyribonucleic acid
ds	Double-stranded
EBM-2 MV	Endothelial basal medium 2 - microvascular
EDTA	Ethylenediaminetetraacetic acid
EGF	Epidermal growth factor
EGFR	Epidermal growth factor receptor
EM	Electron microscopy
EMSA	Electrophoretic mobility shift assay
FBS	Foetal bovine serum
FDA	Food and Drug Administration
FPLC	Fast-performance liquid chromatography
HBSS	Hank's balanced salt solution
hCMEC/D3	Human cerebral microvascular endothelial cells D3
HPLC	High-performance liquid chromatography
ICP-MS	Inductively-coupled plasma mass spectroscopy
IC	Intracarotid
IgG	Immunoglobulin G
IV	Intravenous
JAM	Junctional adhesion molecule
LRP-1	LDL-receptor-related protein 1
MRPs	Multidrug Resistance-associated Proteins
NP-Gal	Galactose coated nanoparticles
NP-DNA-20^{ss}	Single stranded 20nt-DNA nanoparticles
NP-DNA-20^{ds}	Double stranded 20nt-DNA nanoparticles
NP-DNA-40^{ds}	Double stranded 40nt-DNA nanoparticles
NP-DNA-40^{LO}	Low-density 40nt-DNA nanoparticles
NP-DNA-40^{HI}	High-density 40nt-DNA nanoparticles
PB	Phosphate buffer
PBS	Phosphate-buffered saline
PEG	Poly(ethylene glycol)
Pgp-1	p-glycoprotein
PLA	polylactides
PLGA	poly (D,L-lactide-co-glycolate)
RNA	Ribonucleic acid
ROS	Reactive oxygen species
SEM	Scanning electron microscopy OR standard error of the mean
siRNA	small interfering RNA
ss	Single-stranded
SPR	Surface plasmon resonance
TBE	Tris/Borate/EDTA buffer
TEM	Transmission electron microscopy
TGFβ	Transforming growth factor beta
VEGF	Vascular endothelial growth factor

1 GENERAL INTRODUCTION

Drug delivery to the brain is drawing major attention, and researchers are working on how to solve the issues of treating central nervous system (CNS) diseases. Currently, CNS diseases account for a large proportion of disease burden and societal costs, with a proportionally lower research budget than other disease areas (Feigin et al, 2019). Several pharmaceutical companies are stopping or significantly reducing major efforts in the area of CNS diseases due to difficulties in drug delivery. Not a single pharmaceutical company worldwide has a drug-discovery programme targeting the blood brain barrier therefore, the area needs attention and that collaboration and new knowledge is needed to understand and handle these issues in the future.

The real obstacle of delivering drugs into the CNS is the blood-brain barrier, which consists of endothelial cells, astrocytes and pericytes with tight junctions (Pardridge W. M, 2005). It forms a highly selective semipermeable membrane barrier that protects the brain from brain-disrupting compounds found in the blood. It acts as a kind of 'firewall', which allows the passage of oxygen and essential nutrients into the brain, but at the same time blocks the entrance of most of the harmful or toxic molecules into the brain. Therefore, it prevents the entry of about 98% of drugs from crossing the BBB pathway (Pardridge W. M, 2005). Thus, large molecules, monoclonal antibodies, gene therapies, recombinant proteins, antisense and RNA interference compounds cannot cross through the BBB. Researchers have come up with several potential agents to treat CNS diseases but end up running into a major roadblock when trying to deliver them to the nervous system (Pardridge W. M, 2005).

Limited strategies designed to deliver therapeutics into the brain exist, either invasive or non-invasive. The invasive route involves administering drug directly into the brain through surgical intracerebral injection, which provides a sufficient dosage of the drug without causing systemic toxicity (Agrawal et al, 2018). However, intracerebral injection is painful and complicated procedure and relies mainly on cerebral diffusion, hence being dependant on the concentration which can decrease from the site of administration. Non-invasive strategies include systemic drug delivery, based on the anatomical structure of brain capillaries, cells, and extracellular environment and the nasal route to transfer fluids across the brain using the olfactory bulb (Agrawal et al, 2018). The limitations of nasal delivery include inadequate drug infusion through the nasal mucosa, and that drug clearance might occur without reaching the site of interest. For the systemic drug delivery

to work effectively, the drugs need to enter the brain parenchyma and the cerebrospinal fluid and further diffuse through the brain extracellular matrix to the targeted site (Agrawal et al, 2018). Although there are multiple crossing pathways (detailed in chapter 1.1.3), yet approximately 98% of small molecules and most large molecules are unable to reach the brain through the BBB (Pardridge W. M, 2005).

Gene editing or gene silencing through nucleic acids currently is one of the promising approaches to treat neurodegenerative diseases. However, securing consistent delivery into the CNS presents several challenges. One of the potential ways to cross BBB without affecting its properties is to use nanoparticles as nanocarriers to deliver therapeutics into the brain. Here in this thesis we focused on gold nanoparticles as nanocarriers to deliver therapeutic oligonucleotides into the brain.

1.1 Blood-Brain Barrier

The CNS has developed a series of barriers to protect itself from invading pathogens, neurotoxic molecules, and circulating blood cells. The CNS structure, with diverse degrees of permeability, includes the blood-cerebrospinal fluid (CSF) barrier, the blood-brain barrier (BBB), the blood-retinal barrier and the blood–spinal cord barrier (Abbott et al., 2010). Of the three main CNS barrier layers, the BBB at the brain endothelium is the most crucial interface for molecular fluxes between blood and cells as a result of the very extensive microvascular bed, and proximity of the finest branches to individual neurons, typically 8– 25μm (Abbott et al., 2010).

The first evidence for a BBB arose in 1885 when Paul Ehrlich described the existence of a physical interface between the CNS and the peripheral circulation (Serlin et al., 2016). Ehrlich injected aniline dyes into a rat's bloodstream to stain tissues. Surprisingly, the dye injected into the blood circulatory system stained peripheral organs but not the brain and the spinal cord.

Thirty years later, Ehrlich's student, Edwin Goldmann, noticed the opposite phenomenon by injecting trypan blue into the cerebrospinal fluid (CSF), which stained cells within the CNS, but not in the periphery (Serlin et al., 2016). The two experiments showed that a tight seal existed between the blood and the brain. However, the nature of that seal did not

become apparent until the late 1960s, when electron micrographs of brain capillaries revealed that they differ from capillaries in the rest of the body. The endothelial cells that make up the walls of brain capillaries form tight junctions, restricting the passage of ions and many metabolites and biomolecules between the cells of the endothelium.

The BBB structure is formed by a complex system of endothelial cells, pericytes, astrocytes, and basal lamina (Masserini, 2013), preventing the passage of most circulating cells and blood-borne molecules (de Boer & Breimer, 1998; Petty & Lo, 2002). This is achieved by the presence of tight junctions between brain endothelial cells interconnected side by side to form a seal, which restricts the paracellular movement of molecules. Next, specialized transporters and the efflux transporters control substances that enter the brain. Lastly, enzymatic components protect the brain from toxins or neurotransmitters (Hersh et al., 2016)

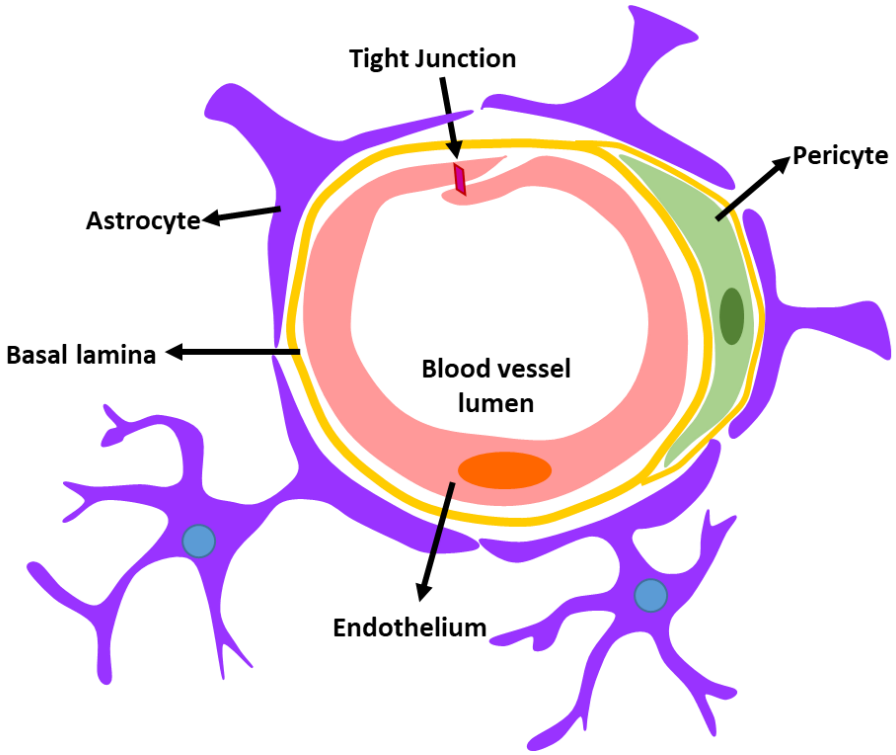

Figure 1.1 *The structure of the Blood brain barrier.*

1.1.1 Building blocks of the Blood-Brain Barrier

- **Brain endothelial cells** – the BBB is made up of endothelial cells that form the walls of the capillaries. These cells are required for proper barrier formation and interaction with adjacent cells. The brain endothelial cells have continuous tight junctions. Tight junctions between the brain endothelial cells prevent paracellular movement of molecules and restrict passive diffusion of molecules into the brain. Brain endothelial cells also help to shuttle essential nutrients and metabolites across the BBB, via their ATP-binding cassette (ABC) transporters (Abbott et al., 2010). These transporters contribute to the BBB properties by efflux of small lipophilic molecules that can diffuse into the brain endothelial cells and back to the bloodstream. Although the endothelial cells form the primary barrier of the BBB, they also interact with surrounding cells (Abbott et al., 2010), including astrocytes and pericytes, which contribute to the maintenance of the barrier function *(figure 1.1).*
- **Basal lamina** is made up of type IV collagen, fibronectin, and laminin that cover the whole capillary endothelial cell layer, keeping the BBB structure integral. The primary function of the basal lamina is to restrict the movement of solutes (Cardoso, Brites, & Brito, 2010).
- **Pericytes** are embedded in basal lamina forming a cellular layer around the endothelial cells. They play an essential role in the formation and maintenance of the BBB. Their contractile properties also help to regulate capillary blood flow and phagocytosis, clearing out cellular debris as well as inhibiting any CNS immune cells from damaging the proper formation of BBB (Liu et al, 2012).
- **Astrocytic End-Feet** are processes extended by astrocytes – the star-shaped glial cells found in the brain and spinal cord. Astrocytes have various roles, but mostly they support neurons (Cardoso, Brites, & Brito, 2010). Their other functions include biochemical support of the brain endothelial cells, providing essential nutrients to the nervous tissues, maintaining a balance of extracellular ions, and a role in scarring and repair processes of the brain following traumatic injuries (Cardoso, Brites, & Brito, 2010).

1.1.2 Molecular Composition of BBB

The vital components of the BBB are tight junctions between brain endothelial cells, which restrict the paracellular diffusional movement of molecules passing between the endothelial cells, from blood to brain. The effectiveness and integrity of these tight junctions are controlled by transmembrane and cytoplasmic accessory proteins, which help to form a tight seal by linking to intracellular actin and the cytoskeleton (Cardoso, Brites, & Brito, 2010). The transmembrane proteins include occludin, claudin, and junction adhesion molecules (JAM). Occludin helps with only the formation of tight junctions, whereas JAM and claudin (claudin-1 and claudin-5) help with both formation of tight junctions and contribute to creating the BBB high electrical resistance (Cardoso, Brites, & Brito, 2010). Besides this, there are also cytoplasmic accessory proteins, which include Zona occludens (ZO-1, ZO-2 and ZO-3) and cingulin, which are necessary for the structural support (Kaur, Foulds, & Ling, 2008). Cytoplasmic proteins play a vital role in the structural support of tight junctions and creating low permeability of the BBB. The absence of cytoplasmic proteins can cause disruption of the tight junctions and thereby permit the entry of infected monocytes into the CNS (Wolburg & Lippoldt, 2002).

The BBB structure also includes adherens junctions, which are located on the endothelial cells, and which contribute to the structural integrity of the tight junction. The adherens junction complex is composed of cadherin proteins. Cadherins are linked to the cytoplasm through the association of alpha, beta, and gamma catenins, allowing cell-cell adhesion and ensuring tissue structural support (Wolburg & Lippoldt, 2002).

Additionally, the presence of tight junctions and their respective trans-membrane proteins generate a high electrical resistance across the endothelium. This resistance restricts movement of electrolytes across the endothelial cells and reduces ion movements via the paracellular route (Cardoso, Brites, & Brito, 2010).

1.1.3 Routes across blood–brain barrier

Brain endothelial cells possess many different transport systems in order to supply the brain with nutrients. Passage of molecules across the brain endothelial cells can occur via the paracellular pathway (between adjacent cells) or through a transcellular pathway (through the cells) (Hersh et al., 2016). Paracellular and transcellular pathways play a vital role in BBB permeability. In the paracellular pathway, the ions and solutes diffuse between two adjacent cells according to their concentration gradient (Petty and Lo, 2002). Whereas, the transcellular pathway involves different mechanisms of both passive diffusion of lipophilic compounds and receptor mediated shuttling and transcytosis of molecules.

The passage of all the compounds that cross the brain endothelium via paracellular and transcellular pathways can be categorised as passive diffusion, carrier-mediated transport, or endocytosis/transcytosis (Gromnicova et al. 2016).

1.1.3.1 Passive diffusion

Small lipid soluble and non-polar molecules with size less than 500 Da can enter the brain through passive diffusion (Pardridge, 2005). The exchange of the blood gases, oxygen and carbon dioxide is diffusive, and these gases move down their concentration gradients. Oxygen supply to the brain and carbon dioxide removal is blood-flow dependent, as long as cerebral blood flow remains within physiological limits (Pardridge, 2005).

Usually, higher lipid solubility and several other physico-chemical factors favour the process of BBB penetration, but some factors may restrict the passive diffusion of the compounds into the CNS. These include; compounds with molecular weight higher than 500 Da, compounds that have high polar surface area and compounds that have a tendency to form 6 or more hydrogen bonds, as having more hydrogen bonds moves the molecule from the aqueous phase into the lipid phase of the cell membrane, which can reduce the diffusion by increasing the free energy requirement (Pardridge, 2005). However, these molecular and physico-chemical factors are not always an absolute indication for CNS penetration and there are many examples of effective CNS active drugs in clinical use which do not comply with these BBB penetration rules (Bodor, 2010). One example is that bases that carry positive charge have an advantage over acids when penetrating the BBB. Their cationic nature allows them to interact with the negatively-charged glycocalyx and

phospholipids of the plasma membrane of endothelial cell that facilitate their entry (Johansson, 2001).

1.1.3.2 Carrier-mediated (solute) transport

Most hydrophilic or polar molecules, such as peptides and proteins, cannot diffuse through cell membranes. Thus, brain endothelial cells express many carrier-mediated transporters in the cell membrane (Zhang et al., 2002). The carrier-mediated transporters work by either facilitating diffusion or use sodium or proton gradients (Abbott et al. 2010). The transported molecules include a wide range of molecules such as glucose, amino acids, nucleosides and nucleotides, small peptides, organic cations, and anions (Abbott et al. 2010).

Brain endothelial cells express these transport proteins on the luminal and abluminal endothelial cell membranes (Cardoso, Brites, & Brito, 2010). The transport of these molecules is influx and (going in from blood to the brain) and also efflux (going back into the blood from the brain endothelium) or from brain endothelium via specific efflux transporters of the ATP-binding cassette (ABC) transporters (Cardoso, Brites, & Brito, 2010) (figure 1.2). The ones of the greatest significance for efflux transport are P-glycoprotein (Pgp-1) (i.e. ABCB1), the Multidrug Resistance-associated Proteins (MRPs) (i.e. ABCC1), and Breast Cancer Resistance Protein (BRCP) (i.e. ABCG2). These efflux transporters are located on the luminal side of the brain endothelial cells. They remove lipophilic molecules, including many potentially harmful molecules and drugs from the brain endothelium back into the blood (Begley, 2004). These transporters are also responsible for excluding useful drugs from entering the brain and present a major challenge for the pharmaceutical industry in developing therapeutics for the brain.

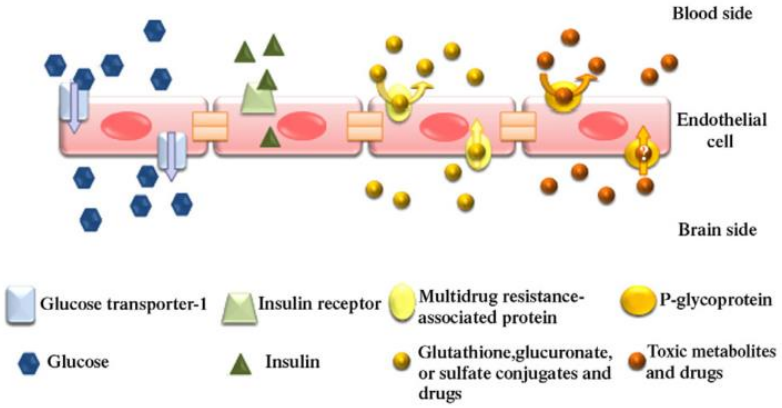

Figure 1.2 *Endothelial cells express a variety of transporters and receptors, which regulate brain concentrations of nutrients, hormones, metabolites and xenobiotics. For simplicity, the diagram only presents a few of the main transporters and receptors, the glucose transporter-1, the insulin receptor, the ABC transporters, the multidrug resistance-associated protein and p-glycoprotein (figure taken from Cardoso, Brites, & Brito, 2010).*

1.1.3.3 Endocytosis and transcytosis

Large proteins/peptides and macromolecules are transported across the BBB via transcytosis. Transcytosis is a transport process that transports large molecular weight solutes by two mechanisms; endocytosis (macromolecules are taken up into vesicles) and/or exocytosis (vesicles containing macromolecules are released from the cell). Transcytosis of macromolecules across the BBB provides the main route by which large molecular weight solutes can enter the CNS intact (Abbott et al. 2010). Although most large blood-borne molecules are physically prevented from entering the brain by the presence of the blood–brain barrier and tight junctions, specific and some non-specific transcytosis mechanisms exist to transport a variety of large molecules and complexes across the BBB (Abbott et al. 2010).

The overall mechanism of endocytosis involves molecules being pinched off or coated in a vesicle. The vesicular mechanism of transport involves either receptor-mediated transcytosis (RMT) or adsorptive-mediated transcytosis (AMT) (Abbott et al. 2010). Receptor-mediated transcytosis (RMT) involves a specific receptor, such as transferrin receptor or insulin receptor, on the cell surface, which triggers an endocytosis event. The receptors and their bound ligand form a cluster and a caveolus is formed, which pinches off into a membrane-enclosed vesicle. Then, both the receptor and ligand are internalised into the endothelial cell and transported across the cytoplasm to be either exocytosed at the opposite side of the cell or moved into a lysosomes to be digested, for the cell to use the

nutrients within the vesicle. In contrast, adsorptive endocytosis involves binding of charged macromolecules, which renders macromolecule cationic and causes interaction with cell surface binding sites and causes endocytosis (Sauer et al., 2005). The details of these transport systems are outlined in Table 1.1.

Table 1.1 Examples of few of the macromolecule systems on the BBB which deliver molecules from blood to brain (Sauer et al. 2005).

Transport system	Receptor (if known)	Ligand	Type
Transferrin	Transferrin receptor (TfR)	Transferrin-Fe	RMT
Insulin	Insulin receptor (IR)	Insulin	RMT
Lactoferrin	Lactoferrin receptor (LfR)	Lactoferrin	RMT
Tumour necrosis factor	Tumour necrosis factor receptor (TNFR)	TNFα	RMT
Apolipoprotein E	Apolipoprotein E receptor 2 (ApoER2)	Lipoproteins	RMT
LDL-receptor-related protein 1 and 2	LDL-receptor-related protein 1 and 2 (LRP1, LRP2)	Lipoproteins, Amyloid-β, lactoferrin, α 2-macroglobulin, melanotransferrin, ApoE	RMT
Cationised proteins	+	Cationised albumin	AMT
Cell penetrating peptides	+	SynB5/pAnt-(43–58)	AMT

Macromolecule transport can be exploited or targeted to overcome the BBB. Examples of the most commonly targeted are transferrin receptor or LRP-1 (LDL-receptor-related protein 1) receptor. This is because the expression of the transferrin and LRP-1 receptor is high in brain endothelium *in vivo*. (Helms et al. 2016).

1.1.4 Enzymatic blood-brain barrier

In addition to tight Junctions and efflux pathways, brain endothelial cells also express various enzymes that can metabolize lipophilic toxic substances or neurotransmitters and thus protect the brain. These enzymes are metabolically highly active and are localised in large numbers within the cytoplasm of the endothelium, such as peptidase and cholinesterase (Pardridge, 2005). These enzymes limit the entry of various endogenous and exogenous substances (Pardridge, 2005). Some enzymes functionalize lipophilic substrates, such as cytochromes P-450, other enzymes covert metabolites to polar molecules, by conjugating them with a small molecule, so that they can be excreted (Minn et al. 1991).

1.1.5 Models to study the Blood-Brain barrier models for in vitro research

BBB models are used to test drug transport and the simplest way to model a BBB is to use brain endothelial cells, as these are the first line of cells that will be in contact with the blood and with the tested substances. Using an *in vitro* cell line of brain endothelium also makes it easy to mimic the characteristics of BBB, such as the relative expression of molecules that provide the phenotype of brain endothelial cells' tightness and lack of permeability and high electrical resistance (reviewed in Gromnicova, 2016). Also, *in vitro* BBB models reduce animal testing and are overall less expensive than *in vivo* experiments.

Since the 1970's, researchers in both academia and industry have attempted to isolate cerebral micro-vessel endothelial cells (CECs) in order to model a human BBB *in vitro* that closely mimics the *in vivo* phenotype, which is reproducible and easy to grow. Although primary human CECs would be an ideal model of choice, the rarity of available fresh human cerebral tissue makes the studies impractical.

On the other hand, brain microvascular endothelial cell line hCMEC/D3 was developed to model human BBB. It can be easily grown and is amenable to cellular and molecular studies on pathological and drug transport mechanisms with relevance to the central nervous system (CNS) (Weksler, Romero, & Couraud, 2013). The immortalised hCMEC/D3 cell line retains some important characteristics of primary brain endothelial

cells, and expresses cell surface adhesion molecules, tight junction proteins, chemokine receptors, ABC transporter proteins, and brain microvascular endothelial markers throughout the course of 35 cell-split passages (Sreekanth, 2012). However, hCMEC/D3 lacks high electrical resistance that primary brain endothelial cells possess. Despite its downside, many researchers have used the cell line since its introduction in 2005 and to date; over 500 research articles have been published using hCMEC/D3 cells.

1.1.5.13D co culture model of blood-brain barrier

Cells behave differently in an *in vivo* environment compared to the monolayer they are cultured in (2D environment). Cells in an *in vivo* environment are in 3D matrix along with other cell types of the BBB and therefore, receive physical support, nutrients, and biochemical signals from all directions.

It is possible to mimic 3D *in vivo* environment for which 3D co-cultures have been developed. Using a 3D co-culture model of the BBB can provides a quick solution compared to animal experiments in understanding fundamental biology and the development of therapeutic products. 3D co-culture model of the BBB can be designed using collagen gel cultures seeded with glial cells, astrocytes or pericytes or both. Then, a monolayer of hCMEC/D3 cells is seeded on top of the collagen gel (Sreekanth et al, 2012). To prepare a 3D co-culture model, hCMEC/D3 can be co-cultured with astrocytes. Astrocytes from various sources, including mouse, rat, porcine, bovine, and human, can be used. In our project, primary human astrocytes were used as they may potentially increase the translational findings to humans *in vivo.* Primary human astrocytes are obtained from brain tissue of a foetus or an adult - in the present study we used human foetal astrocytes due to the limited availability of human tissue from the adult brain.

1.2 Overcoming the Blood-Brain barrier

A number of approaches have been developed to improve therapeutic drug delivery across the BBB into the CNS. Strategies range from bypassing the BBB to deliver drugs directly into the brain, modifying the drug agent and its carrier for effective delivery, or even disrupting the BBB itself (illustrated in figure 1.3). All current strategies have their own specific features, advantages and limitations that are summarized in the Table 1.2 (Hersh et al, 2016).

Table 1.2 Different approaches for drug delivery across BBB into brain featuring their advantages and limitations (table taken from Hersh et al, 2016).

Method	Route	Advantages	Limitations
Osmotic Disruption of BBB	Paracellular	Transient	Invasive Transient cerebral oedema Non-specific
Chemical Disruption of BBB	Paracellular	Transient	Conflicting results in clinical trials
Receptor mediated transport	Transcellular	Targeted	Low efficiency
Cell-mediated delivery	Transcellular	Targeted	Toxicity to cell carrier Low therapeutic loading
Focused Ultrasound	Paracellular	Non-invasive Targeted	High cost
Intrathecal and Intraventricular Delivery	Bypass BBB	Elevated concentrations in CSF	Invasive Limited parenchymal concentrations Rapid CSF turnover
Intranasal Delivery	Bypass BBB	Non-invasive Simple administration	Irritation of nasal mucosa Low efficiency
Interstitial Wafers and Microchips	Bypass BBB	Sustained and/or controlled release	Invasive Limited distribution through extracellular space
Convection Enhanced Delivery	Bypass BBB	Enhanced distribution via bulk flow	Invasive Back flow of infusate Risk of catheter misplacement

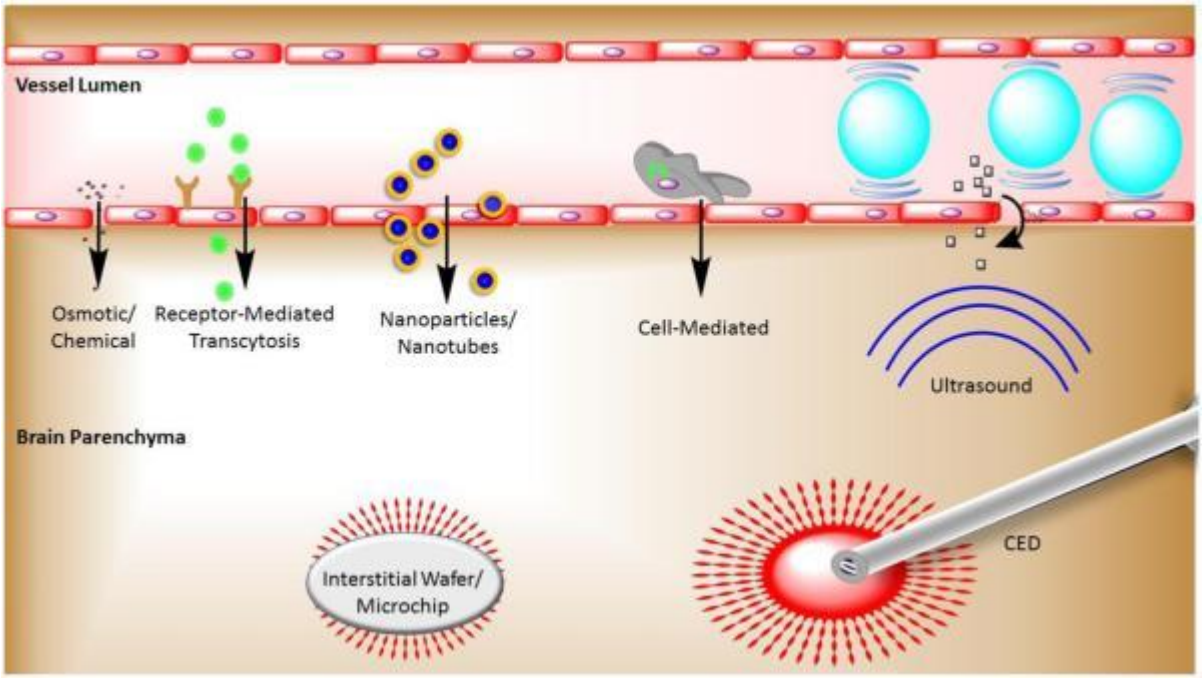

Figure 1.3 *An illustration of different strategies for delivering therapeutic drugs across the BBB. Therapeutic drugs are transported from the blood vessel lumen across the BBB via various strategies: osmotic or chemical disruption of tight junctions; receptor-mediated transcytosis; nanoparticle-based carriers (including targeted nanoparticles); cell-mediated delivery, and Focussed ultrasound-mediated oscillation of microbubbles causing disruption of tight junctions and enhanced transcytosis. Interstitial wafers and microchips, in addition to convection-enhanced delivery CED, bypass the BBB and deliver therapeutic agents directly to the brain parenchyma (figure taken from Hersh et al, 2016).*

Although there are multiple drug delivery approaches, approximately 98% of small molecules and most large molecules (Pardridge W. M, 2005) are unable to reach the brain through the BBB due to various limitations - inadequate drug infusion, being painfully invasive or disrupting the BBB.

1.2.1 Overcoming the Blood-Brain barrier with nanocarriers

As discussed before, the BBB prevents many types of molecule from entering the brain. Therefore, potential drugs and therapeutic molecules that are designed to target the brain must be delivered in a way that overcomes the impermeable BBB. One of the approaches to overcome this problem is to use nanocarriers.

Currently, advances in the field of nanomedicine have generated several platforms that can improve the unmet problem of drug transport across the BBB, namely nanoparticles (NPs)

(Khan et al. 2014). NPs are colloidal carriers that can have a natural or synthetic origin and vary in sizes between 1 and 100 nm (Masserini, 2013). NPs provide a promising approach for drug delivery into the brain due to their different functional groups. The possibility of drug reaching the brain after coupling with NP will primarily depend on the physiochemical features of the NPs that will be carrying the drug rather than on the chemical structure of the drug, as in most cases the drug is inactive with the NPs (Masserini, 2013). NPs also have high chemical and biological stability. Moreover, they can incorporate both hydrophilic and hydrophobic therapeutics and be administered into the brain by a variety of routes (including oral, inhalation, and parenteral) (Masserini, 2013). Moreover, NPs can bind its therapeutic ligands (i.e. cargos) either covalently or non-covalently. They can carry proteins, antibodies, aptamers, or nucleic acids to target specific tissues. Having a large surface area to volume ratio gives them the ability to bind to multiple copies of ligands and dramatically increase their binding affinity (Masserini, 2013).

There are two types of NPs - synthetic NPs, and natural NPs.

1. **Synthetic NPs** can be made from organic or inorganic material;
    - Organic materials NPs - made of polymeric materials such as Poly (e-caprolactone) (PCL), poly(ethylenimine) (PEI), poly(amidoamine) dendrimers (PAMAM), poly(alkylcyanoscrylates), poly(lactic-co-glycolic acid) (PLGA) and polyesters (poly(lactic acid) (PLA)).
    - Inorganic materials NPs- made from gold, silver, silicon dioxide (silica).

These NP carriers can transport therapeutic drugs mainly by adsorbing, entrapping, or binding covalently to the therapeutics (Khan et al. 2014). The inorganic NPs offer a great advantage over the organic and natural polymeric NPs in terms of simplicity of preparation and functionalization. Due to their distinctive physical properties, inorganic NPs are easier to track by microscopy (such as transmission electron microscopy (TEM), magnetic resonance imaging (MRI)), or analytical techniques (such as ICP-MS). Disadvantages of inorganic NPs are that they cannot be degraded naturally, and some might present undesired toxicity (such as silver nanoparticles).

2. **Natural NPs** – are made from natural polymers such as amino acids (poly(lysine), polysaccharides (chitosan and alginate), poly(aspartic acid), or proteins (albumin and gelatin) (Khan et al. 2014). The NPs made up of natural materials have

advantages of providing biological signals to interact with specific receptors/transporters that are expressed on endothelial cells. However, their downsides are limited ability to control their modification, inadequate tracking capacity on imaging platforms, and batch to batch variability (Khan et al. 2014).

The types of nanoparticles that are popular for biomedical research are reported in table 1.3.

Table 1.3 The types of nanoparticles those are popular for biomedical research.

Type of nanomaterial	Advantages	Disadvantages	Review article
Silica nanoparticles	Synthesis in variety of shapes and sizes Drug loading inside the pores of the material	If coating not stable, nanoparticles can cause haemolysis	(Roggers et al. 2014)
Magnetic nanoparticles	MRI agents already in medicine Theranostic application	If uncoated, can interact with proteins and lead to opsonisation	(Veiseh et al. 2010)
Gold nanoparticles	Synthesis in variety of shapes and sizes Optical properties useful for theranostic application	Ligand attachment limited to thiols and amines	(Dykman & Khlebtsov 2012)
Quantum dots	Optical properties useful for bioimaging	Typically made out of heavy metals, concerning for clearance, Toxic for in vivo applications	(Angela et al. 2019)
Carbon nanotubes	Drug loading inside the material Theranostic application	Low biocompatibility and safety, Toxic for in vivo applications	(He et al. 2013)
Liposomes	Biocompatible Biodegradable Drug loading inside the material	Quick capture by reticuloendothelial system Accumulation in liver and spleen Main delivery via passive targeting	(Bozzuto & Molinari 2015)

1.3 Gold Nanoparticles

Gold nanoparticles hold several advantages over other types of nanoparticles. Their physical properties allow them to be used in several applications in biomedical applications, and they are easy to synthesize. Gold nanoparticles also have low toxicity that can vary according to their design/way of synthesis.

1.3.1 The chemical and physical properties of the gold nanoparticles

Gold nanoparticles have the great advantage of being able to be synthesized in several shapes and sizes, such as nanospheres and nanorods. The most commonly used shape for drug-delivery research is nanospheres; therefore, this thesis is also focused on using gold nanospheres (Gromnicova et al. 2016). The most common size of gold nanoparticles that is used for application in biology ranges between 1.5 nm to 50 nm in diameter (Guerrero et al. 2010; Sadauskas et al. 2007; Gu et al. 2009; Libutti et al. 2010; Sandhu et al. 2002; Prades et al. 2012; Fraga et al. 2013; Yang et al. 2005). The shape and size both are very useful determinants of surface properties of the nanoparticle, i.e., how many surface atoms might have the ability to react and form a bond. The surface atom reactivity can be calculated to determine how many potential ligands can be attached to the gold nanoparticle core. For example, gold nanoparticles of 2.2nm diameter have been calculated to have about 162 surface atoms (Hostetler et al. 1998). However, Hostetler also calculated that not all of them could form bonds. The smaller nanoparticles have a large surface area-to-volume ratio and might have over 50% of their surface atoms available for reaction (reviewed in Gromnicova, 2016).

Not only their size and shape are easily tuneable, but the gold nanoparticles also have many other useful properties, such as their optical and heat-generating properties (used for temperature-dependent killing of tumor cells (Zhang et al, 2018)). The optical properties of gold nanoparticles are useful for their detection, measuring the gold concentration or characterization of nanoparticle size, shape, or ligand coating (Huang et al. 2007). Gold nanoparticles (less than 40 nm in diameter) are also able to quench fluorescence (Swierczewska et al. 2011), which is a very favourable quality if trying to detect the gold

or attached ligands in biological environments. Quenching happens when a gold nanoparticle is within a few nanometers of a fluorophore (Dulkeith et al. 2005), when the nanoparticle's surface plasmon resonance (SPR) changes the excitation/emission property of the fluorophore, preventing it from emitting light (Kang et al. 2011).

1.3.2 Synthesis of gold nanoparticles

The synthesis of gold nanoparticles is a simple process, the gold nanoparticles are produced in a liquid form by the reduction of the gold salt chloroauric acid (H[AuCl4]). Chloroauric acid is dissolved by rapid stirring during which a reducing agent is added. This procedure produces neutral gold atoms as the Au^{3+} ions are reduced. There are two general methods of doing this to synthesize gold nanoparticles, the Brust-Schiffrin method, and the Turkevich method (Brust et al. 1994 and Turkevich et al. 1951).

In 1951, the Turkevich method was first applied by using sodium citrate as the reducing and stabilizing agent, which yields spherical gold nanoparticles suspended in the water of about 10-20 nm in diameter. Larger nanoparticles can be produced by using lower concentration of sodium citrate (so there is not enough reducing agent to reduce all the gold). If there is less sodium citrate used in the reaction, the lower amount of citrate ions available for stabilizing the particles causes small particles to aggregate into larger ones (until the total surface area of all particles becomes small enough to be covered by the existing citrate ions).

The second method of synthesizing gold nanoparticles is "Brust-Schiffrin", which was discovered by Brust and Schiffrin in the early 1990s. It is used to produce gold nanoparticles of about 2-6 nm in diameter that are very stable. The reaction occurs in organic liquids that are normally not miscible with water (like toluene). The reducing agent used in this method is sodium borohydride, and the stabilizing agent is tetraoctylammonium bromide (Templeton et al. 1998; Ackerson et al. 2005). If gold nanoparticles are not coated or stabilized with ligands, they will retain their reactive abilities (aggregate into bigger nanoparticles). For example, gold nanoparticles can be stabilized with sugars (i.e. galactose) along with PEG-amine and insulin, to form a stable monolayered protected nanoparticle in a single reaction (Templeton et al. 1998; Ackerson et al. 2005).

1.3.3 Coating of gold nanoparticles

It is essential to coat (i.e. with galactose or PEG-amine) the gold nanoparticles used in biological systems because if absent, then the gold nanoparticles would aggregate once they enter a physiological environment. Aggregation can happen because once the gold nanoparticles enter a physiological environment, there is rapid adsorption of proteins from the bloodstream to the NP surface, forming a protein coating “the protein corona” (Khan et al. 2014). The formation of this protein corona may cause the NPs to aggregate or alter the surface chemistry of the NPs. Additionally, protein corona can accelerate blood clearance of the NPs and localise them mostly in spleen and liver, which may decrease the dose available for accumulation in the brain as well as induce inflammation (Rampado et al, 2020). Therefore, coating gold nanoparticles with molecules that stabilize them may help to maintain the performance and safety of the material (Rampado et al, 2020).

Gold nanoparticles that transport therapeutics across the BBB need to be stabilized, and then a therapeutic cargo attached. Finally, a targeting ligand may be attached to facilitate their uptake into target cells or tissues.

1.3.4 Ligand place exchange reaction

One way to attach cargo molecules onto gold glyco-nanoparticles is to use place exchange reaction. Since our project involves attaching of DNA onto gold nanoparticles, an explanation using DNA follows.

The reaction occurs when there is an excess of free thiolated DNA molecules added to the mixture of thiol-coated gold nanoparticles (figure 1.4). The excess of free thiols react with the gold core, where some bind, exchanging for the already attached ligand.

The place exchange reaction is an easy procedure being very useful for coating gold nanoparticles with thiol ligand in a non-reducing environment as reaction is sensitive to the reducing environment and may cause to detach the ligands from gold nanoparticles. Therefore, this reaction has been used both for coating nanoparticles as well as the release of ligands from nanoparticles in cells in reducing conditions (Cervellera et al, 2017).

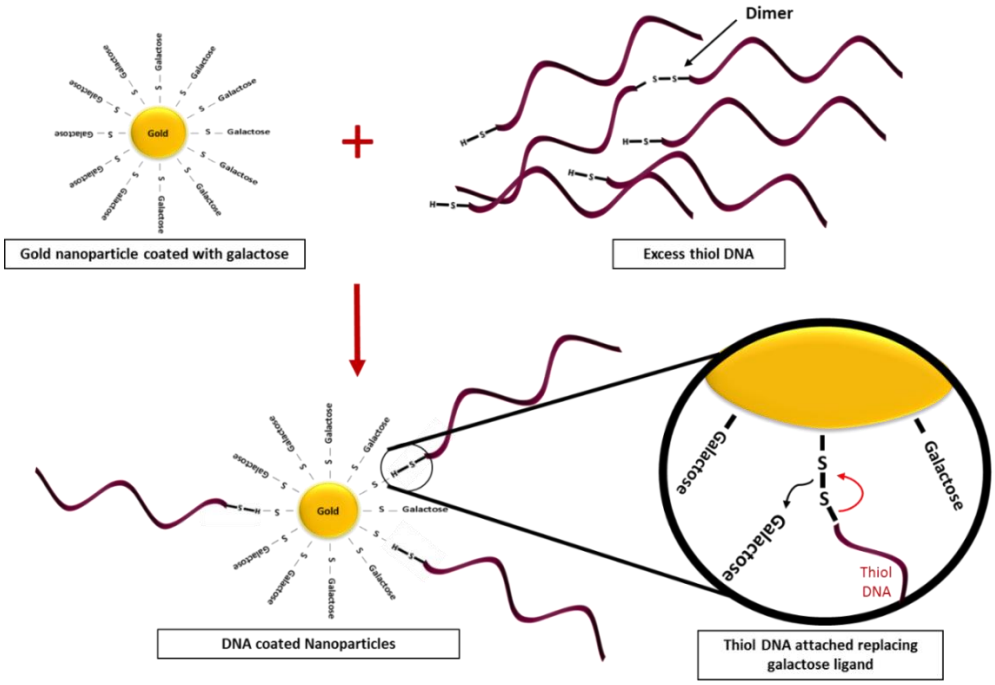

Figure 1.4 *Mechanism of place exchange reaction. Thiol ssDNA covalently attaches to the gold nanoparticle by replacing the galactose ligand.*

1.3.5 Covalent and non-covalent attachment of ligands on the gold nanoparticles

Gold nanoparticles have been used to deliver several therapeutically useful molecules, such as proteins, drugs, or nucleic acids (Daraee et al. 2014).

Ligands can be attached to spherical gold nanoparticles either covalently or non-covalently. The covalent bond is stronger than the non-covalent one and thus results in more stable ligand attachment. However, sometimes a weaker non-covalent bond is preferred as the release of the ligand is faster (Daniel & Astruc 2004).

The most common and stable covalent linkages to the gold core include a thiol bond and its variations (disulfides, dithiols, trithiols, tetrathiols, or xanthates). The strength of the covalent bond can be changed by adding several thiols to attach a single ligand to the gold core or adding a cyclic thiol at the end group, which increases the strength of the ligand (Letsinger et al. 2000).

Non-covalent binding of ligands occur via electrostatic interactions, where a charged group attracts an oppositely charged molecule. For example, a NH_3^+ group on the nanoparticles can carry a charge and thus bind to other oppositely charged ligands (Letsinger et al. 2000).

1.3.6 Toxicity of gold nanoparticles

Gold nanoparticles are generally considered to be non-toxic (Fratoddi et al, 2011). However, if taken up and stored inside cells, the catalytic action of NPs can cause mitochondrial damage or interact with DNA and/or generate reactive oxygen species (ROS) (Manke et al, 2013). It has been suggested that different properties of the gold nanoparticles may change their interaction with cells - whether they are taken up or become toxic (Fratoddi et al, 2011). The properties that affect the toxicity of gold nanoparticles include the size, shape, charge and ligand coating, as well as proteins that may attach to nanoparticles (protein corona) from serum. Currently, the most widely accepted examples of nanomaterial toxicity are oxidative stress and inflammation. Moreover, nanoparticles can also have harmful effects on the autophagy and lysosomal pathways, resulting in toxicological consequences. Endocytosis of nanomaterials by both phagocytic and non-phagocytic mechanisms mostly ends with lysosome internalization. The lysosomes have acidic pH and variety of hydrolytic enzymes (e.g., proteases, esterases, phosphatases, nucleases, and lipases) providing an extremely hostile environment to degrade all but the most bio persistent nanoparticles. In addition to the endo-lysosomal pathway, recent evidence suggests nanoparticles can also induce autophagy (Stern and Johnson, 2008). Among the many physiological functions, the lysosome, uses autophagy (macroautophagy) pathway to degrade intracellular pathogens, damaged organelles and long-lived proteins (Klionsky, 2007). Autophagy induction by nanoparticles may be an attempt to degrade what is observed by the cell as foreign or abnormal. While the autophagy and endo-lysosomal pathways have the potential to influence the disposition of nanoparticles, there is also a growing body of literature suggesting that biopersistent nanopartciles can, in turn, negatively impact these pathways (Stern and Johnson, 2008).

Overall, in general gold nanoparticles have been found to be non-toxic in in vitro experiments according to many studies. Connor et al, 2005 showed that gold nanoparticles

(spheres) of different sizes (4, 12, and 18 nm in diameter) with capping agents (citrate, cysteine, glucose, biotin, and cetyltrimethylammonium bromide) were found to be non-toxic based on the MTT assay on human leukemia cell line. Similar results were showed for gold nanoparticles (spheres, 3.5 nm in diameter) on immune system cell lines by Shukla et al, 2005, where gold nanoparticles entered the cell by endocytosis, did not induce any toxicity, and reduced the level of reactive oxygen species. In contrast to these results, other groups have found that gold nanoparticles are "toxic". For example, Goodman et al, 2004 found that cationic 2 nm gold nanoparticles are toxic (at certain doses). Interestingly, the same gold nanoparticles with a negatively charged surface were found to be non-toxic used at the same concentration in the same cell line. Pan et al, 2009 also showed that 1.4nm gold nanoparticles triggered necrosis, mitochondrial damage, and induced an oxidative stress on number of examined cell lines (Human colon carcinoma cells, HeLa, Human lung carcinoma cells, Human liver carcinoma, baby hamster kidney cells, Human dermal fibroblast and many more). However, Pan et al, 2009 found no evidence for cellular damage for 15nm gold nanoparticles of the same surface group. The study highlights, there may be a possible size-dependent toxicity of gold nanoparticles (Pan et al. 2009). In particular, gold nanoparticles smaller than 2 nm in diameter show evidence of chemical reactivity that does not occur at larger sizes (Turner et al. 2008).

For in vivo toxicity there is a real need to investigate the long term exposure of gold nanoparticles before any potential therapeutic applications.

The available literature reports, both in vitro and in vivo, vary widely in their methods and conclusions (Ostrowski et al. 2009). Many reports indicate that gold nanoparticles are nontoxic; however, others contradict this finding. The conflicting cytotoxicity results can arise from the variability of the different cell lines used, different toxicity assays or due to different chemical/physical properties of nanoparticles. For example, cytotoxicity results can vary with the different cell lines i.e. citrate coated 13nm gold nanoparticles were found to be toxic to a human carcinoma lung cell line but non-toxic to the human liver carcinoma cell line used at same dose concentration (Patra et al. 2007).

1.3.7 Gold nanoparticles clearance

According to FDA guidelines, pharmaceutical drugs should be eliminated via metabolism or excretion processes after they enter the body as it reduces toxicity and prevents drug accumulation. Similar to pharmaceutical drugs, nanoparticles should be designed to be eliminated in the body. Many studies have found that the nanoparticles with hydrodynamic diameters ≤5.5 nm are generally to be excreted from the rat body by the renal route (Choi et al. 2007). Since the majority of the gold nanoparticles used in studies are larger than the renal filtration cut-off, the gold nanoparticles are not always excreted in urine, instead they were found to be eliminated from the blood by the reticuloendothelial system and therefore to accumulate in the spleen and liver (Sadauskas, et al. 2007).

1.3.8 Gold nanoparticles in clinical trials

FDA has approved few gold nanoparticle based technologies for diagnostic and therapeutic purposes in medicine.

- Clinical trials carried out by Astra Zeneca in partnership with Cytimmune; on gold nanoparticle-based cancer treatment. Aurimune (CYT-6091) (pegylated colloidal gold particles) was used as a vehicle to deliver the recombinant human tumor necrosis factor alpha (rhTNF) into tumors, which disrupted the blood vessels, enabling chemotherapeutic drugs to penetrate the tumor and damage the cancer cells. Safe delivery of highly effective doses of rhTNF to tumor cells was observed (Libutti et al. 2010).

- AuroLase® (silica-gold nanoshells coated with (poly)ethylene glycol (PEG)) nanoparticles are also in clinical trials for localized therapy for the treatment of primary or metastatic lung tumors (NCT01679470) (Anselmo et al. 2016). A currently active trial uses AuroLase® as an imaging technology during focal ablation of prostate tissue using nanoparticle-directed laser irradiation. Since no active drug is used in this approach, AuroLase® is activated externally at the target site, thus avoiding any toxicity towards the normal cells (Anselmo et al. 2016).

- Gold nanoparticles conjugating with spherical nucleic acid formulation (composed of siRNAs) targeting the Bcl-2-like protein 12 (BCL2L12) sequence that has potential antineoplastic activity are in clinical trials for the safety evaluation. (Kharlamov et al. 2015). Kharlamov et al. 2015 studied the safety and feasibility of two delivery techniques

for gold nanoparticles for the treatment of atherosclerosis. Results obtained in the trial suggested that gold nanoparticles are associated with a significant regression of coronary atherosclerosis and an acceptable level of safety for clinical practice.

- Another gold nanoparticle based therapy in clinical trial is to use gold nanoparticles for breath analysis with a nanosensor array for identifying gastric diseases. It has been suggested that the nanosensor array could provide the missing non-invasive screening tool to distinguish gastric cancer and related precancerous lesions (Xu et al . 2013).

1.3.9 How nanoparticles can cross the BBB

As previously mentioned, many therapeutic drugs are not able to reach the brain. Gold nanoparticles could potentially enhance drug delivery as they can cross the BBB via intracellular traffic pathways (Sarin et al. 2008). Different pathways affect the delivery of gold nanoparticles to the different intracellular compartments and therefore, may affect their delivery and ultimate destination. Intracellular localization detected by transmission electron microscopy is the first tool to analyse the transport mechanism. Gold nanoparticles have been observed in the cytosol, vesicles, or in the nucleus of the brain endothelial cells (Gromnicova et al, 2016). The different ways NPs can cross the BBB are described below.

1.3.9.1 Crossing the BBB without functionalization

Nearly all nanomaterials are BBB impermeable, however, gold nanoparticles have been shown to reach the brain and accumulate in neurons even in the absence of any specific functionalization (Masserini, 2013). Gromnicova et al, 2014 showed a rapid movement (within 10 mins) of <5nm glyco-nanoparticles into all neuronal cells within rat cortex. Such movement was too quick to be employed by diffusion via intercellular spaces. Hence, NPs may possibly cross BBB using active transport.

1.3.9.2 Adsorptive-mediated transcytosis

The concept of adsorptive-mediated transcytosis involves binding of cationic proteins to endothelial cell surface and crossing the BBB. The mechanism involves functionalization of the surface of the gold nanoparticles in a way that will allow electrostatic interaction with the luminal surface of the BBB. Since endothelial cells have negative (due to the sulphated glycocalyx) or positive charges (some cells or some regions in cells have positive charge due to existence of positive proteins), this interaction can be promoted by conferring a positive and/or negative charge to the gold nanoparticles surface.

1.3.9.3 Receptor mediated transcytosis

Transcytosis is the process by which extracellular cargo is internalized at the plasma membrane (the apical side) of the cell and is transported via vesicular transport to the basal side (see section 1.3). The transcytosis transport mechanism of macromolecules relies on the presence of specific receptors on the luminal surface of brain endothelial cells. For example, insulin, transferrin, and apolipoproteins are some of the proteins that reach the brain through receptor-mediated transcytosis.

1.3.10 Exocytosis of nanoparticles

Nanoparticles administered into the body are eventually cleared by organs such as the kidney, liver or spleen. However, they can remain in the organs for a long time if taken up by macrophages (Oh et al, 2014), thus increasing the likelihood of acute or chronic toxicity.

Therefore, it is important to evaluate exocytosis (from brain and other organs) of gold nanoparticles for biosafety purposes. Previous research has shown that exocytosis may depend on the incubation time of nanoparticles with cells. For example, Bartczak et al, 2012 showed that 14nm peptide coated gold nanoparticles exhibited a faster rate of exocytosis compared to larger 74nm peptide coated gold nanoparticles investigated on endothelial cells.

1.3.11 Detection of gold nanoparticles in vitro and in tissues

Depending on experimental design, there are different ways to detect and quantify gold NPs in biological applications. Two of the methods for analysis of gold NPs uptake used in this project included electron microscopy and inductively coupled plasma mass spectrometry (ICP-MS).

1.3.11.1 Electron microscopy

The most common method for imaging, detecting and quantifying gold NPs is transmission electron microscopy (TEM). Gold NPs can be detected on the cells' surface by scanning electron microscopy (SEM) or inside the cells and their intracellular compartments by TEM. Gold NPs smaller the 10nm may not be visible by standard SEM or TEM, but methods such as silver enhancement can be used (deposition of silver atoms onto gold NPs increase the particle size to up to ~20 nm in diameter).

There are several advantages of using TEM for analysis of the uptake of gold NPs into the cells and tissues. The data produced can be both quantitative and qualitative. Moreover, once the sample has been processed for electron microscopy, it can be repeatedly analysed.

There are also some disadvantages of using electron microscopy. It is an expensive and time-consuming technique. Moreover, imaging of real-time events is not possible due to the nature of the technique that requires thoroughly dehydrated sample for observations.

1.3.11.2 Inductively-coupled plasma mass spectrometry (ICP-MS)

ICP-MS is a technique that is used for quick and accurate measurements (lower limit of sensitivity <1 pg/ml) of metals in experimental samples. In terms of detecting gold NPs, the method can be used to measure number of nanoparticles in biological cultures (cells with gold NPs) as the gold concentration is directly related to the number of nanoparticles in the cell culture.

1.4 Gold nanoparticles to transport oligonucleotide-based therapeutics for CNS drug delivery

Short fragments of nucleic acids, such as CRISPR/Cas9 system (gene editing) and antisense oligonucleotides (ASOs) (gene silencing) provide promising approaches to treat neurodegenerative diseases. By direct intervention at the mRNA level, they may bind to a mutated gene and reduce production of pathogenic proteins (Sah & Aronin, 2011). Their conceptual simplicity, the possibility of rational design, relatively inexpensive cost, and developments in the sequencing of the human genome has led to use oligonucleoties as therapeutic agents or as tools to study gene function (Verma, 2018).

Over the last few years, there has been remarkable progress in the development of oligonucleotide therapeutics. Currently, oligonucleotide-based therapeutics form the third major drug development platform (Sah & Aronin, 2011), mainly focusing on modulating gene expression by targeting RNA or the genome itself. Oligonucleotides can be used to manipulate thousands of messenger-RNAs (mRNA) that play an essential role in cellular functions.

Antisense oligonucleotides can alter mRNA function through several distinct mechanisms, making them a diverse tool (Dias & Stein, 2002). They can be used to restore protein expression, reduce the expression of a toxic protein, or modify mutant proteins to reduce their toxicity. Antisense oligonucleotides can be synthesized as small as 8 – 30 nucleotides and easily hybridized to a complementary sequence of gene of interest (Choung et al., 2006) (i.e., in treating HD, these oligonucleotide strands would be complementary to the mRNA that codes for the mutant Huntington protein) (Sah & Aronin, 2011). Oligonucleotides are specifically designed to modulate the transfer of genetic information to protein i.e. oligonucleotides with a complementary sequence can hybridize to a specific mRNA and can inhibit its expression inducing a blockade in the transfer of genetic information from DNA to protein (Verma, 2018)

Oligonucleotides can be divided into two forms according to their mode of action:

- The RNase H-dependent oligonucleotides, which work by inducing the degradation of mRNA
- The steric-blocker oligonucleotides, which work by physically preventing or inhibiting the progression of splicing or the translational machinery.

This way, the information in the DNA that codes for the harmful protein causing the disease does not pass onto the ribosome, and the harmful mutated protein is never formed (Rader et al., 2014).

For neurodegenerative disorders such as Huntington disease, antisense oligonucleotide therapy has moved from preclinical to the clinical stage, facilitated by the remarkable distribution and cellular uptake of antisense oligonucleotides when delivered into the brain (Sah & Aronin, 2011). However, since Huntington disease is a chronic disease, long-term and repeated administration is required to provide sustained benefits.

An alternative to antisense oligonucleotides is CRISPR/Cas9 system. CRIPSR/Cas9 is a gene editing therapeutic approach based on natural mechanism of editing the target-specific DNA sequence of the genome by using three molecules; nuclease (Cas9), responsible for cleavage of the double-strand DNA; an RNA guide (short sequence), which guides the complex to the target; and the target DNA. The mechanism involves designing a stretch of 20nt base pairs (target DNA) that matches the gene that needs to be edited. An RNA molecule complementary to those 20nt base pairs is constructed (guide RNA).Then the protein [Cas9] will cut the DNA sequence of interest at a specific site (Cong et al, 2013). Once the DNA is cut, the cell's natural repair mechanisms kick in and work to introduce mutations or other changes to the genome. CRIPSR/Cas9 has a potential to achieve the same benefits antisense oligonucleotides in treatment of Huntington disease but with a lasting effect, since it permanently inactivates the defective gene (Heidenreich & Zhang, 2016). Therefore, CRISPR/Cas9 can treat other single gene defect disorders because it involves gene editing which changes the sequence of DNA (by inserting a cut or break in the DNA). This changes the message the gene is giving and “tricks” a cell's natural DNA repair mechanisms into introducing therapeutic changes (Cong et al, 2013).

1.4.1 Current development of gene therapy

Advances in gene therapy in recent years have led to numerous studies investigating the therapeutic potential of oligonucleotides in various in vitro cell models, animal disease models, and in human clinical trials (Verma, 2018). Gene therapy is emerging as potentially beneficial treatment for several diseases such as tumors, cancer anaemia,

rheumatoid arthritis, cardiovascular diseases, HIV/AIDS, cystic fibrosis, diabetes mellitus and obesity, and renal diseases (Verma, 2018).

In 2013 in the US, the food and drug administration (FDA) approved two antisense oligonucleotide drugs, lomitapide, and mipomersen, for the treatment of familial hypercholesterolemia. Lomitapide and mipomersen antisense oligonucleotide drugs work by targeting expression of the gene apolipoprotein-β, which promotes lowering the cholesterol (Rader et al., 2014).

A pharmaceutical company Isis pharmaceuticals has been successful in treating an eye disease associated with AIDS with their antisense drug, Vitravene©. The company is currently working on $9.9 million project to engineer an antisense drug for Huntington disease. Besides that, they have made promising advances in scientific trials of antisense technology to treat other conditions including high cholesterol and Parkinson's disease (ISIS pharmaceuticals, 2010).

1.4.2 Challenges for delivery of naked oligonucleotides into the brain

Delivery of oligonucleotides across the BBB, for diseases like Huntington's disease, is challenging because the therapeutics cannot simply enter the brain. Therefore, our research has mainly focused on solving the problem of delivering therapeutic oligonucleotides into the CNS by not having to disrupt the BBB. The novel approach used for this project consists of using ~2nm gold nanoparticles as a nanocarrier to deliver oligonucleotides (covalently attached) into the brain.

1.4.3 Thiol-modified oligonucleotides

Thiol-modified DNA oligonucleotides have been used extensively, not only on gold nanoparticles. They can be used for reaction with a broad array of activated accepting groups, such as maleimide, cysteines in proteins and are suitable for binding to gold nanoparticles. Next, they have characteristics that make them useful as probes for detection of target molecules. For example, the infrared dye IRDye® 750 (Li-Cor) widely used in microscopy, is available in either NHS ester (amino groups with activated N-

hydroxysuccinimide esters) or maleimide form. Horseradish peroxidase (HRP) can be also used as a modifier of oligonucleotides in several target detection applications, such as in situ hybridization and immunoassays. Most importantly, owing to the strong affinity of thiol groups for gold surfaces, thiol oligonucleotides are extensively used for the preparation of functionalized gold nanoparticles (Zimmermann et al. 2010).

Lastly, thiol-modified oligonucleotides can be easily synthesised by incorporating the thiol modification at either the 5′- end or the 3′-end of the oligonucleotide.

1.5 Aim of thesis

As mentioned previously, effective drug delivery to the brain is challenging due to the existence of the BBB. As new therapeutic molecules emerge with the potential to treat brain disorders, there is a need for a therapeutic nanocarrier that can be transported into the brain while retaining its therapeutic cargo. Gene editing or silencing through nucleic acids is currently one of the most promising approaches to treat neurodegenerative diseases. However, securing consistent delivery into the CNS presents several challenges. One approach is to use gold nanoparticles to deliver therapeutic oligonucleotides into the brain parenchyma. Previous work in our group (Gromnicova et al., 2014) showed that gold glyco-nanoparticles of <5 nm in diameter can enter rat brain and have the potential to act as a delivery system of oligonucleotide therapeutics into the brain.

Hence, gold glyco-nanoparticles of <5 nm in diameter were investigated as a delivery system of oligonucleotides into the brain.

Aims of the following chapters include:

Chapter 3: To determine a suitable methodology of attaching 20nt and 40nt oligonucleotides to the ~5nm gold glyco-nanoparticles via place exchange reaction and to assess cell uptake efficiency of the DNA coated nanoparticles using 2D cellular models of the BBB.

Chapter 4- To isolate NP-DNA-40^{ds} with different numbers of 40nt DNA molecules attached to each nanoparticle using FPLC and to assess uptake efficiency of the different sized NP-DNA-40^{ds} using the 3D co-culture model of the BBB.

Chapter 5- To assess nanoparticles intracellular localisation in brain, kidney, liver and spleen using transmission electron microscopy and to determine overall bodily distribution by measuring gold concentration in each organ using ICP/MS of the different sized NP-DNA-40^{ds} when injected in rats intravenously and intracarotidly (in vivo).

Chapter 6 – To quantify how much DNA was transported across the brain endothelial cells in 2D cellular models of the BBB

2 MATERIAL AND METHODS

2.1 Nanoparticle associated methods

2.1.1 Synthesis of gold glyconanoparticles

Gold glyconanoparticles were obtained from Midatech Pharma Plc. They were synthesised using a modified Brust-Schriffrin method. The procedure consisted of mixing gold salt and SH-C2 -alpha-galactose ligands in water and methanol at a specific molar ratio (not known; confidential synthesis protocol by Midatech). The addition of reducing agent, sodium borohydride, to the mixture resulted in instant formation of small gold nanoparticles. Gold nanoparticles were dissolved in water and characterized by Midatech using HPLC (high-performance lipid chromatography) and DLS (dynamic light scattering) on a Nano ZSP Zetasizer (Malvern instruments). The nanoparticles have gold core of 2nm in diameter, determined by transmission electron microscopy, and the size of the glycol-nanoparticles is 3.63 ± 1.09 nm (mean ± SD) measured by DLS. These nanoparticles have approximately 100 gold atoms in the core and 40 covalently bound C2-galactose molecules on the outside, attached by disulphide bonds, as determined by molecular mass of the gold core (~20,000) and physical size.

Two batches of galactose-coated gold nanoparticles were used in this work (size by DLS is 3.63+/- 1.09 nm (mean SD)):

- **Batch A (100% C2aGalNP)-** 2.33 mg/ml – batch used for the (unfractionated) in vitro 2D transfer assay; NP-DNA-20^{ss} vs NP-DNA-20^{ds} and NP-DNA-20^{ds} vs NP-DNA-40^{ds} (in chapter 3 respectively).

- **Batch B (100% C2aGalNP)**- 5mg/ml – batch used to prepare one large batch of (fractionated) NP-DNA-40^{LO} and NP-DNA-40^{HI} used for *in vivo* experiments, 3D co culture transfer assays and qPCR quantification (in chapter 4, 5 and 6 respectively).

No batch variability was observed.

The nanoparticles were used at concentrations of 8 μg/ml for cell studies unless described otherwise.

2.1.2 Preparation and characterisation DNA-coated gold glyconanoparticles

2.1.2.1 DNA Sequences

For the sequence of DNA with 5' C6 spacer with thiol group we selected a 20 nt DNA sequence. The selected DNA sequence was derived from a GFP gene (green fluorescence protein), obtained from a plasmid of Neisseria gonorrhoeae (pCmGFP) (GenBank: FJ172221.1). Oligonucleotide sequence to make;

1) NP-DNA-20^{ss} and NP-DNA-20^{ds}

- 20nt **thiol**-DNA – ssDNA;
  5' Thiol-C6- AAT ATC GCG GAC AGA AGA CG 3' (Sigma)

- 20nt DNA complementary to thiol-DNA – to make dsDNA;
  5' CG TCT TCT GTC CGC GAT ATT 3' (Sigma)

```
5′ HS-C6-AAT ATC GCG GAC AGA AGA CG      3′
3′       TTA TAG CGC CTG TCT TCT GC      5′
```

2) NP-DNA-20^{ds} with biotin tag

20nt DNA complementary to thiol-DNA with Biotin for EMSA analysis

5' Biotin - CG TCT TCT GTC CGC GAT ATT 3' (Sigma)

```
5′ HS-C6-AAT ATC GCG GAC AGA AGA CG      3′
3′       TTA TAG CGC CTG TCT TCT GC-Biotin 5′
```

NP-DNA-20^{ss}

NP-DNA-20^{ds}

NP-DNA-20^{ds} with Biotin

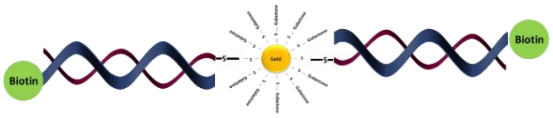

Figure 2.1 *Illustrative images of NP-DNA-20ss and NP-DNA-20ds*

3) NP-DNA-40^{ds}

- 5’ HS-C6-AAT ATC GCG GAC AGA AGA CG 3’ (Sigma) = 20nt thiol-DNA strand 1
- 5’ – AAAAGCTCTGCCTTGGTTTCCGTCTTCTGTCCGCGATATT-3’ (Sigma) = 40nt DNA strand 2
- 5’- GAAACCAAGGCAGAGCTTTT- 3’ (Sigma) = 20nt DNA for extension on strand 1

```
5′  HS-C6-AATATCGCGGACAGAAGACGGAAACCAAGGCAGAGCTTTT   3′
    3′    TTATAGCGCCTGTCTTCTGCCTTTGGTTCCGTCTCGAAAA   5′
```

4) NP-DNA-40^{ds} with biotin tag

- 5’- GAAACCAAGGCAGAGCTTTT---Biotin 3’ (Sigma) = 20nt DNA for extension on strand 1 with **Biotin** for EMSA analysis.

```
5′  HS-C6-AATATCGCGGACAGAAGACGGAAACCAAGGCAGAGCTTTT-Biotin 3′
    3′    TTATAGCGCCTGTCTTCTGCCTTTGGTTCCGTCTCGAAAA   5′
```

NP-DNA-40^{ds}

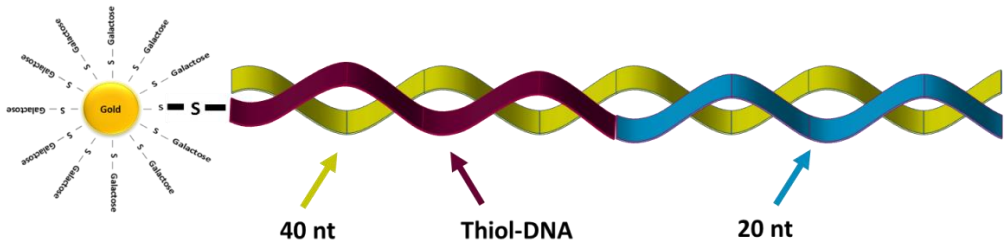

NP-DNA-40^{ds} with Biotin

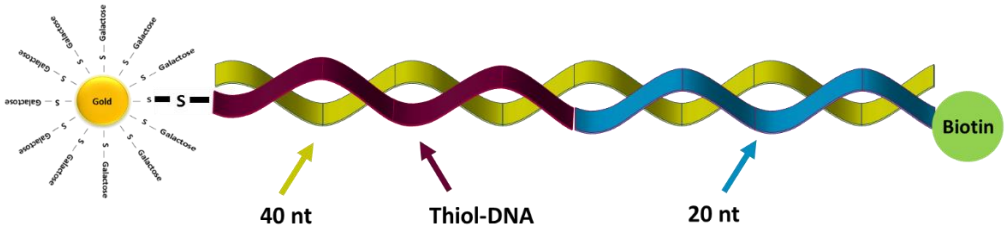

Figure 2.2 *Extension of the NP-DNA-20ss by the addition of 40nt complimentary DNA to make NP-DNA-40ds (illustrative images).*

2.1.2.2 Reduction of thiolated DNA

The purchased thiol DNA from Sigma (Poole, Dorset) came protected because the thiol bonds are strong nucleophiles, and if they are unprotected, they spontaneously form disulphides in neutral aqueous solution.

Tris(2-carboxyethyl)phosphine (TCEP) was used to reduce the thiol DNA to yield free thiol. Molar ratio of 1 nmol of DNA to 1.25 nmol of TCEP (made up in 0.1M tris/HCL (pH 7.5)) was used and mixture incubated at RT for 4 hours.

The procedure of the reaction was as follows:

- Prepared 1mM TCEP – 2.8mg TCEP added in 10 ml of 0.1M tris/HCL (pH 7.5)
- Thiol DNA had 376.5 nmol DNA in powdered form.
- Reaction performed at 1 : 1.25 molar ratio;

  376.5 nmol DNA : 470.625 nmol TECP

  10mM ($x10^{6}$) …….. 1 Litre (TCEP)

  470.625 nmol ..…….. 4.70625 ($x10^{-5}$)

  = 47 µl /2 (TCEP breaks 2 molecules)

= **23.5** µl of 1mM TCEP used to reduce 376.5 nmol of Thiol DNA

- Incubated at room temperature for 4 hours.
- Added 26.5 µl 0.1M tris/HCL (pH 7.5) to make up final volume of 50 µl. *(Note: end volume of 0.1M tris/HCL (pH 7.5) can be adjusted to make up final desired volume aliquot of Thiol DNA).*

2.1.2.3 Ligand place-exchange reaction to prepare DNA coated gold nanoparticles

20 nucleotide DNA-coated nanoparticles (NP-DNA-20)

To prepare 20 nucleotide DNA-bound nanoparticles, galactose-coated gold nanoparticles were mixed with 20nt thiol DNA to make NP-DNA-20^{ss} at a molar ratio of 1 (nanoparticles) to 14 (Thiol DNA). The place exchange reaction occurred over 2 days at 37 °C. The 0.5mL reaction tube was kept in a storage container flushed and sealed with nitrogen gas to prevent spontaneous oxidation between free DNA thiols.

The step-by-step procedure for ligand place-exchange reaction:

- 14:1 molar ratio of DNA : nanoparticles. Each Thiol DNA aliquot contained 1.4 nmol DNA in a 10 µl volume.
- Nanoparticles required – 0.1 nmol for 1.4 nmol DNA
- Stock galactose nanoparticles = 2.33 mg/ml. molecular weight = 20,300
- For place exchange reaction: 0.1 $x10^{-9}$ x 20,300 = 2.03 $x10^{-6}$ g nanoparticles
  = 2.03 x 10^{-6} / 2.33 (mg/ml) = **0.87 µl stock nanoparticles**
- **Added 0.87** µl nanoparticles to 1.4 nmol Thiol DNA aliquot, flushed with nitrogen gas in sealed container and incubated at 37 °C for 48 hours.

20nt dsDNA-coated gold glyconanoparticles

To make NP-DNA-20^{ds}, equimolar amount of 20nt DNA complementary to the thiol-DNA (with or without biotin depending on the nature of the experiment) was added. Biotinylated

complementary DNA was used for EMSA analysis. Nanoparticle transport assay required the com plementary DNA to be un-biotinylated.

After the reaction to exchange galactose with DNA was finished, equimolar amount (1.4 nmol) of 20nt complementary DNA (dissolved in nuclease-free water) to thiol-DNA was added. The pure DNA comes in powder form and nuclease free water is added to liquefy.

40 nucleotide DNA-coated nanoparticles (NP-DNA-40)

40 nucleotide DNA-coated nanoparticles (NP-DNA-40) were prepared as described above, using place exchange reaction to attach 20nt thiol DNA onto gold nanoparticles first. After the reaction, a 40nt DNA (strand 2) and 20nt ssDNA DNA (for an extension on strand 1) was added to NP-DNA-20^{ss} at an equal molar ratio to thiol-DNA. The mixture was incubated at room temperature for 30 mins for hybridisation to take place **(figure 2.2).**

Step-by-step procedure of the elongation of 20nt DNA-coated nanoparticles to form 40nt DNA-coated nanoparticles:

- Place exchange reaction was performed between nanoparticles and Thiol 20nt DNA for 48 hours ***(refer to chapter 2.1.4.1)***
- After the reaction, equimolar amount (1.4 nmol) of 40nt DNA and (1.4 nmol) extended 20nt ssDNA was added to NP-DNA-20^{ss}.
- The mixture hybridised for 30 mins at room temperature.

2.1.3 FPLC of 40nt DNA-coated nanoparticles

A large batch of NP-DNA-40^{ds} was fractionated to prepare nanoparticles with different densities of DNA molecules attached (NP-DNA-40^{LO} and NP-DNA-40^{HI}). These fractions were used for all *in vitro* 3D BBB transfer assay and *in vivo* experiments.

9.14 mg (1386 nmol) of reduced thiol-DNA was added to 2mg (99 nmol) of galactose-coated nanoparticles (batch B, Midatech Pharma), and the mixture was incubated at 37 °C for 48 hours.

The nanoparticles were analysed on FPLC ÄKTA pure (GE Healthcare) and separated using Superdex 200 10/300 GL column (with PBS as elution solvent), a gel filtration and/or Size-exclusion chromatography (SEC). The elution volume for all fractions was set at 0.5ml at flow rate of 0.4 ml/min and UV wavelength of 260nm. The fraction **(described in figure 2.3a)** of 20nt DNA bound nanoparticles eluting out at fraction-15, 16, 17 were pooled together **(illustrated in figure 2.3b)** to prepare formulation of nanoparticles with High DNA ratio bound nanoparticles (NP-DNA-40^{HI}) by adding equimolar 40nt ssDNA (strand 2) and 20nt extension ssDNA onto strand 1 **(Section 2.1.2.1 for DNA sequences).** Fractions eluting out at fraction-19, 20, 21 were pooled together to prepare formulation of nanoparticles with Low DNA ratio bound nanoparticles (NP-DNA-40^{LO}) by adding equimolar 40nt ssDNA (strand 2) and 20nt extension ssDNA onto strand 1. The rest of the fractions eluting out much further down the column were identified as excess DNA dimer and free DNA molecules, unbound onto the nanoparticles.

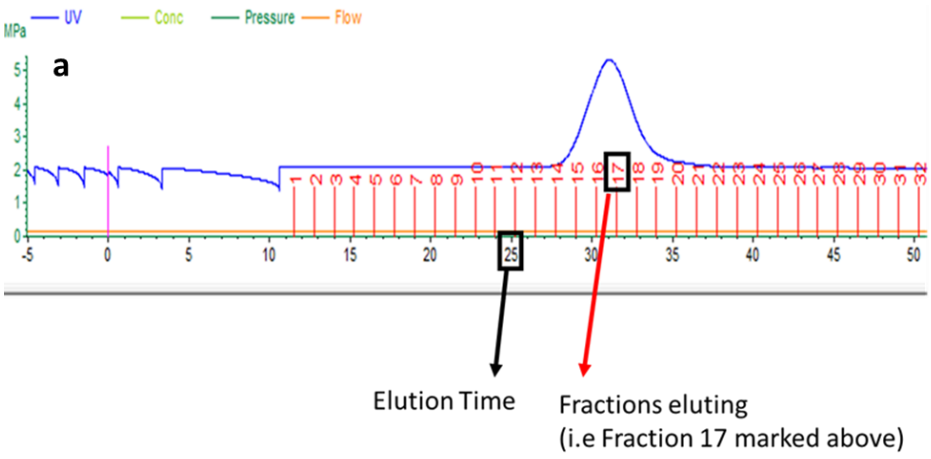

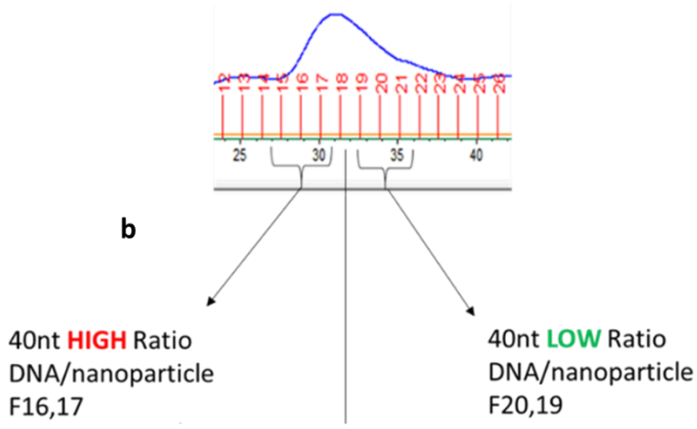

Figure 2.3 *Representative fractions eluting at different times.* ***b)*** *Illustrating which fractions were pooled to make NP-DNA-40^{LO} and NP-DNA-40^{HI}.*

2.1.4 Analysis of gold concentration by spectrophotometric gold assay

Formulations prepared and purified on FPLC of NP-DNA-40^{LO} and NP-DNA-40^{HI} were measured for their gold concentration against a standard (Gold standards for AAS 1000 mg/ml, Sigma). 5 different gold standard concentrations were used: 0.857 mg/ml, 1.75 mg/ml, 2.5 mg/ml, 5 mg/ml and 10 mg/ml.

The assay was performed in a 96 well plate, with a total volume of 200µl in each well. In each well, 10µl of sample, 10µl H_2O and 30µl of 100% freshly prepared aqua regia (kept on ice) were added. The liquids were then mixed by gentle tapping and left to incubate for a 1 min. Next, 150µl of 2M NaBr was added. The absorbance was read on a plate reader using OPTIMA FluoSTAR, at 390 nm.

2.1.5 Electrophoretic mobility shift assay (EMSA) to analyse DNA bound nanoparticles

2.1.5.1 Sample preparation

- **NP-DNA-20^{ds} with Biotin tag**

Complementary biotinylated DNA was hybridised with NP-DNA-20^{ss} to form NP-DNA-20^{ds} in order to perform EMSA detection. Molar ratio of 1nmol of NP-DNA-20^{ss} to 1.15 nmol of 20nt biotinylated ssDNA (complementary to thiol DNA) (1 : 1.15) was used. The sample mixture was adjusted to pH ~ 8 by adding 10X TBE buffer, leaving the final concentration of the TBE buffer 0.5X (pH 8.3) in the sample mixture. The mixture was incubated for 30 min at room temperature for the hybridization to take place.

- **NP-DNA-40^{ds} with Biotin tag**

40nt DNA (which has its first 20nt complementary to the thiol DNA bound on to nanoparticles) and a biotin DNA (complementary to the last 20nt of 40nt DNA), was added in the mixture of NP-DNA-20^{ss} to hybridize the ssDNA bound on nanoparticles and extend the 20nt DNA to a 40nt long dsDNA. The samples were incubated for 30 mins at room temperature to permit hybridization. Later, samples were x100 diluted in water (purite; high performance water purification system is needed as EMSA is highly sensitive technique).

After preparation of NP-DNA-20^{ds}-Biotin and NP-DNA-40^{ds}-Biotin, samples were prepared to run on gel.

2.1.5.2 Preparation of Gel

Samples of NP-DNA-20^{ds}-Biotin were run on a 6% polyacrylamide gel whereas, a sample consisting of NP-DNA-40^{ds}-Biotin were run on a 5% polyacrylamide gel. Gels were prepared as indicated:

5% Acrylamide gel: 3.3ml 30% acrylamide/Bis Solution (37.5:1) (Bio-Rad), 1ml 10X TBE, 15.7ml H_2O, 13mg ammonium persulfate (APS), 40 µl tetramethylethylenediamine (TEMED). Overall volume was 20 ml, which is enough to make two gels.

6% Acrylamide gel: 4ml 30% acrylamide/Bis Solution (37.5:1), 1ml 10X TBE, 15ml H_2O, 13mg ammonium persulfate (APS), 40 µl tetramethylethylenediamine (TEMED). Overall volume is 20 ml, which is enough to make two gels.

The gel was pre-run in 0.5X TBE at 85 V for 1hr. The sample (20µl in each gel well) was loaded on the gel using the following mixture: 1 µl DNA-bound nanoparticle stock, 6 µl 5X TBE, 13 µl Water, 5 µl loading dye (6X, Fermentas). The gel was run in 0.5X TBE at 90V for 1hr and 10 mins for NP-DNA-20^{ds}-Biotin and 1hr and 20 mins for NP-DNA-40^{ds}-Biotin. The gel was transferred onto a nylon membrane Amersham Hybond N+ (GE Healthcare) at 100 V for 1hr and 15 mins in 0.5X TBE at 4° C. DNA was then cross-linked onto the membrane with UV (120mJ/cm^2) and developed using the manufacturer's instructions of chemiluminescent nucleic acid detection module kit (Thermofisher). GelDoc system was used to photograph the membrane.

2.2 Cell culture methods

Table 2.1 Cell cultures.

Cell line	
Brain endothelial cell line	**Abbreviation** - hCMEC/D3 **Source/supplier** - Weksler et al. 2005 **Passage used** - 26-30 **Medium:** modified EBM-2 (Lonza) - contained 0.025% VEGF, IGF and EGF; 0.1% bFGF, 0.1% (v/v) rhFGF, 0.1% (v/v) gentamycin, 0.1% (v/v) ascorbic acid, 0.04% (v/v) hydrocortisone. The amount of serum was reduced to 2.5% (v/v) of foetal bovine serum. **Maintenance** - Frozen hCMEC/D3 cells (p25) cells thawed and grown on collagen coated (type I from calf skin (Sigma, Gillingham, UK)) T-25 culture flask with EBM-2 *MV* medium (changed every 2-3 days). The cell's medium was kept to surface area ratio at 1ml per 5 cm^2. The cells were split when 90% confluent, and once confluent, they were washed X2 with HBSS and trypsinized with 0.05% trypsin-EDTA Invitrogen™ Life Technologies) for 3-5 mins. The cells were seeded according to the seeding density of cells/cm^2. At all times, the cells were incubated at 37 °C. All cultures were kept in a humidified atmosphere with 5% CO_2.
Human primary astrocytes	**Abbreviation** – hA **Source/supplier** - ScienCell **Passage used** – 2-7 **Medium** - Astrocyte medium (ScienCell) – supplemented according to manufacturer's instructions with FBS (2%), astrocyte growth supplement (1%), and Penicillin/streptomycin solution (1%). **Maintenance** – Frozen hA cells (passage 2) thawed and grown on collagen coated (type one from calf skin) T-25 culture flask with astrocyte media (changed every 2 days). The cell medium was kept to surface area ratio at 1ml per 5 cm^2. The cells were split when 70-80% confluent and once confluent, they were washed X2 with HBSS and trypsinized with 0.05% trypsin-EDTA (Invitrogen™ Life Technologies) for less than 3-5 mins. The split cells were transferred into T-75 flasks to grow more cells. At all times, the cells were incubated at 37 °C. All cultures were kept in a humidified atmosphere with 5% CO_2

2.2.2 2D uptake and transport assay of DNA-coated gold nanoparticles in brain endothelial cells

A 2D nanoparticle transport assay was performed on hCMEC/D3 cells to compare the uptake and transport of nanoparticles with oligonucleotide cargos as follows:

- **NP-DNA-20^{ss} compared with NP-DNA-20^{ds} transport assay**
- **NP-DNA-20^{ds} compared with NP-DNA-40^{ds} transport assay**

For all 2D nanoparticle uptake and transport assays, hCMEC/D3 cells (of passages between 26 and 30) were seeded on collagen coated 0.4 µm polyester membrane trans-well inserts (Corning Costar). The trans-well inserts used were either 6.5 mm (seeding density 20,000 cells/insert) or 12 mm (seeding density 70,000 cell/insert). The hCMEC/D3 cells were grown until confluent (2-3 days). The trans-well system consists of the top chamber (inside of trans-well insert), in which the cells grow and bottom chamber (well plate) volume with culture medium. The medium applied in each chamber depended on size of trans-wells used, which is summarised in table 2.2.

Table 2.2 Recommended trans-well inserts medium volumes.

Trans-well insert (diameter)	Multiple well plate (to place inserts)	Medium added in top chamber	Medium added in bottom chamber
6.5mm	24 well	0.1 ml	0.5 ml
12mm	12 well	0.5 ml	1.5 ml

The nanoparticles at a final concentration 8 µg/ml were applied to the upper chamber (of insert) in EBM-2 MV medium and incubated at 37 °C for 3 hours. After the incubation, both chambers were washed 3x in 0.5ml Hank's Balanced Salt Solution (HBSS). The cells were fixed for 1 hr at room temperature in 2.5% glutaraldehyde in 0.1M PB (Sörensons phosphate buffer). The fixative was removed and the chambers were washed 3X in PBS (phosphate buffer saline) and stored in 0.1M PB at 4 °C (summarized in figure 2.3). The inserts were then processed for electron microscopy as described in **Section 2.3.1.**

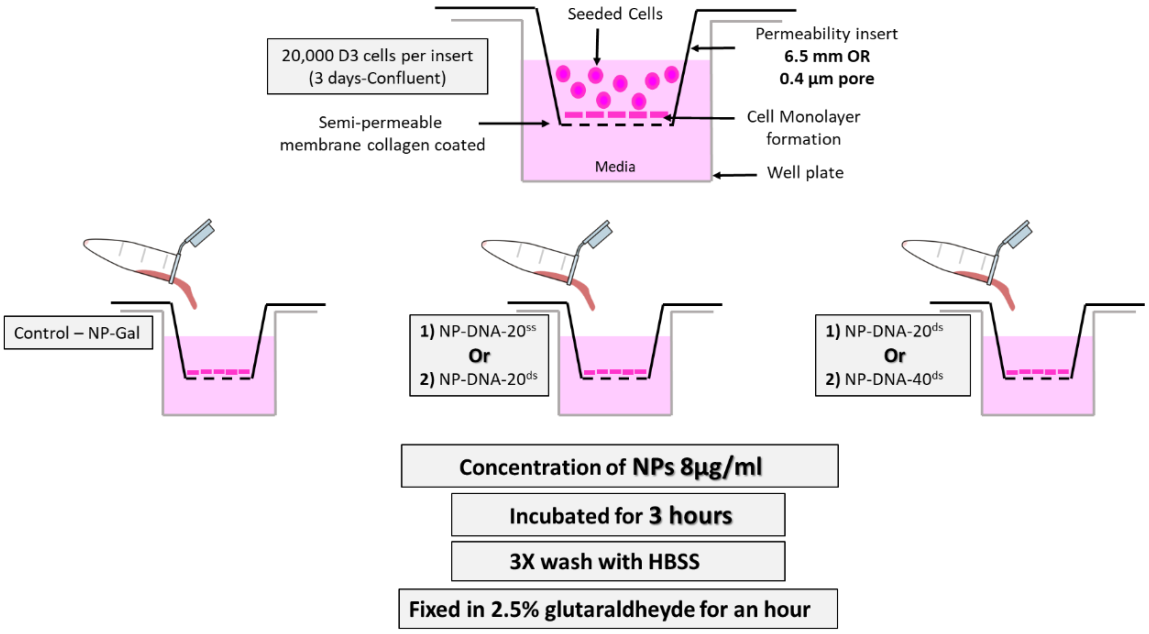

Figure 2.4 *Nanoparticle uptake and transport assay*.

2.2.3 3-dimensional co-cultures for uptake and transport assay of DNA-coated nanoparticles

3-dimensional co-cultures of human brain endothelial (hCMEC/D3) cells and human astrocytes (hA) were used for nanoparticle uptake and transport assays. Astrocytes of 1.5 x10^6/ml were seeded into a collagen gel solution. The collagen gel solution was prepared using 80% (v/v) rat type I collagen with a stock concentration of 2 mg/ml, 10% 10x MEM, 10% human astrocyte cell suspension in astrocyte medium, and plated in a 24 well plate (500µl/well). Before adding the cell suspension to the collagen and 10x MEM solution, 5M NaOH was added drop by drop, followed by careful mixing to raise the pH (colour changed from yellow to orange/pink), which will formed the gel. The gel was incubated for 20 min at 37 °C. RAFT^{TM} absorber plungers (Lonza) were dropped carefully on top of the collagen gels to absorb liquid. The RAFT^{TM} absorber plunger was removed after 20 mins, the astrocyte medium was added to the compressed gels, and the culture was incubated for 24hr. hCMEC/D3 cells were seeded on top of the gel and grown over 2 days in modified EBM-2 medium (Table 2.1) until they formed a monolayer.

Then, nanoparticles were added to the 3-dimensional co-culture gels at a final concentration of 8 µg/ml in modified EBM-2 media and incubated for 3 hrs at 37 °C. After the incubation, the medium was removed, the cultures were washed 3x in 0.5ml HBSS and fixed in 2.5% glutaraldehyde for 1 hr.

The compressed gels were washed x3 in PBS and gently detached from the bottom of the 24 well plates with a spatula. They were then stored in phosphate buffer at 4 °C and processed for electron microscopy as described in **Section 2.3.1.**

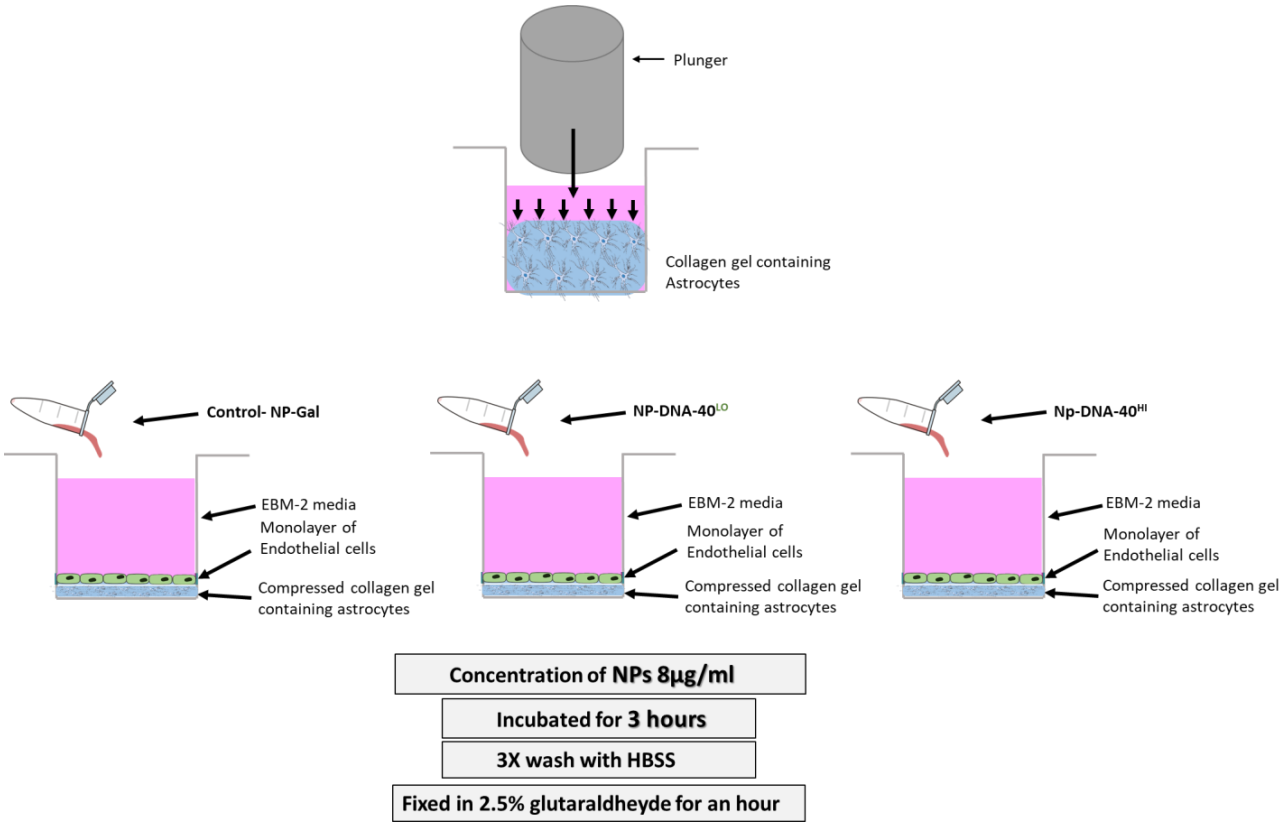

Figure 2.5 *3-Dimensional co-cultures for nanoparticle uptake and transport assay.*

2.2.4 Alamar Blue assay to assess cell viability

To assess toxicity of DNA-coated gold nanoparticles, Alamar Blue assay was performed. hCMEC/D3 cells were seeded in collagen-coated 96-well plates at $3x10^4$ cells/per well and incubated in 5% CO_2 in air at 37°C until they formed a monolayer (24 hours). Nanoparticle solution (100 µL/well) was then added at final concentrations between 8-50 µg/mL, testing nanoparticle formulations of NP-Gal, NP-DNA-40^{LO} or NP-DNA-40^{HI}. The cells were incubated with the nanoparticles for 24 hours. For positive control of toxicity 30 µg/ml digitonin was used by applying it for 30 mins on cells. As a negative control, no nanoparticles were applied on cells.

After the incubation, the cells were washed with HBSS 3X and treated with 10% (v/v) Alamar Blue diluted in EMB-2 medium for 5 hours. Absorbance was then measured at 570

nm (to measure reduced form of Alamar Blue) and 620 nm (to measure oxidised form of Alamar Blue) using FLUOstar OPTIMA micro plate reader (BMG LABTECH, Ortenberg, Germany). The cell viability was calculated by the ratio of E570 (reduced form) /E620 (oxidised form).

2.2.5 Immunofluorescent microscopy of human astrocytes with GFAP marker

Table 2.3 List of antibodies used in this study.

Antibody	***Clonality***	***Immunogen***	**Concentration**	**Company**
Primary ***GFAP***	Rabbit, IgG	*Purified bovine GFAP*	*1/2000*	*#AB5804, Millipore (U.K.) Ltd.*
Secondary ***Anti rabbit IgG antibodies AlexaFluor ® 488 conjugated, raised in Goat***	*Goat IgG (H+L)*	*Rabbit IgG*	*10µg/ml*	*#A11008 Invitrogen Ltd.*

Human astrocytes were grown on collagen-coated coverslips. Once they were about 90% confluent, they were rinsed with HBSS and fixed with 4% (w/v) paraformaldehyde (PFA) in PBS for 20 min at room temperature. Cells were washed 3x in PBS. Coverslips were permeabilized and blocked in a solution of saponin (0.05% w/v) and normal goat serum (5% v/v) in PBS for 30 min. Then, cells were incubated with a primary antibody (1/2000 in PBS containing 2.5% goat serum and 0.05% saponin) for 1hr at room temperature. Then, coverslips were washed 3X in PBS containing 0.05% saponin on a shaker for 5 min and incubated with secondary antibody (10µg/ml in PBS containing 2.5% goat serum and 0.05% saponin) for 1 hr at room temperature. After final 3X washes with PBS containing 0.05% saponin on a shaker for 5 min, the coverslips were mounted with Dapi-Fluoromount medium (VECTASHIELD) and stored in the dark at 4 °C until they were imaged. Images were captured with an Olympus BX61 microscope using CellP imaging software. As a negative control, cells were incubated with diluent without primary antibody.

2.3 Localisation and quantification of nanoparticles in cells by Transmission Electron Microscopy

2.3.1 Processing of samples for transmission electron microscopy

During processing for transmission electron microscopy, all incubations mentioned in this section were performed at room temperature, and all solutions mentioned in this sections were applied to both insert and the bottom chamber.

The cells were permeabilized in 0.01% Triton X100 for 15 minutes on a rocker and then washed 3x in 0.1 M PB). Silver enhancement (Aurion) was prepared according to the manufacturer's instructions. Its function was pre-tested using a dot blot test – a drop of goat-anti-mouse IgG-gold (ultrasmall) (Aurion) was placed onto a membrane Amersham Hybond N+ (GE Healthcare) and incubated in silver enhancement solution for 30 min to show dark staining.

Silver enhancement solution was applied to the inserts for 1 hr and 10 mins on a rocker and then washed 3x in distilled water. Cells were then osmicated in 1% (w/v) osmium tetroxide (in 0.1 M PB) for 30 min and then washed 3x in 0.1 M PB. The insert was removed from the well and its membrane was cut out. Then, the membrane was cut in half, where the middle part of one half was cut into a strip (~3 mm wide), which was then cut in half and edges were removed to create 2 squared pieces. The part towards the edge of each piece was noted by cutting the corner off. Finally, dehydration on the membranes was performed. Both insert membrane pieces were directly immersed in increasing concentrations of alcohol. The timings and concentrations of ethanol were as follows:

30% ethanol for 5 min,

50% ethanol for 5 min,

70% ethanol for 10 min,

100% ethanol for 10 min (performed twice),

100% ethanol with molecular sieve for 10 min.

After dehydration, the membrane pieces were incubated in a 50:50 mixture of 100% ethanol and Epon resin (Agar) and placed on a rocker overnight. The next day the insert membrane pieces were penetrated with freshly prepared Epon resin and changed twice, each change was incubated for 2 hrs. The insert membrane pieces were embedded in Epon resin a cushion pad for 48 hrs at 60 °C.

Samples embedded in resin blocks were prepared for microsectioning by removing the excess tip of the block to reach the sample. The block was then microsectioned to 80 nm thick sections (silver to gold coloured layers) using a diamond knife (Diatome, Switzerland). The 80 nm cut sections were collected onto pioloform film-covered copper grids. After at least 2 hrs of air drying, they were counterstained with 3% aqueous uranyl acetate for 30 mins followed by Reynolds lead citrate for 10 mins.

2.3.2 TEM quantification of nanoparticle uptake

The sections were observed at a magnification of 20,000 x on JEM 1010 (Jeol). The nanoparticles were counted in cells and sorted into 3 – 4 cell compartment categories; vesicles, cytosol, basal plasma membrane (under cell) and nucleus (illustrated in figure 2.5) at the time of viewing on the electron microscope. The nanoparticles are easily distinguished on electron microscope as they are very sharp black dots and decreasing contrast and brightness of electron microscope does not change their appearance, whereas other cell components fade/disappear. The length of the insert which was assessed on TEM (ranged usually between 300 – 1500 microns in length) was then imaged at low magnification (200x for JEM 1010) to get the length of the section assessed, using Image J software (NIH). The number of nanoparticles was then recalculated per micron of insert.

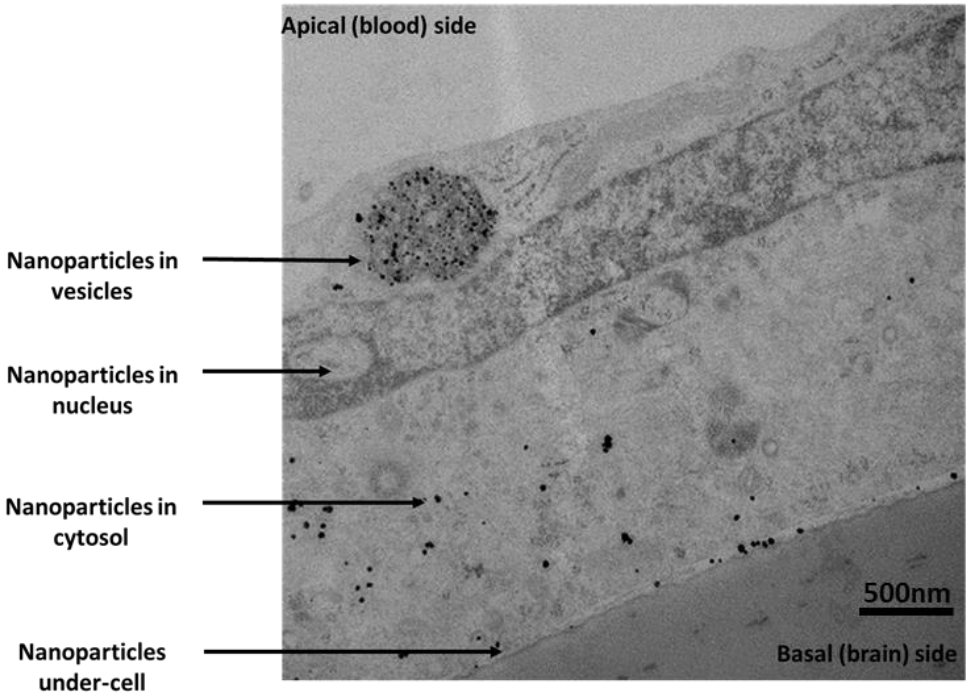

Figure 2.6 *Illustration of counting nanoparticles in different cell compartments.*

2.4 DNA-coated gold nanoparticles *in vivo*

All animal-related experiments of injection, perfusion, fixation, and organ removal were performed in Istanbul in collaboration with Mehmet Kaya and his colleagues. There were 5 groups of rats, Wistar albino's, males, aged approx. 3 months. Each group consisted of 3 rats that were injected with 200µg of gold nanoparticles/kg bodyweight as indicated in Table xx. 100 µL sterile isotonic saline was added to the dose of nanoparticles. The final volume of injected amount per animal was about 120 µl.

Table 2.4 Number of animals per treatment group.

	Intracarotid injection	Intravenous injection
NP-Gal	3	3
NP-DNA-40^{LO}	3	-
NP-DNA-40^{HI}	3	3

Nanoparticles were infused into the left external carotid artery (intracarotid injections) or penile vein (intravenous injections) for over 1 minute. The nanoparticle solution was allowed to circulate for 10 minutes, after which the animals were perfused with cold isotonic saline for 20 mins. Before perfusion with isotonic saline, 2 ml of blood was removed and kept on heparin.

After perfusion, brain, kidney, liver, lung, spleen, and heart were collected. Each one of the paired organs was immersed in fixative of 2% (w/v) PFA and 2.5% (w/v) glutaraldehyde (made in 0.1 M phosphate buffer) for TEM analysis, and the other was rapidly snap frozen for ICP-MS and qPCR analysis. Heart was cut in half (vertically) and the two halves treated as above. Brain was also cut in half (coronal) at bregma +1 and the posterior half was fixed whilst the anterior half was frozen. [Note was made of which side was injected for intracarotid injections]. The fixed collected tissues for TEM analysis were kept in fixative (as above) for 2 hours at +4^{o}C, and then the tissues were stored in PBS at +4^{o}C.

2.4.1 Light and electron microscopy of fixed animal tissue samples

Tissue samples were sectioned to 100µm thick vibratome sections (Leica). The sections were stored in 0.1M PB at 4°C for up to a week, then stored in a storage solution (high sucrose and ethylene glycol) at -20 °C.

2.4.1.1 Light Microscope (LM) - silver staining for tissue samples

100 µm tissue sections were stained using Aurion LM Silver enhancer (prepared using manufacturer's instructions). The tissue samples were incubated for 40 mins with silver enhancement and imaged using a camera or a light microscope (Nikon, 1x).

2.4.1.2 Transmission Electron Microscope processing

A similar tissue section to the one stained with LM silver enhancer was selected. Selected tissue sections for all groups for all organs were placed in glass vials and permealized with 0.05% Triton X100 for 30 mins and washed 3X with 0.1M PB. About 5-6 drops Aurion EM silver enhancer (prepared according to manufacturer's instructions) were applied to each sample, and incubated for 2 hours at room temperature. Tissues were washed 3x with distilled water, and 1% (w/v) osmium tetroxide (in 0.1 M PB) was applied for 45 min. The sections were rewashed 3x with 0.1M PB, and subjected to the following dehydration in acetone procedure;

- 30% acetone - 10 mins
- 50% acetone - 10 mins
- 90% acetone - 10 mins
- 100% acetone x2 – 20 mins
- 100% sieve (pure) acetone – 20 mins

After dehydration, the tissue sections were incubated in a 50:50 mixture of 100% acetone and Epon resin and placed on a rocker overnight. The next day the tissue sections were penetrated with fresh resin with 2 changes, each incubated for 2 hrs. After that, tissue sections were flat embedded in Aclar sheets and incubated for 48 hrs at 60°C. Meanwhile, capsule-shaped resin blocks were prepared using gelatin capsules that were filled with Epon resin and polymerised for 48 hrs at 60 °C.

Once polymerised, a small piece (about 2 mm x 2 mm) was cut out of the flat-embedded tissue sections and glued (Super Glue) onto the resin capsules. Each block was microsectioned as **described in 2.3.1**.

2.4.2 ICP-MS Analysis of gold present in animal tissues

Quantification of the amount of gold by ICP-MS in the brain, kidney, liver, lung, spleen, heart, and blood was performed with help of Ibon Perera at Midatech in Bilbao, Spain. Due to their strictly confident methodology, they were not allowed to share more details with me apart of the digestion procedure of the tissues: 25% tetramethylammonium hydroxide (TMAH) + 0.2% x100 Triton and 1% HCL + 2 ng/ml iridium (Ir).

The obtained values from the ICP-MS were levels of gold (ng) per g of tissue.

2.5 Quantification of DNA in solution and cells by qPCR

SYBR Green 2X master mix kit was ordered from Qiagen. Forward and reverse primers were prepared with a stock concentration of 10 µM in order to have 0.5 µM concentration in a final 20 µl sample/reaction volume. Samples containing DNA template were diluted to working concentration. At all times, reaction component preparation was performed on ice. Table 2.5 summarises the concentration and volume of reagents used per single reaction.

Table 2.5 Components needed to run single qPCR reaction.

Reaction	**Target Final Concentration**	**Volume per single 20 µl reaction**
2x SYBER Green Mix	1X	10 µl
Forward Primer (10 µM stock)	0.5 µM	1 µl
Reverse primer (10 µM stock)	0.5 µM	1 µl
PCR grade water	Make up to 20 µl	7 µl
DNA template	1-10 pg	1 µl

For qPCR quantification purposes, 4 treatment groups were selected; 40nt dsDNA alone, NP-Gal, NP-DNA-40^{LO}, NP-DNA-40^{HI}. 8µg/mL of nanoparticles for each group was applied for 3 hours incubation time in a 2D cellular transport assay. Media was collected from top chamber (apical side) and bottom chamber (basal side) of the trans-well, and from the hCMEC/D3 cell layer. Media collected from top and bottom of trans-well was immediately frozen and cells were lysed with 1% triton and frozen immediately at -20 ºC. The lysed cells, top and base media samples were used for DNA quantification. A positive control (40nt DNA template) was always included to make sure all the kit components are working correctly. A non-DNA template as negative control was included to determine if contamination was present. During qPCR, it was very crucial to avoid DNA cross-contamination. Therefore, a designated clean laboratory set-up area was used as well as designated equipment. Extra care was taken to avoid pipetting errors during qPCR set up as the accuracy of qPCR is highly dependent on accurate pipetting and thorough mixing of solutions. Amplification and detection conditions were performed according to SYBR Green manufacturer's guide; 2 min at 50°C, followed by 10 min at 95°C, followed by 40 cycles of 15 s at 95°C, and 1 min at 55°C. The Ct values given out from qPCR for each sample were normalised using a standard curve (discussed in detail in chapter 6).

3 PREPARATION, CHARACTERISATION AND UPTAKE OF GOLD NANOCARRIERS WITH DNA

Aim:

The aim for work in this chapter was to prepare oligonucleotides attached to galactose-coated gold nanoparticles NP-Gal and investigate their potential as a therapeutic delivery system into the brain.

1. To prepare and characterize DNA coated NP-Gal.
2. To understand what size oligonucleotide cargo can bind onto the NP-Gal and whether it can be transported across the brain endothelium in vitro
3. To compare the cellular uptake and transport of different cargo sizes of DNA-coated nanoparticles crossing the brain endothelium in vitro, such as;

- NP-DNA-20^{ss} compared with NP-DNA-40^{ds}
- NP-DNA-20^{ds} compared with NP-DNA-40^{ds}

3.1 Introduction

As discussed earlier, drug delivery to the brain has many challenges due to the intrinsic properties of the BBB. The interface between blood plasma and brain consists of brain endothelium cells with tight junctions and the surrounding glia. BBB significantly restricts the passage of water-soluble, charged, and high-molecular weight therapeutics to the brain while allowing penetration of small and/or lipophilic molecules into the brain (BMC Neurology, 2009). In order to progress with effective treatment for neurodegenerative diseases such as Huntington Disease, brain cancer and stroke, which are extremely prevalent diseases, novel strategies must be developed to enhance the passage of therapeutic agents across the BBB.

One approach is to use nanoparticle carriers, especially gold nanoparticles. Gold nanoparticles may be a useful agent in treating brain disorders. Gold nanoparticles have many advantages such as simple synthesis, chemical stability, narrow-size distribution, easy surface functionalisation, and low toxicity providing promising methods to solve many challenges in contemporary medicine (Freese et al. 2013). Previous experimental data obtained by Gromnicova et al, 2016 in our research group showed that gold glyconanoparticles <5 nm can enter rat brain. Therefore, they may have potential as a delivery system of therapeutic molecules into the brain. Therefore, my research has mainly focused on delivering therapeutic oligonucleotides into the CNS without disrupting the BBB. The novel approach consists of using <5nm gold galactose coated nanoparticles (NP-Gal) as a nanocarrier to deliver oligonucleotides (thiol DNA) into the brain. For this project, covalently attached oligonucleotide-gold nanoparticles were prepared using 20nt and 40nt thiol-DNA and ~2nm gold core NP-Gal. DNA was used instead of RNA due to its higher stability.

3.2 Results

Place exchange reaction was used to attach thiol-DNA to gold nanoparticles. In this reaction, excess amount of thiolated DNA attaches covalently to the stable nanoparticle coated with thiolated galactose ligands, whilst releasing galactose ligands in exchange.

3.2.1 Selection of gold nanoparticles

Nanoparticles used throughout the project were ~2nm gold core and had covalently attached galactose ligands. Galactose ligand was attached to gold nanoparticles because the previous study by our research group (Gromnicova et al, 2014) showed that galactose coated nanoparticles did not aggregate and remained stable at 4 °C for up to 1 year.

3.2.2 Selection of DNA sequence

20nt Thiol-C6-DNA selection - For the sequence of DNA with 5' C6 spacer and thiol group (referred to as thiol-DNA), we selected a 20nt DNA sequence - AAT ATC GCG GAC AGA AGA CG. The selected DNA sequence was derived from a GFP gene (green fluorescence protein), obtained from a plasmid of a bacteria Neisseria gonorrhoeae (pCmGFP) (GenBank: FJ172221.1). The selected sequence is not present in the genome of mammalian cell or human cell.

Homology of the sequence was assessed by BLAST search (NCBI) to any gene in the mammalian and human genome, as we used human brain endothelial cells and astrocytes for in vitro studies and in vivo experiments on rats. The maximal homology with the human genome was 29/40 nucleotides with three gaps. There was no detectable homology with the rat genome.

40nt DNA selection – For the sequence of 40nt DNA, we selected a sequence of 5' – AAAAGCTCTGCCTTGGTTTCCGTCTTCTGTCCGCGATATT-3' by BLAST search (NCBI). The 40nt sequences had the first 20nt base pairs complementary to the thiol-DNA (above). During the selection, we made sure that the selected sequence is not present in the genome of a rat or human genome.

3.2.3 Detection of DNA attached to the galactose gold nanoparticles by electrophoretic mobility shift assay (EMSA)

EMSA (electrophoretic mobility shift assay) was used to detect nanoparticles with different numbers of DNA molecules attached to each nanoparticle. EMSA is generally used to detect proteins (i.e. transcription factors) binding onto a specific sequence of DNA. The binding of a protein to DNA affects the mobility of DNA in the gel as it migrates at a slower rate than the free linear DNA fragments once the current is applied. In our case, we were detecting DNA molecules bound onto gold nanoparticles. The more DNA molecules the gold nanoparticles had attached to it, the nanoparticles would move slower through a

polyacrylamide gel and thus producing a DNA-NP band that is towards the top of the gel (figure 3.1- right).

Additionally, using EMSA for the separation of nanoparticles with different numbers of DNA molecules attached to the gold nanoparticle is a novel use of this technique. Other techniques have been used to separate DNA-coated gold nanoparticles from uncoated ones. For example, fluorescent-based methods or agarose gel electrophoresis can isolate the nanoparticles from the gel. (Pellegrino et al. 2007) (Sandstrom et al. 2003; Pellegrino et al. 2007; Zanchet et al. 2001).

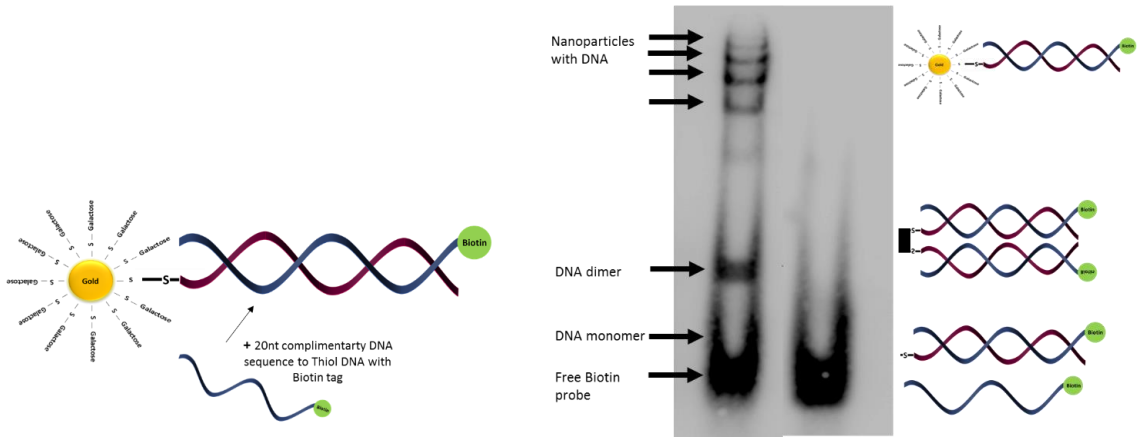

Figure 3.1 *Gold nanoparticle attached with double stranded DNA thiol-ssDNA hybridized with complementary 20nt-bp of biotinylated DNA for EMSA detection (left), summarising what each band on the acrylamide gel for EMSA detection represents (right).*

3.2.4 Optimising place exchange reaction to maximise DNA molecule attachment to the nanoparticle

Initial experiments were carried out to optimise the best time of incubation at which the place-exchange reaction took place. This was important as we needed to attach the maximum number of thiol DNAs to each nanoparticle. The experiment was set to test incubation time for reaction over a different number of days (day 1, 2, 3, 4, and 7), with molar excess ratio of thiol-DNA of 14: 1 DNA: NP at 37° C (the DNA used was in non-reduced form as supplied).

Figure 3.2 of EMSA gel of the place exchange reaction set over a different number of days shows no bands higher up in the gel. This could suggest that the DNA was not attaching to the nanoparticles, and hence, no bands were observed. The reason for no DNA molecules attaching to the nanoparticles might have been that the thiol-DNA was in oxidised form. Oxidised form of DNA (dimer) is not able to attach onto the nanoparticles due to having its thiol group occupied.

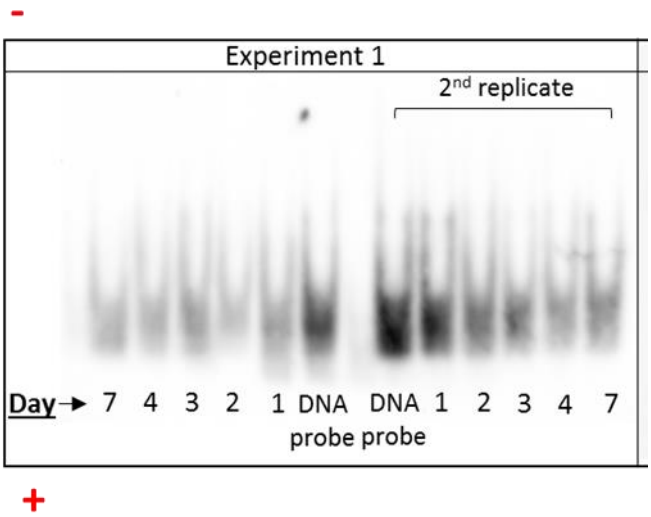

Figure 3.2 *Initial experiment of place exchange reaction with 14nmol DNA : 1nmol NP ratio set over different number of days (day 7, 4, 3, 2 &1) shows no bands of DNA-attached to gold nanoparticles. The control (DNA probe); 20nt-Biotinlayted DNA. The experiment was performed on 6% acrylamide gel and blotted on nylon membrane and detected by a chemiluminescence detection kit.*

3.2.4.1 DNA reduction

Since oxidised (dimer) disulphide DNA does not have free thiol group to attach onto the nanoparticles, the next step comprised reducing dimerized DNA to free up thiol groups to attach onto the nanoparticles. Reducing reagents dithiothreitol (DTT) and tris(2-carboxyethyl)phosphine (TCEP) were tested (Figure 3.3 –A). The addition of DTT to DNA (molar ratio of 2nmol DTT: 1nmol DNA) left most DNA dimers in oxidised form, similarly to control treatment with water only. On the other hand, TCEP reduced most of the DNA dimers.

Therefore, TCEP was selected as a reducing agent. Then, we tested different number of molar ratio concentrations of TCEP versus DNA (1.25nmol TECP: 1nmol DNA & 2nmol TCEP: 1nmol DNA) with a different number of the incubation time (1 hr, 2hrs, & 4 hrs).

Figure 3.3- B shows that the most suitable conditions to reduce thiol-DNA were molar ratio of 1.25nmol TCEP: 1nmol DNA) and incubated for 4hours (as all DNA was in reduced form by 4 hours). The ratio of 1.25nmol: 1nmol compared to 2nmol: 1nmol was selected to keep minimal concentration of the reducing agent. In that way, there was very little free reducing reagent left in the nanoparticle-DNA mixture. The reason for this is that excess reducing reagent can detach thiol-DNA from the nanoparticles after the place exchange reaction has taken place.

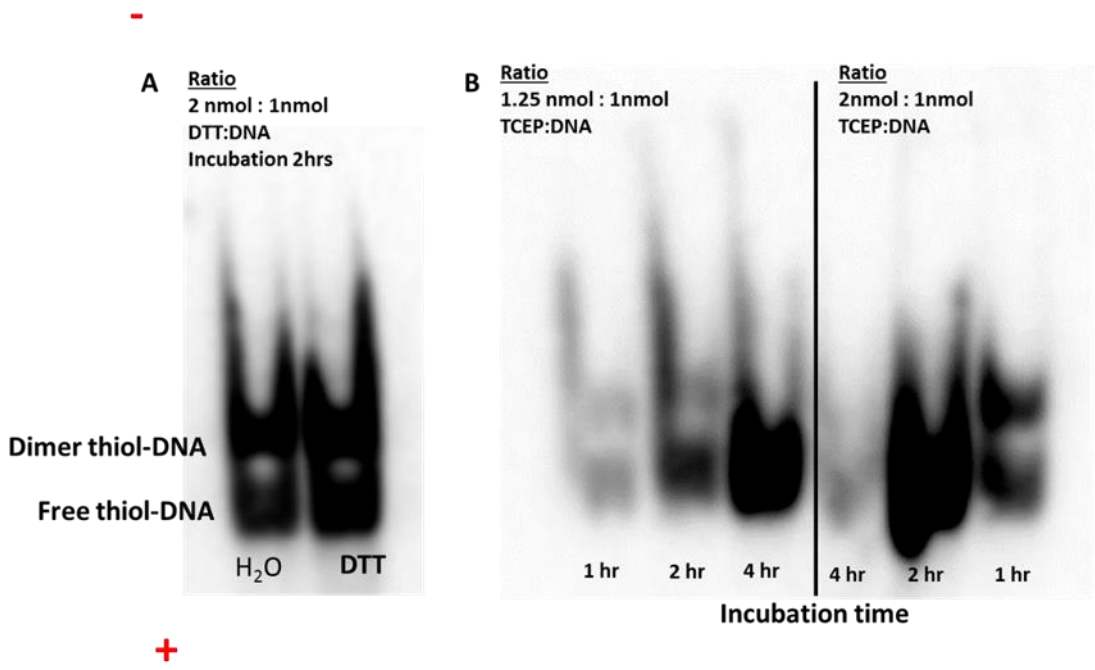

Figure 3.3 *Different reaction conditions to reduce dimer-DNA. Image A represents DTT reducing reagent. Image B represents TCEP reducing reagent. The experiment was performed on 15% acrylamide gel and blotted on nylon membrane and detected with a chemiluminescence.*

3.2.4.2 Optimisation of incubation time for the place exchange reaction

Following reduction to unprotect the thiol-DNA, a place exchange reaction to bind thiol-DNA onto gold nanoparticles was performed. The incubation time for the place exchange reaction to take place was set over a different number of days; day 1, day 2, day 3, and 4. The ratio was kept at 14nmol-DNA (DNA in excess) to 1nmol gold nanoparticles (14:1). Mixed gold nanoparticles and reduced thiol-DNA was immediately flushed with nitrogen

gas (to avoid oxidation of free DNA molecules) in a sealed box and kept at 37 °C for day 1, 2, 3 and 4.

The results in figure 3.4 show the incubation time that was needed for the place exchange reaction to form DNA-attached gold nanoparticles. The probe is biotin attached 20nt DNA, which represents a band of monomeric DNA only. At day two, strong gel bands and the highest number of bands were observed at the top of the gel, compared to other days. After two days, the dimer (oxidised DNA) band starts to get darker/stronger. At this point, the gold nanoparticle may have reached the maximum number of DNAs they could attach, and the free DNA in the mixture has started to dimerize.

When the band density was measured (Figure 3.5), day 2 showed higher DNA loading on nanoparticles (band 5 and 6) compare to the rest of the days (results summarised in graph-1 below). Therefore, for all future experiments, an incubation time of 2 days was selected for the place exchange reaction to get the maximum number of DNA attached to the nanoparticles.

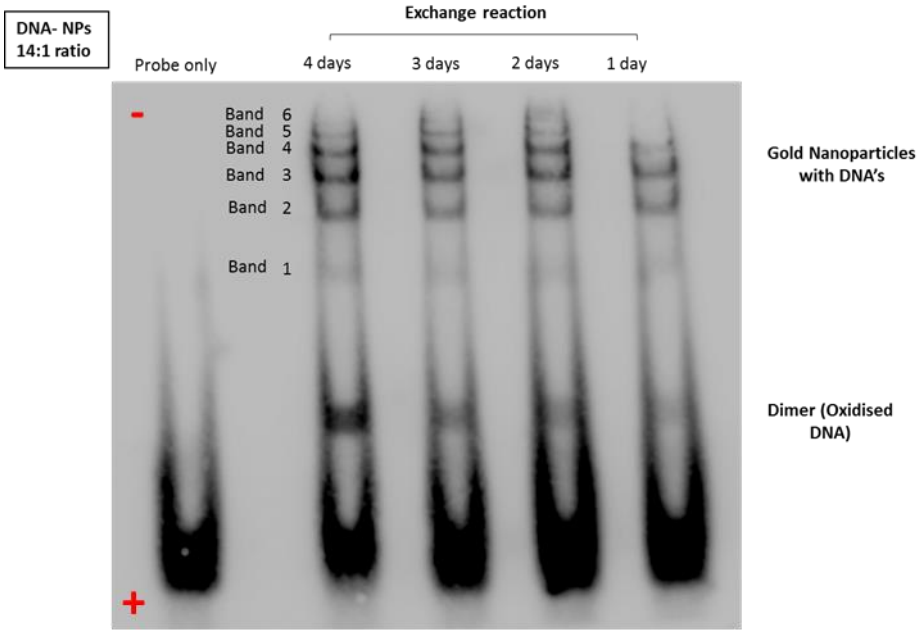

Figure 3.4 *Electrophoretic mobility shift assay of DNA attached gold nanoparticles using a biotinylated DNA probe. Probe only = biotinylated complementary sequence of thiol-DNA. The bands identified as nanoparticles with DNA and free DNA, in a monomeric form (Thiol-DNA), or dimerized. The probe of biotin DNA alone is used as a control, which shows the bands for monomeric DNA only.*

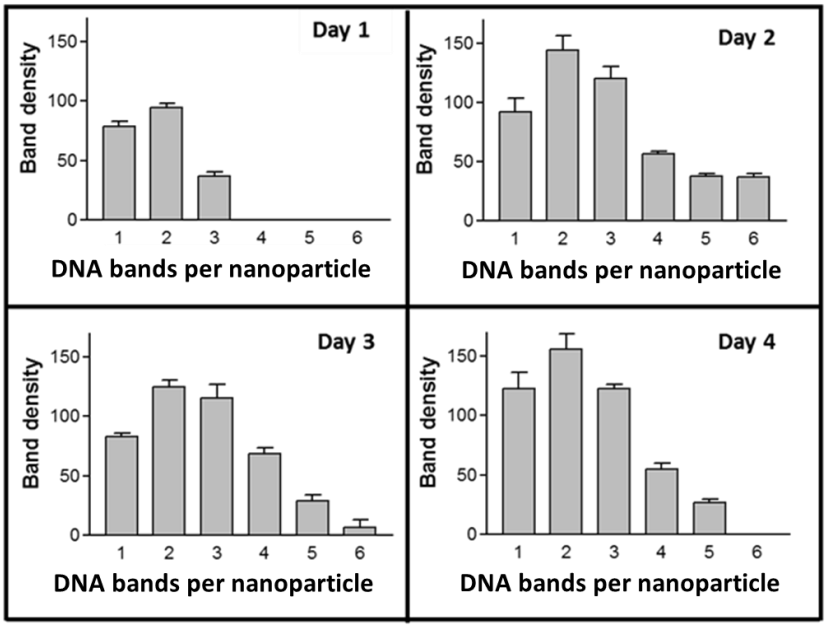

Figure 3.5 *Analysis of band density from the EMSA blot of the 4 days-place exchange reaction. The band density was analysed with ImageJ by measuring the darkness of the each band on the EMSA blot.*

3.2.5 Cellular uptake comparison of DNA attached gold nanoparticles

Aim- Compare the transport rate across brain endothelium of nanoparticles with different numbers of DNA molecules (2D in vitro experiments).

In a previous study, Gromnicova et al, 2014 pointed out the possibility that higher DNA density coated nanoparticles may increase the uptake efficiency of gold glyco-nanoparticles. Therefore, we compared the uptake rate of nanoparticles with different amounts of DNA attached into cells.

In vitro BBB model in the form of human brain endothelial cell line hCMEC/D3 was used to test the uptake rate of DNA-attached gold nanoparticles. Since brain endothelial are the first line of cells that are in contact with the blood plasma in vivo, and therefore would interact with DNA-attached gold nanoparticles.

3.2.5.1 Cellular Uptake of pre-fractionated 20nt ssDNA attached nanoparticles compared to pre-fractionated 20nt dsDNA attached nanoparticles

To test the uptake rate of different quantities of DNA attached gold nanoparticles, three dose groups (illustrated in figure 3.6) were prepared, i.e. control NP-gal, ssDNA-coated nanoparticles and dsDNA coated nanoparticles.

They contained an excess free DNA and unbound gold nanoparticle in the mixture. Therefore we called this a pre-fractionated preparation. (*Fractionation terminology and procedure is detailed in chapter 4).

Control – NP-Gal (no DNA attached)

ssDNA attached nanoparticles (NP-DNA-20^{ss})

dsDNA attached nanoparticles (NP-DNA-20^{ds})

A complementary DNA was hybridized with the **NP-DNA-20^{ss}** in order to form **NP-DNA-20^{ds}**.

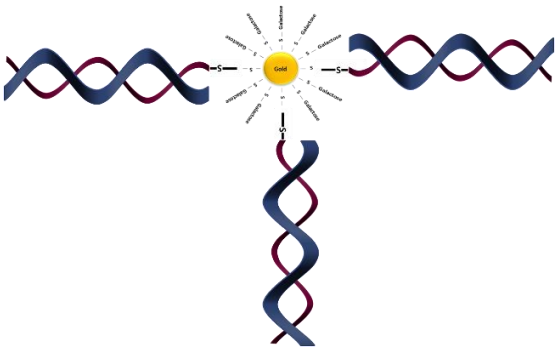

Figure 3.6 *Illustrative images for NP-Gal, NP-DNA-20ss and NP-DNA-20ds; the images are diagrammatic (heterogeneous with respect to how many DNA molecules were attached and not to scale).*

The results of comparing the uptake of NP-DNA-20^{ss} with NP-DNA-20^{ds} into brain endothelial cells are shown in figure 3.7 and figure 3.8. Nanoparticles were quantified in the cell cytosol, vesicles, in the nucleus and under-cell (**illustrated in figure 2.6 in chapter 2**). As the NP-Gal used had ~2 nm gold core, they were not visible within cells by the electron microscopy unless silver-enhanced. Silver enhancing the gold nanoparticles increased the size of these ~2 nm nanoparticles to about 20 nm. Therefore, for all nanoparticle transport assay studies, electron microscopy along with silver enhancing the ~2nm gold nanoparticle was used in order to track the nanoparticles intracellularly.

NP-DNA-20^{ds} had a significantly greater number of nanoparticles in vesicles compared to both the control NPs and the NP-DNA-20^{ss}. The NP-DNA-20^{ss} showed increased uptake in

vesicles compared to the control alone. Notably, there is an unusual increase in cell uptake in the nucleus, which may be due to damage to the nuclear membrane.

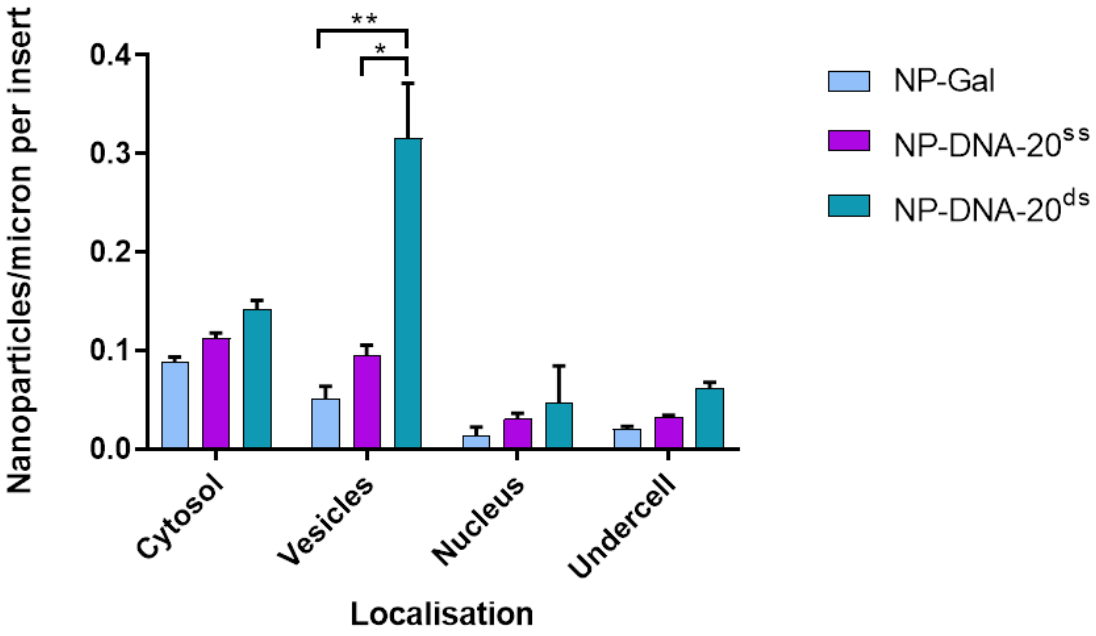

Figure 3.7 *Uptake comparison of NP-DNA-20^{ss} with NP-DNA-20^{ds} into brain endothelial cells. Nanoparticles quantified in cell cytosol, vesicles and in nucleus. The control= NP-Gal. Three experiments were performed, each individual experiment having three technical repeats. Tukey's multiple comparisons test was performed using GraphPad. There is significant difference for NP-DNA-20^{ds} compared to NP-Gal in vesicles (p-value: 0.0034) and NP-DNA-20^{ds} compared to NP-DNA-20^{ss} in vesicles (p-value: 0.0133).*

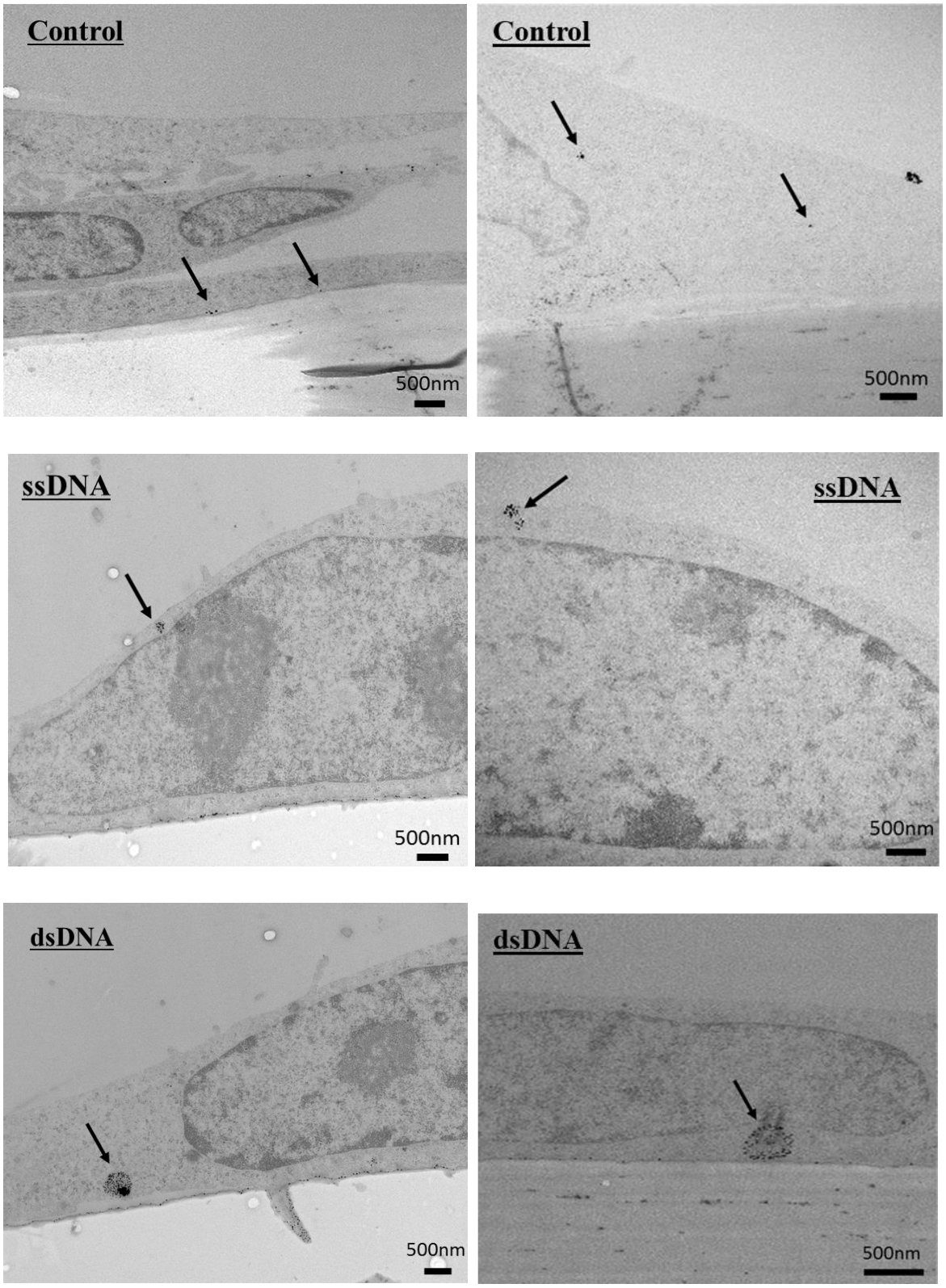

Figure 3.8 *Electron micrographs of silver enhanced gold nanoparticles with attached DNA in hCMEC/D3 cells. More number of NP-DNA-20^{ds} (dsDNA) nanoparticles were observed in vesicles in comparison with NP-DNA-20^{ss} (ssDNA) and NP-Gal (Control). The arrows point towards gold nanoparticles.*

3.2.5.2 Pre-fractionated NP-DNA-20^{ds} compared to pre-fractionated NP-DNA-40^{ds}

Since we observed higher cellular uptake of NP-DNA-20^{ds} compared to NP-DNA-20^{ss} in the brain endothelial cells, we decided to prepare nanoparticles with longer (40nt) DNA attached. Longer DNA molecule would allow us to quantify DNA in the cells/tissue with PCR and RT-qPCR. Moreover, we wanted to determine if a larger oligonucleotide cargo can be transported into and across brain endothelial cells.

To keep costs at minimum, we decided to keep the 20nt thiol-DNA and hybridise it with a 40nt ssDNA which had 20 base pairs complementary to the thiol-DNA. Another 20nt ssDNA was added to compliment the last 20 nucleotides on the end of the 40nt ssDNA to make a NP-DNA-40^{ds} (**refer to chapter 2.1.2.1**).

3.2.5.2.1 Detection of 40nt dsDNA nanoparticles

EMSA was performed to analyse the attachment of 40nt DNA onto the gold nanoparticles. As shown in figure 3.9, there is a shift up of the bands for 40 nucleotides compare to the 20 nucleotides. This confirms hybridization of 40nt DNA onto the nanoparticles. Band B is relatively strong and it likely indicates presence of free monomer of 40nt ssDNA and dimerized thiol 20nt DNA.

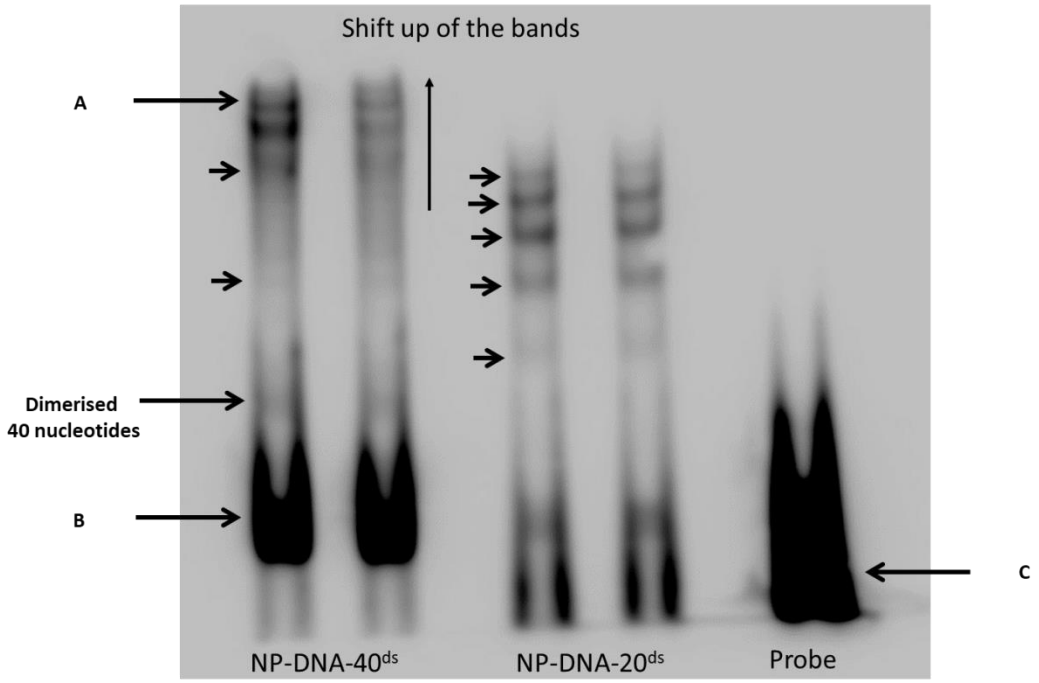

Figure 3.9 *A representative electrophoretic mobility shift assay of NP-DNA-20ds and NP-DNA-40ds. The probe (biotin DNA) is used as a control, which shows the bands for monomeric DNA only. There are duplicate bands for each NP-DNA-20ds and NP-DNA-40ds. The bands higher up the gel (A) represent the nanoparticles attached with DNA, the band (B) shows dimerized DNA, and right at the bottom (C) is the free DNA in a monomeric form (Thiol-DNA). Three EMSA experiments were carried out to confirm the results.*

3.2.5.2.2 Cellular Uptake of pre-fractionated NP-DNA-20^{ds} compared to pre-fractionated NP-DNA-40^{ds}

NP-DNA-40^{ds} were investigated in their uptake efficiency in brain endothelial cells.

Three dose groups (illustrated in figure 3.10) were prepared to compare the transport rate of NP-DNA-20^{ds} compared with NP-DNA-40^{ds} on D3 cells. These groups contained excess free DNA and gold nanoparticles in the mixture.

1) **Control – NP-Gal**

2) **NP-DNA-20^{ds}**

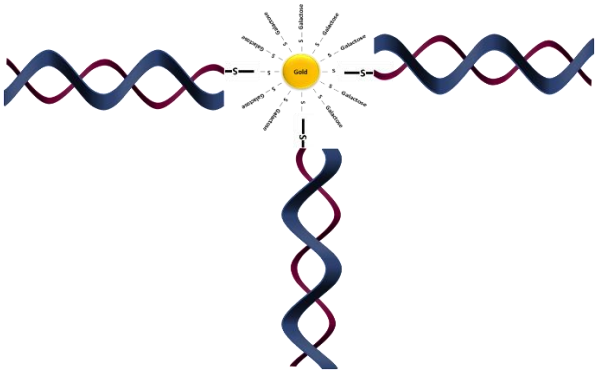

3) **NP-DNA-40^{ds}**

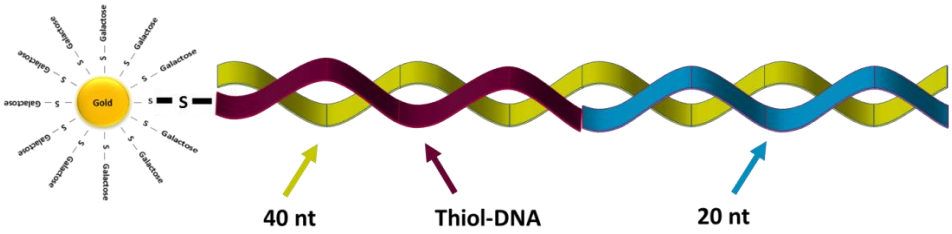

Figure 3.10 *Illustrative images for NP-Gal, NP-DNA-20ds and NP-DNA-40ds; the images are diagrammatic (heterogeneous with respect to how many DNA molecules were attached and not to scale).*

The cellular uptake of NP-DNA-20^{ds} compared withNP-DNA-40^{ds} into brain endothelial cells is shown in Figure 3.11 and Figure 3.12 Nanoparticles were quantified in the cytosol, vesicles, nucleus, and at the basal membrane (under-cell). As a control, we used NP-Gal with no DNA attached. There was a statistically significant increase in cell uptake of NP-DNA-40^{ds} compared to both NP-Gal and NP-DNA-20^{ds}. The NP-DNA-40^{ds} nanoparticles showed almost three times more cell uptake in cellular vesicles. Since the amounts of nanoparticles observed at the basal membrane (under-cell) was higher, it is possible that the nanoparticles were more likely crossing through the cells in comparison with the NP-Gal and NP-DNA-20^{ds}.

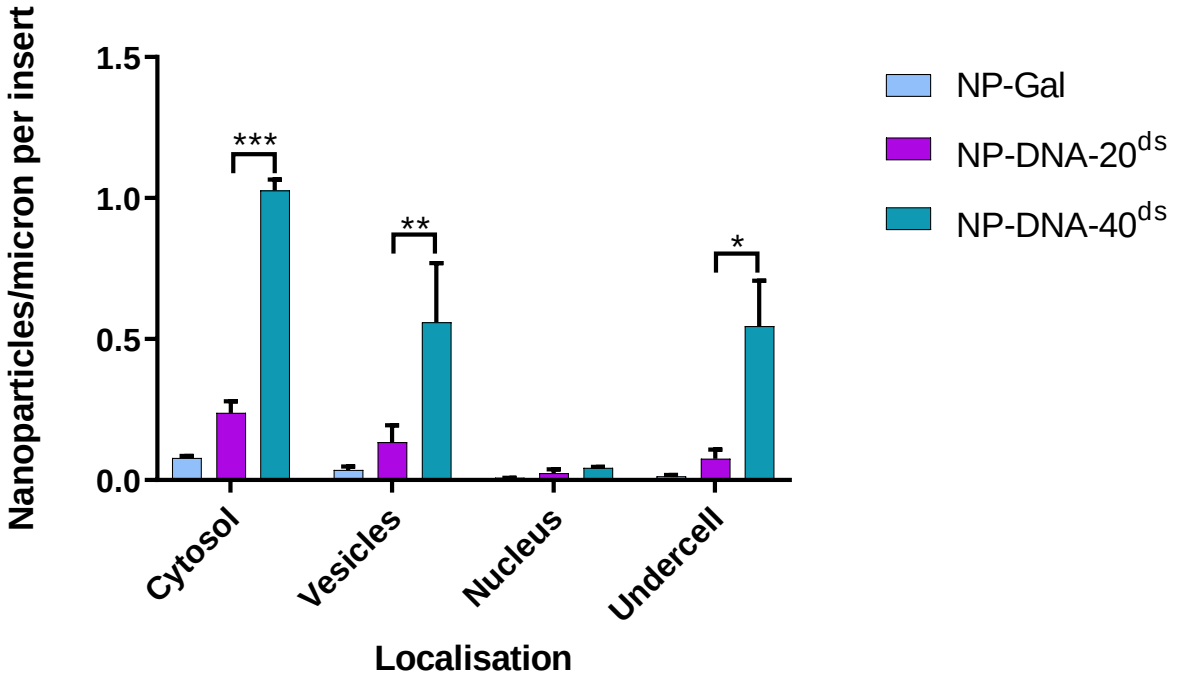

Figure 3.11 *Comparison of uptake of NP-DNA-20^{ds} and NP-DNA-40^{ds} into brain endothelial cells. Nanoparticles were quantified in the cell cytosol, vesicles, nucleus, and at the basal membrane (under-cell). NP-Gal was the nanoparticle control, no DNA attached. Three experiments were performed, each experiment having three technical repeats. Tukey's multiple comparisons test showed significant difference for NP-DNA-40^{ds} compared to NP-DNA-20^{ds} in cytosol (p-value: 0.0003), vesicles (p-value: 0.0082) and under cell (p-value: 0.0108).*

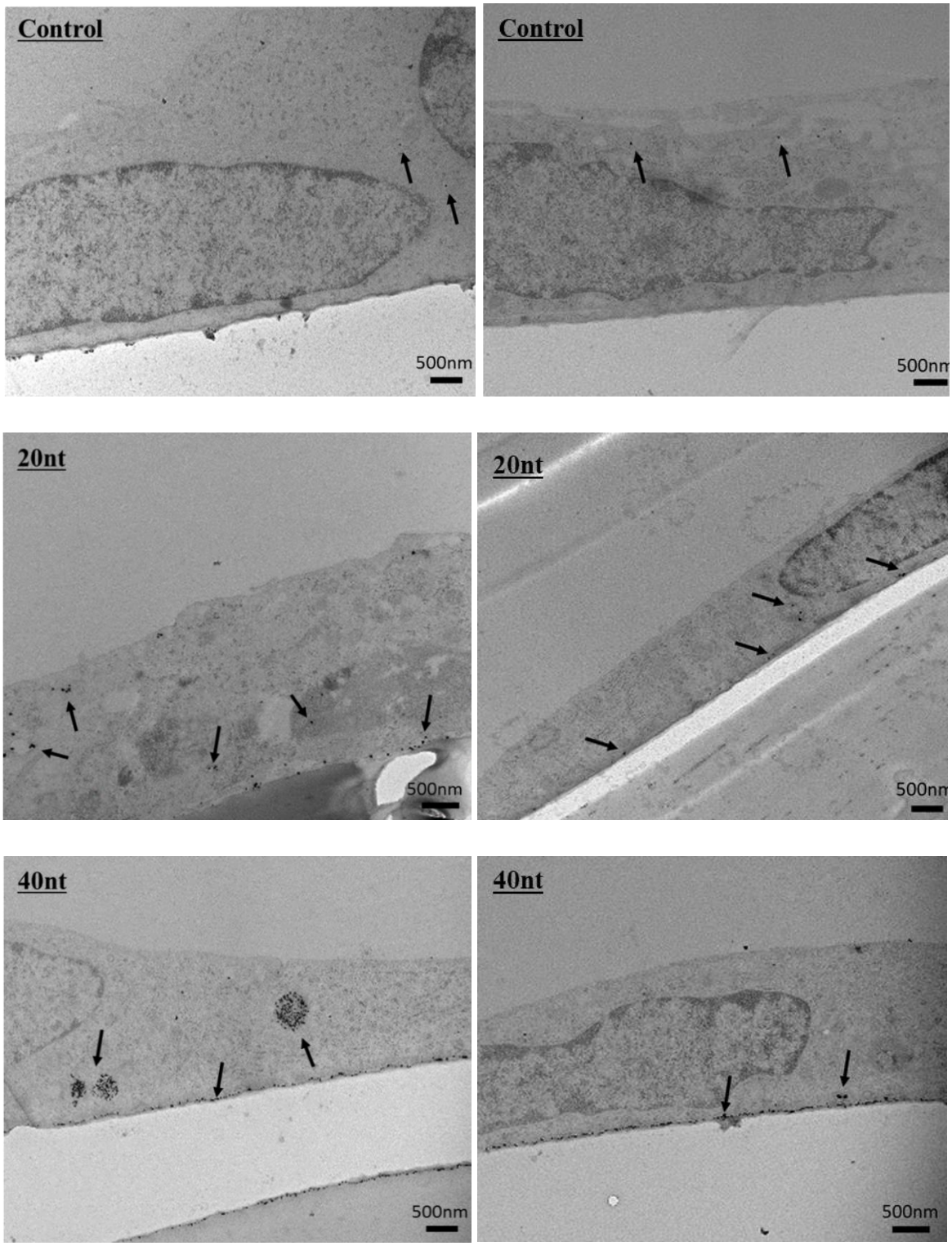

Figure 3.12 *Electron micrographs of DNA-attached gold nanoparticles of various nucleotide lengths on hCMEC/D3 cell line. Many nanoparticles were observed in vesicles and crossing through the cell for the NP-DNA-40^{ds} (40nt) compared to NP-DNA-20^{ds} (20nt) and NP-Gal (Control). The arrows point towards gold nanoparticles.*

3.3 Summary/Discussion

For effective brain drug delivery, we used galactose coated gold nanoparticles with a 2nm gold core as nanocarriers of DNA into brain endothelial cells. DNA coated gold nanoparticles were synthesized by place exchange reaction, a simple method to attach DNA onto gold nanoparticles. The thiol DNA attaches covalently to the nanoparticle coated with thiol galactose ligands, releasing the galactose ligand in exchange. We found that molar ratio of 14:1 (DNA: NP) with an incubation time of 48 hours, flushed with nitrogen gas, and incubated at 37 °C were the optimal conditions to coat nanoparticles with maximum number of DNA molecules.

To assess the effectiveness of the reaction, EMSA gel filtration was used. It effectively separated nanoparticles with different densities of DNA molecules. Six different bands were observed on EMSA, which possibly demonstrated that up to 6 DNA molecules attached per nanoparticle. However, it is not proven that the equally-spaced EMSA bands correspond to 1, 2, 3, 4, 5 and 6 DNA molecules attached to each nanoparticle. As EMSA is a novel technique for detection of DNA attached to gold nanoparticles, no NP-DNA standards were available to compare our samples.

After preparing DNA attached gold nanoparticles with 20nt or 40nt long DNAs were assessed for their cellular uptake efficiency across human brain endothelial cells (hCMEC/d3). We examined the difference in uptake ofNP-DNA-20^{ss} compared to NP-DNA-40^{ds} and of the NP-DNA-20^{ds} to NP-DNA-40^{ds}.Nanoparticle cell uptake assays for NP-DNA-20^{ds} showed significantly higher vesicular transport compared to NP-DNA-20^{ss}. In comparison to the control uncoated nanoparticles, NP-Gal, NP-DNA-20^{ss} had significantly higher vesicular transport.

When comparing double-stranded version on DNA-coated nanoparticles, the more negatively-charged nanoparticles (40nt) had significantly higher uptake efficiency in both cytosolic and vesicular localisations. Furthermore, more nanoparticles were observed at the basal membrane for NP-DNA-40^{ds}. This may mean that a higher number of nanoparticles was crossing the cell from the apical side (blood) compared with NP-DNA-20^{ds} and the uncoated NP-Gal. Additionaly, from the electron micrographs of NPs uptake experiments, one may question that the NPs may just remain attach to the collagen coated trans-well and not pass through to the basal side into the medium. Due to set up of our experiment it was not possible to test the basal side media on TEM, as only fixed cells were possible to image. Therefore, in chapter 6; experiments were performed for detection of DNA on the

other side of the trans-well membrane (in basal media) using quantitative PCR. The movement of free 40nt dsDNA and 40nt dsDNA attached NPs was tested across the trans-well system. Chapter 6 experiment of DNA movement is a good evidence of transcellular migration as it shows that the gold nanoparticles seen on the basal side of cells did not remained attached to the collagen-coated trans-well membrane (as seen on the electron micrographs) but to passed through into the basal side media.

Overall, we found that pre-fractionated (crude) mixture of larger (in size due to more nucleotides) and negatively-charged DNA attached nanoparticles had increased cellular uptake in human brain endothelial cells when compared with uncoated nanoparticles.

A possible way our DNA attached nanoparticles may have crossed brain endothelial cells is via adsorptive-mediated transcytosis. The adsorptive-mediated transcytosis involves binding of the proteins (by electrostatic interaction with the luminal surface of the endothelium) to the endothelial cell surface to cross the endothelium. Charge is a key parameter of NPs known to influence their cellular uptake as well as cytotoxicity (Hühn et al, 2013). For example, Cho et al, 2017 reported that the uptake rate of cationic gold nanoparticles into the SK-BR-3 cell line was fivefold higher than their anionic counterparts. The authors also explained that half of the cationic gold nanoparticles diffuse into cells by non-endocytosis pathways. This may occur by creating holes or other disruptions in the plasma membrane. In contrast, anionic and neutral gold nanoparticles are internalized into cells only via endocytosis pathways. Additionally, an alternative cell uptake assay of charged gold nanoparticles coated with galactose/PEG-amine was completed in our group (Gromnicova et al., 2014). I confirmed in my own observations that positively charged gold nanoparticles coated with galactose/PEG-amine had higher cell uptake in both the cytosol and vesicles compared to only galactose nanoparticles. The uptake of positively charged nanoparticles may be promoted because the positive charge of nanoparticles may have interacted with endothelial cells negative surface charge (negative surface charge due to glycocalyx; a negatively charged layer that covers the luminal surface of endothelial cells). Behzadi et al, 2017 also pointed out that electrostatic interaction between charged nanoparticles and the cell membrane is of great importance. Their study showed the adhesion of positively charged nanoparticles to the cell membrane which may promote membrane-wrapping phenomena. A fully membrane-wrapped nanoparticle does not easily detach from the cell membrane and has more chances of entering the cell. Likewise the positively charged nanoparticle, perhaps our negatively charged nanoparticles may have been attracted towards positive proteins found on the

endothelial cells that may have helped to facilitate their uptake, though this area still needs thorough investigation; of how the negative charge interacts with endothelium cell surface proteins.

Furthermore, from electron micrographs we observed that our gold nanoparticles coated with more DNA molecules appeared to have a tendency for active vesicular pathway rather than the passive cytosolic pathway. Size may also be key to determine the uptake pathway of the nanoparticles. Chithrani et al, 2006 investigated gold nanoparticle size and its effect on the transcellular pathway on many different cell lines. In their study, 40nm gold nanoparticles were taken up via active cellular pathway, whereas 2 nm gold nanoparticles used passive pathway to enter cells. For future studies it would be useful to test the "active" pathway by additional experiments of nanoparticles transport in cells using temperature dependant experiments such as 4 °C vs 37 °C.

Nonetheless, there are various other factors apart from the size or charge, which may have affected the uptake efficiency of the DNA attached nanoparticles that we observed. Such factors may be that having more or longer DNA around nanoparticle increases the overall nanoparticle radius, causing the DNA to wrap around the nanoparticle completely. Smith et al, 2007 theoretically showed that a fully membrane-wrapped nanoparticle does not easily detach from the cell membrane and, therefore, has more chances of entering the cell. To explain the difference in uptake of our single stranded versus double-stranded DNA attached to nanoparticles, it is possible that ssDNA rearranges itself around the gold core differently than dsDNA. As dsDNA or 40nt dsDNA has a negatively charged compared to the ssDNA and 20nt DNA, it might rearrange to be as far apart from other strands of DNA as possible due to the negative charge repulsion.

Moreover, as our investigation included a mixture of nanoparticles with attached DNA along with free DNA and uncoated nanoparticles, it was not clear whether the gold nanoparticles we detected via electron microscopy were indeed DNA-coated. Therefore, from these observations, we decided to remove the unreacted free DNA and uncoated nanoparticles from the mixture.

4 FRACTIONATION OF REACTION MIXTURE OF NP-DNA-40 AND ITS UPTAKE EFFICIENCY ON 3D CO-CULTURE MODEL OF THE BLOOD BRAIN BARRIER.

Aims

1. To isolate NP-DNA-40^{ds} with different numbers of 40nt DNA molecules attached to each nanoparticle using FPLC.
2. Next, to assess their uptake efficiency into brain endothelial cells and astrocytes, using the co-culture model of the BBB.

4.1 Introduction

In the previous chapter, we compared the uptake efficiency of NP-DNA-20^{ss} with NP-DNA-20^{ds} and NP-DNA-20^{ds} with NP-DNA-40^{ds}. All the nanoparticle formulations were a mixture of free (unbound) DNA and gold nanoparticles along with nanoparticles coated with DNA. Therefore, to minimise other factors that could affect the uptake of nanoparticles on the cells, it was essential to remove the unreacted free DNA and nanoparticles from the mixture.

For this purpose, we used FPLC (fast protein liquid chromatography) to remove unreacted nanoparticles and unreacted DNA. FPLC provides a high-resolution characterisation and separation of protein (and our DNA-coated nanoparticles) by small-diameter microbeads. Smaller size molecules elute last as they enter inside the microbeads and travel slower. Larger size molecules elute first as they travel faster because they do not enter the microbeads (Madadlou et al, 2011). This technique also allowed us to separate DNA-coated nanoparticles of different sizes by collecting different fractions.

4.2 Results

4.2.1 FPLC (fast protein liquid chromatography) separation of nanoparticle mixture (fractionation)

We decided to use NP-DNA-40 for all further in vitro and in vivo studies because of its higher cellular uptake into brain endothelial cells compared with NP-DNA-20^{ds}. Moreover, using NP-DNA-40 allowed us to amplify 40nt DNA by qPCR and detect DNA in cells. Chapter 6 describes in detail the results of how much DNA can be transported across the endothelial cells in vitro.

However, we came across difficulties when resolving the nanoparticle formulation of NP-DNA-40^{ds}. During separation, the column reached its limit of separating large molecules and it made it difficult to distinguish different sizes of molecules (peaks). Hence, we decided to separate NP-DNA-20^{ss} formulation instead (as shown in Figure 4.1), which our FPLC column separated easily. We then pooled selected fractions together before extending the attached DNA molecule from 20nt to 40nt.

Therefore, we prepared NP-DNA-40 of different DNA densities (low and high density) following these steps:

1. Fractionate NP-DNA-20^{ss} (Figure 4.1)
2. Pool selected fractions to make nanoparticle formulations with high and low DNA density
3. Extend attached DNA molecule to form NP-DNA-40^{ds} by hybridisation
4. Fractionate again the NP-DNA-40^{ds} mixture to remove unreacted DNA.

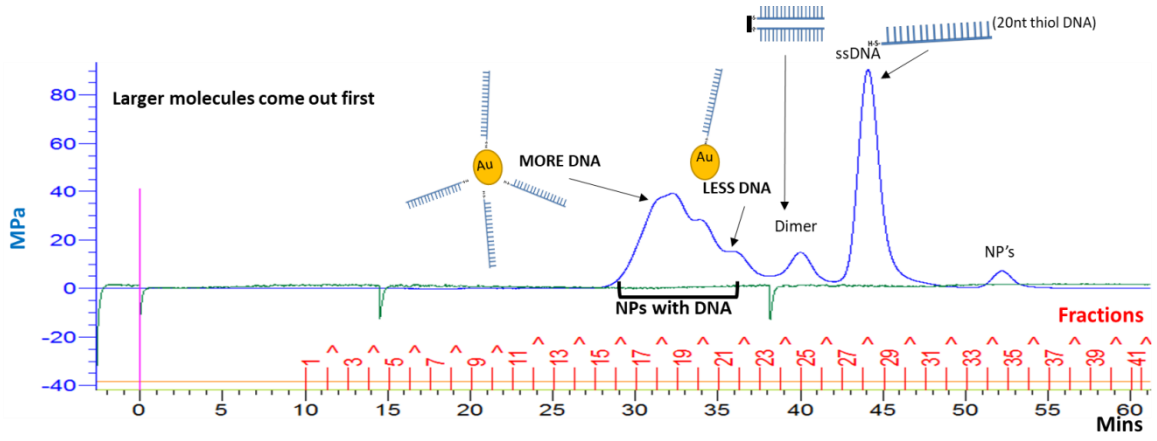

Figure 4.1 *FPLC trace of NP-Gal with 20nt Thiol DNA place exchange reaction. Numbers in red show the fraction number at which the different size molecules were eluted. The elution volume; 0.5ml at flow rate of 0.4 ml/min. All drawings on top of peaks (DNA molecules or NP-DNA molecules) are illustrative for explanation purposes only.*

In order to confirm whether the nanoparticle peaks (in figure 4.1) detected by FPLC corresponded to nanoparticles with an increasing number of 20nt DNA molecules attached on each nanoparticle, EMSA was performed (as described in chapter 3). Figure 4.2 shows free DNA in fraction 28 and 29 with no bands showing higher up the gel, confirming that it does not contain any nanoparticles. Similarly, no bands of NP-DNA were observed in fraction 25 and 26. Dimerised DNA was observed in fraction 25 and 26. Fraction 15, 16, 17, 18, 19 and 20 showed bands at the top of the gel confirming that those fractions contained nanoparticles with DNA molecules attached. The more DNA molecules attached to each nanoparticle, the larger it would be and hence would move slower on the EMSA gel. We observed at least 6 separate bands on the gel, demonstrating that perhaps we had up to 6 different formulations of DNA coated nanoparticles.

To create nanoparticle formulations with high and low DNA density, we decided to pool some of these fractions together. Fractions 19 and 20 lacked the upper bands, hence were pooled to make a formulation of nanoparticles with low density DNAs attached. Fractions 15 and 16 lacked the lower 3 bands while fraction 17 lacked the lower 2 bands, hence were all pooled together to form formulation of nanoparticles with high density DNAs attached. Fraction 18 contained some of each bands and therefore was not used in the above pools.

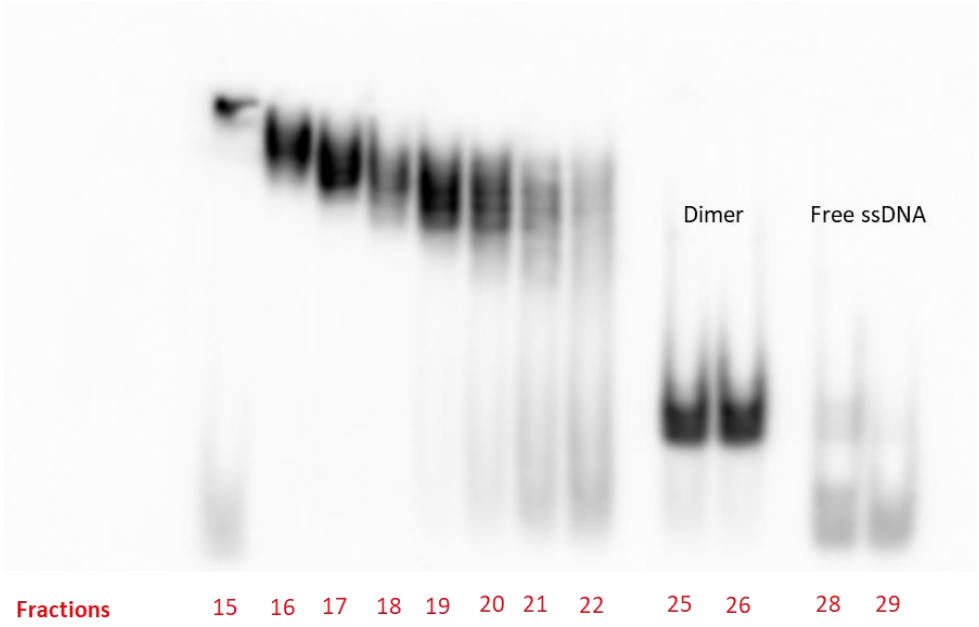

Figure 4.2 *EMSA on a 6% gel was performed to investigate whether the nanoparticle peaks eluted at different fractions detected by FPLC corresponded to nanoparticles with increasing number of DNA molecules attached. Numbers in red are fraction numbers corresponding to Figure 4.1. One time large batch of NP-DNA-40^{LO} and NP-DNA-40^{HI} was prepared and used for cytotoxicity tests, in vitro uptake comparison on the brain endothelial cells and in vivo experiments.*

Next, we extended 20nt single-stranded DNA attached on the nanoparticles into a 40nt double-stranded DNA. The reaction mixture was fractionated again to remove unreacted 40nt and 20nt DNA, as illustrated in figure 4.3a (low-density DNA nanoparticle formulation NP-DNA-40^{LO}) and figure 4.3b (high-density DNA nanoparticle formulation NP-DNA-40^{HI}). The hybridisation and extension of 40nt DNA was successful as the NP-DNA-40 eluted out earlier at fraction 11 rather than fraction 15 (for 20nt DNA). Free 40nt and 20nt peaks were observed on fraction 24/25 (for 40nt) and fraction 29/30 (for 20nt), as expected.

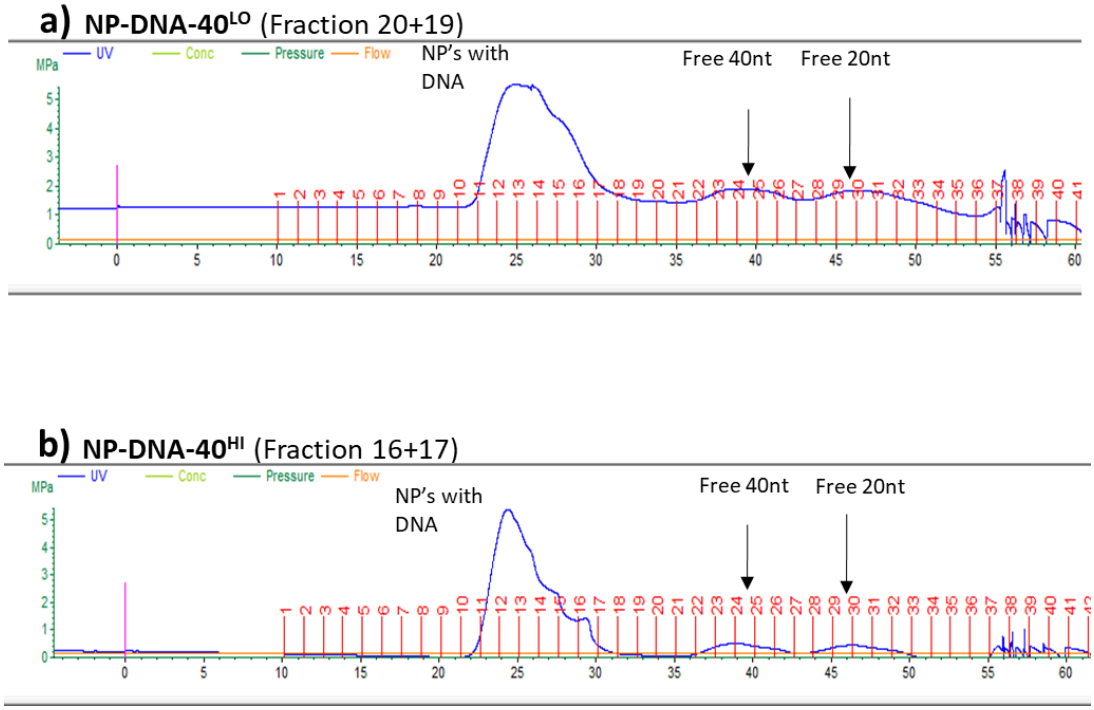

Figure 4.3 *(a) NP-DNA-40^{LO} and (b) NP-DNA-40^{HI}. FPLC fractionation performed to remove excess 40nt and 20nt DNA after hybridisation reaction to create 40nt long dsDNA attached onto the nanoparticles. NP-DNA-40^{LO} has a broader peak than NP-DNA-40^{HI} because of different volumes of NP-DNA-40^{ds} used in fractionation column. We had more of NP-DNA-40^{HI} as three fraction (Fraction: 15, 16 and 17 having 1.5 ml of total sample) were pooled compared to NP-DNA-40^{LO} (Fraction: 19 and 20 having 1ml of total sample).*

To conclude, we prepared two formulations of 40nt DNA attached nanoparticles;

- NP-DNA-40^{LO} – low-density DNA formulation with fewer 40nt DNA molecules attached on each nanoparticle (I.e. probably 1 or 2 strands of 40nt DNA to each nanoparticle)*
- NP-DNA-40^{HI}- high density DNA formulation with more 40nt DNA molecules attached on each nanoparticle (I.e. probably 4-5 strands of 40nt DNA to each nanoparticle)*

[* We hypothesized that the equally-spaced EMSA bands corresponded to 1, 2, 3, 4 and 5 DNA molecules attached to the NP. However, as this is a novel technique, no NP-DNA standards were available to compare with the samples prepared here.]

All the above formulations were free of unreacted DNA and nanoparticles.

4.2.2 Hydrodynamic diameter of DNA-nanoparticles

Hydrodynamic diameter of proteins with known molecular weight was annotated by FPLC to generate standard curve from proteins elution volume (Figure 4.4). To get the hydrodynamic diameter of the nanoparticles, elution volumes by FPLC of each of the nanoparticles were interpolated with the protein standard curve and molecular weights were read off. Once the molecular weights were known, they were converted to nm to get the hydrodynamic diameter value in a nm for a spherical molecule of that particular molecular weight. But to bear in mind our DNA coated nanoparticles are different from globular proteins. The hydrodynamic diameter of different density DNA coated nanoparticles are summarised in table 4.1. NP-DNA-40^{LO} (+1x40nt +2x40nt) has a hydrodynamic diameter of 7.5nm and NP-DNA-40^{HI} (+3x40nt + 4x40nt) has a hydrodynamic diameter of 7.6nm. NP-Gal as expected has hydrodynamic diameter of 1.8nm while, 20nt DNA coated nanoparticles had hydrodynamic diameter ranging from 3nm to 4nm depending on different numbers of DNA strands attached.

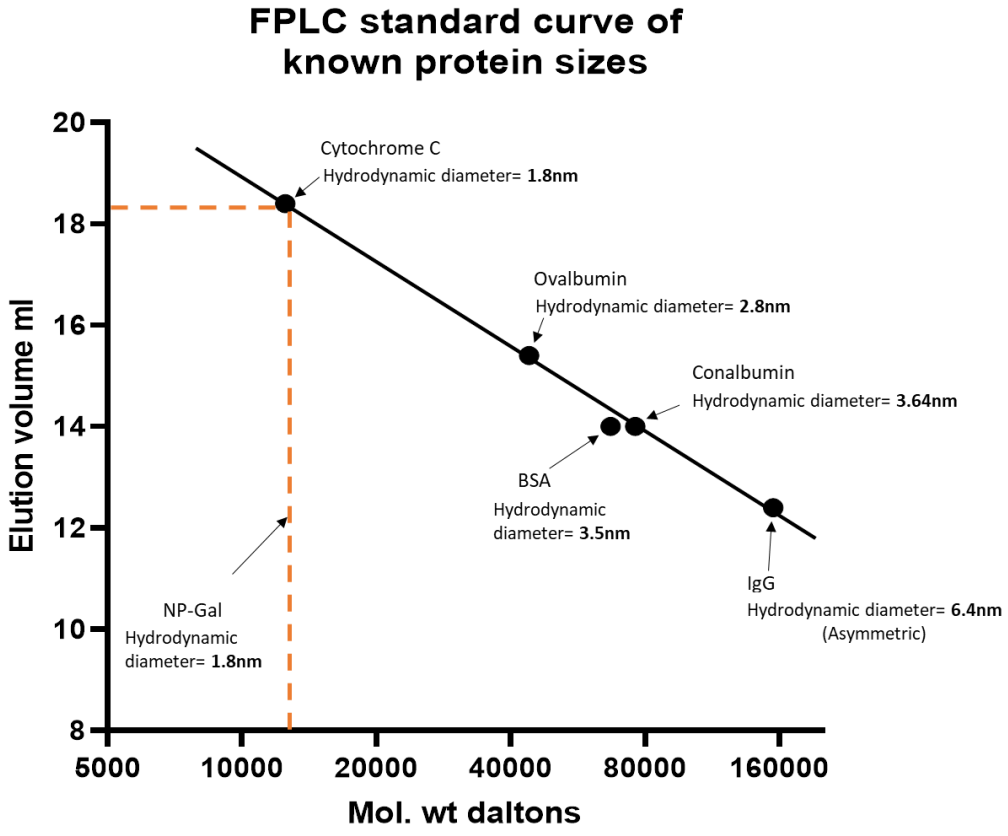

Figure 4.4 *Standard curve of globular proteins (with known molecular weight) annotated by FPLC to get elution volumes.*

Table 4.1 Hydrodynamic diameter of NP-Gal and DNA coated nanoparticles. +1x40nt – refers to nanoparticle with 1 strand DNA.

Particle	Hydrodynamic diameter (nm)		
NP-Gal	1.8		
+ 1x20nt	3.1	**+1x40nt**	7.5
+ 2x20nt	3.6	**+2x40nt**	7.5
+ 3x20nt	3.8	**+3x40nt**	7.6
+ 4x20nt	4.0	**+4x40nt**	7.6

4.2.3 Cytotoxicity of DNA-coated nanoparticles on brain endothelial cells

To investigate cytotoxicity of the NP-Gal, NP-DNA-40^{LO} and NP-DNA-40^{HI}, Alamar blue assay was used. Alamar Blue uses resazurin as an oxidation-reduction (REDOX) indicator where a colour change is formed in response to cellular metabolic reduction. The reduced form of Alamar blue is pink and highly fluorescent, meaning that more living/respiring cells will produce a bright pink colour change from the blue (O'Brien J et al, 2003).

We tested the effect of different concentrations (8µg/ml, 16µg/ml, 32µg/ml and 50µg/ml) of the three nanoparticles formulations on viability of brain endothelial cells at 24hrs. We found no reduction of cell viability on exposure to concentrations of 8µg/ml, 16µg/ml and 32µg/ml for NP-DNA-40^{LO}, NP-DNA-40^{HI} and NP-Gal for up to 24 hours (figure 4.5). At a concentration of 50µg/ml, NP-Gal and NP-DNA-40^{LO} showed low cytotoxicity, whereas, NP-DNA-40^{HI} showed no cytotoxicity at 50µg/ml. It is possible that cells exposed to higher concentration of the nanoparticles will take up and transport higher number of nanoparticles across the cell. This may cause large quantities of nanoparticles gathering at the bottom of the well underneath the cell, perhaps causing it to detach and die.

Since all our experiments of nanoparticle uptake assays were performed using concentration of 8µg/ml, and for 3 hours, we can conclude that such dose was not cytotoxic for hCMEC/D3 cells.

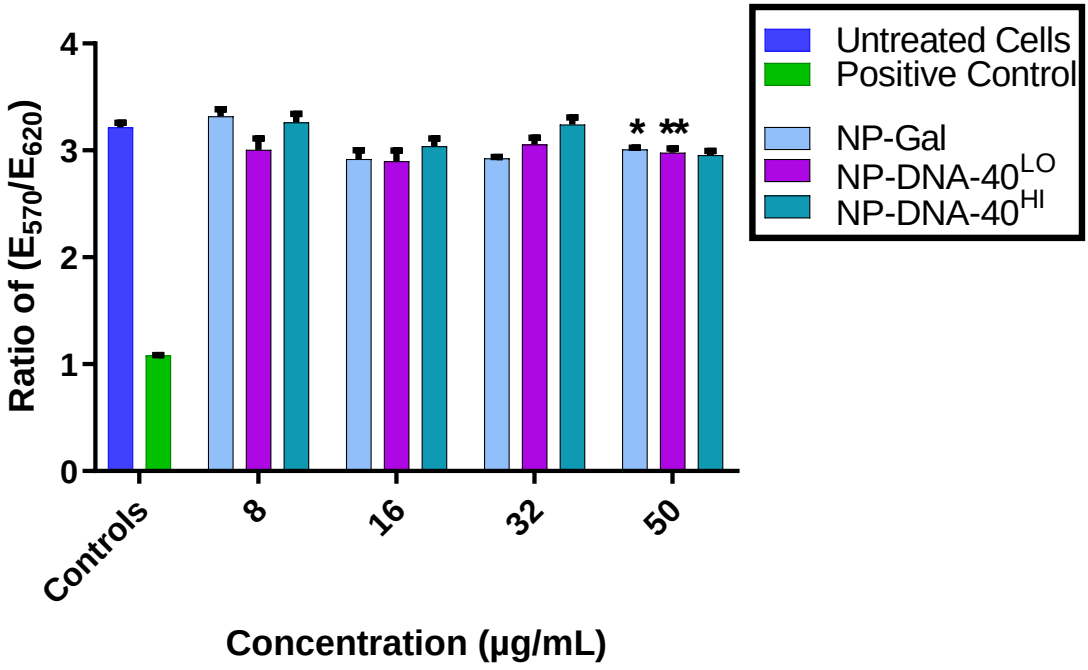

Figure 4.5 *hCMEC/D3 cell viability measured by Alamar blue assay when exposed to 8, 16, 32 and 50 µg/mL of NP-DNA-40^{LO}, NP-DNA-40^{HI} and NP-Gal for 24 hours (n=3). Positive control of cell death is 30 µg/ml digitonin (30 min treatment). Notes: Data are shown as ratio of E570 (reduced form) /E620 (oxidised form) which represents the maximum cell viability. Tukey's multiple comparisons test showed significant difference for NP-Gal and NP-DNA-40^{LO} applied at 50 µg/mL (p-value: * 0.026, **0.0084.*

4.2.4 Uptake comparison of fractionated NP-DNA-40^{LO} and NP-DNA-40^{HI} on the brain endothelial cells

We assessed uptake efficiency of nanoparticle formulations of NP-DNA-40^{LO} and NP-DNA-40^{HI} on brain endothelial cells in 2D cultures, as well as in 3D co-cultures with human primary astrocytes. As mentioned in chapter 2 the nanoparticles were used at concentrations of 8 µg/ml incubated for 3 hours at 37 °C for cell studies unless described otherwise.

4.2.4.1 Uptake comparison on the 2D model of the blood-brain barrier

We found that there were significantly higher numbers of NP-DNA-40^{LO} nanoparticles in cytosol, vesicles and at the basal membrane (Figure 4.6) compared to NP-DNA-40^{HI} and

NP-Gal. NP-DNA-40^{HI} showed higher numbers of nanoparticles in vesicles compared to both the NP-DNA-40^{LO} and NP-Gal.

Overall, both formulations of NP-DNA-40^{LO} and NP-DNA-40^{HI} had higher uptake efficiency and appeared more likely at the basal membrane of the endothelium compared to uncoated NPs, NP-Gal.

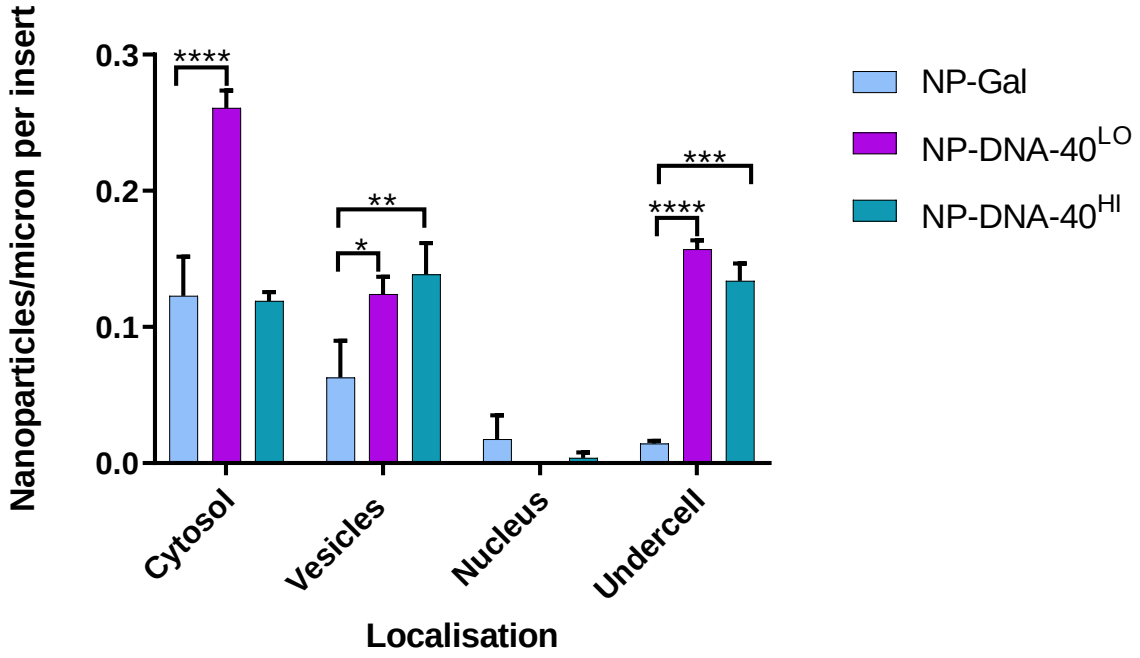

Figure 4.6 *Uptake efficiency of NP-DNA-40^{LO} and NP-DNA-40^{HI} compared with NP-Gal in the brain endothelial cells grown on trans-well inserts (2D BBB model). Nanoparticles were applied at a concentration of 8µg/ml for 3 hours, after which time cultures were prepared as described previously for TEM analysis. Nanoparticles were quantified in cell cytosol, vesicles, in nucleus and at the basal membrane ("undercell"). Three experiments were performed, each individual experiment having three technical repeats. Tukey's multiple comparisons test showed significant difference for NP-DNA-40^{LO} cytosol, vesicles and "undercell" compared to NP-Gal (p-value: * 0.0327, ****<0.0001) and for NP-DNA-40^{HI} vesicles and "undercell" compared to NP-Gal (p-value: **0.01, ***0.0003).*

4.2.4.2 Uptake comparison on 3D co-cultures of the blood-brain barrier

We used co-cultures of endothelial cells grown on astrocytes in a collagen gel as a 3D model of the BBB to assess the nanoparticle uptake by counting cells per astrocyte. We found higher number of NP-Gal nanoparticles in cytosol of astrocytes as compared to NP-

DNA-40^{LO} and NP-DNA-40^{HI} (Figure 4.7). Similar numbers of nanoparticles were observed in vesicles of astrocytes for all three nanoparticles formulations.

Next, we calculated the density of nanoparticles in brain endothelial cells, astrocytes and collagen from electron micrographs with corresponding dimensions of ultrathin sections. Calculating the number of nanoparticles within a known volume provides a true representation of how many nanoparticles were transported across the endothelium and into the astrocytes and collagen. The results represented in in figure 4.8 shows statistically higher numbers of nanoparticles in collagen for NP-DNA-40^{HI} compared to the NP-DNA-40^{LO} and NP-Gal. Fewer nanoparticles were observed in astrocytes and brain endothelial cells compared to collagen for all three NPs formulations (illustrated in figure 4.9).

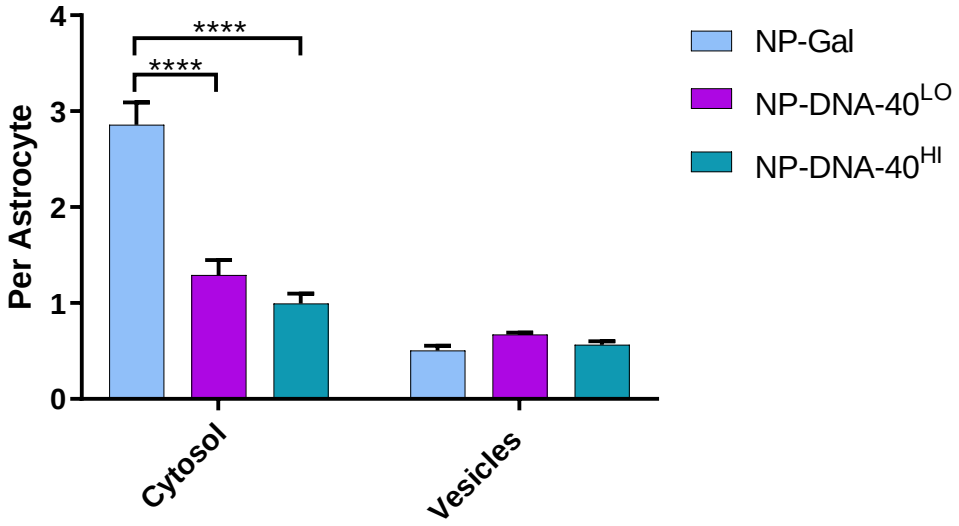

Figure 4.7 *Number of nanoparticles observed in each astrocyte for NP-DNA-40^{LO} and NP-DNA-40^{HI} compared with NP-Gal. Three experiments were performed, each individual experiment having three technical repeats. Tukey's multiple comparisons test showed significant difference for NP-Gal compared to NP-DNA-40^{LO} and NP-DNA-40^{HI} (p-value: **** <0.0001).*

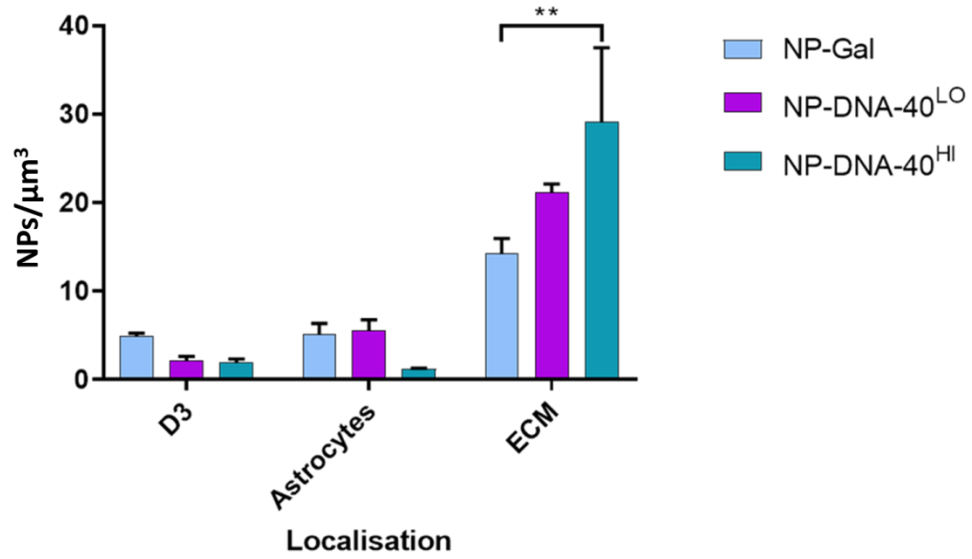

Figure 4.8 *Uptake efficiency of NP-DNA-40^{LO} and NP-DNA-40^{HI} compared with NP-Gal in the brain endothelial cells, astrocytes and in the gel (ECM). Three experiments were performed, each individual experiment having three technical repeats. Tukey's multiple comparisons test showed significant difference for NP-DNA-40^{HI} compared to NP-Gal (p-value: **0.4595).*

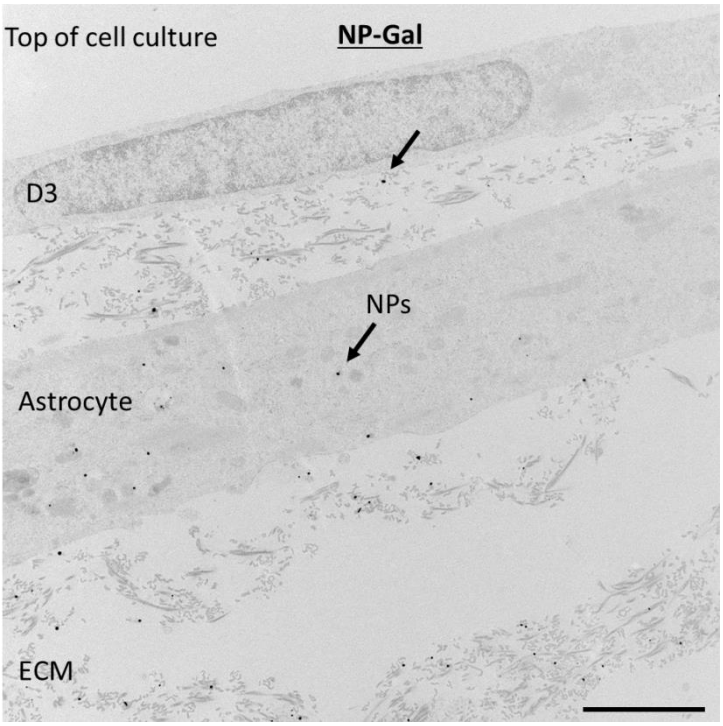

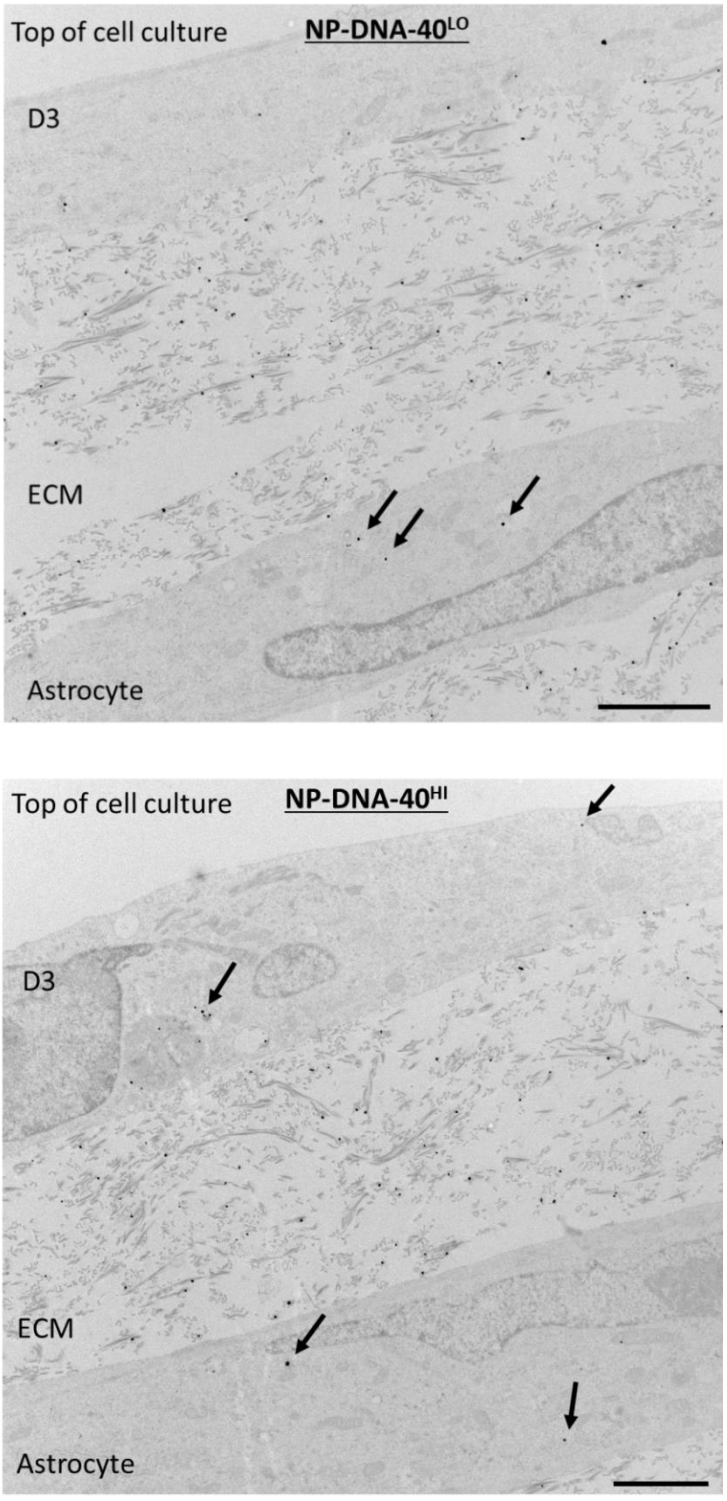

Figure 4.9 *Uptake assay of NP-DNA-40^{LO}, NP-DNA-40^{HI} and NP-Gal with 3D co-culture model of BBB. Brain endothelial cells cultured on top of a collagen hydrogel embedded with astrocytes. Silver-enhanced gold nanoparticles (arrows) present in brain endothelial cells hCMEC/D3, astrocytes and within a collagen gel (ECM). A representative image from three independent experiments is shown, scale bar 2.0 µm.*

4.3 Summary and discussion

In this chapter, we used FPLC as a method to prepare nanoparticle formulations with different densities of 40nt dsDNA molecules attached to each nanoparticle: low-density nanoparticles (NP-DNA-40^{LO}), and high-density nanoparticles (NP-DNA-40^{HI}). We used FPLC because the system is quite advanced with high level of automation which provides number of benefits such as; separating different DNA density nanoparticles automatically without the need for user intervention during the run. It allows automated collection of different DNA density nanoparticles in choice of tubes and in desired volumes while providing inline detection that helps in making informed decisions, for example, when the column has become equilibrated, when to collect fractions. Other separation method available for the fractionating nanoparticles includes electrophoresis (gel or capillary). It has the advantage of low consumption of sample and reagents. Nevertheless, nanoparticles sample collection by electrophoresis is more challenging (Wei and Lie, 1999).

The nanoparticle formulations prepared by FPLC were investigated for their uptake efficiency compared to control nanoparticles (NP-Gal) into and across brain endothelial cells on 2D and 3D models of BBB.

2D transwell BBB models provides an ease of establishing cultures at low cost making it very desirable to be used in various research settings (Cucullo et al. 2008). However, there are substantial limitations to the 2D trans-well models that need to be taken into consideration. For example, the lack of a three-dimensional structure present in vivo; lack of endothelial exposure to physiological shear stress which limits the differentiation of the endothelium into a BBB phenotype (Cuculloet al, 2011). Hence, the cells may be presented with reduced polarized transport, relative low trans-endothelial electrical resistance (TEER) when compared to the BBB in vivo (e.g. isolated brain microcapillaries) and corresponding high paracellular permeability to hydrophilic substances (Gastfriend et al, 2018). Sreekanthreddy et al, 2012 have shown that the junctional tightness of the hCMEC/D3 model may be improved by co-culturing them with astrocytes into a 3D model.

Uptake comparison experiments showed both nanoparticle formulations NP-DNA-40^{LO} and NP-DNA-40^{HI} had higher uptake efficiency and appeared more likely at the basal membrane of the endothelium compared to uncoated NP-Gal. Theoretically, endocytosis of nanoparticles mainly occurs by passive transfer (cytosolic) across the cell membrane into

the cytoplasm or by active endocytosis into vesicles (as observed on the electron micrographs in chapter 3).

Our uptake experiments showed that the route of uptake might be affected by the density of DNA molecules attached on each nanoparticle. The subcellular localization indicated that NP-DNA-40^{LO} used preferentially cytosolic pathway to enter brain endothelial cell, whereas NP-DNA-40^{HI} was entering the cells via vesicular pathways. Both NP-DNA-40^{LO} and NP-DNA-40^{HI} were more effective in using vesicular pathway to enter and perhaps cross the brain endothelial cells and enter the astrocytes compared to NP- Gal. For future studies it would be beneficial to conduct experiments with different time course for the uptake experiments in order to find more about the mechanism/route and dynamics of different density 40nt DNA-nanoparticles.

Moreover, investigations of toxicity confirmed no toxicity of up to 3x higher concentrations than those used in transport studies, and more than 8x longer nanoparticle incubation times. These nanoparticles are safe to use on brain endothelial cells and may be safe for other cell types and cell lines due to their low toxicity.

5 TISSUE DISTRIBUTION AND INTRACELLULAR LOCALIZATION OF NP-DNA-40 IN RATS

Aim:

The aim of work for this chapter was to assess the tissue distribution and intracellular localization of NP-DNA-40 in rats. The objectives were:

1. To examine the effectiveness of two different nanoparticle administration routes; intravenous and intracarotid injections in rats.
2. To assess uptake of NP-DNA-40^{LO} and NP-DNA-40^{HI} compared to control NP-Gal by mass spectroscopy (ICP-MS) to measure gold concentration in the brain, cerebellum, liver, spleen, kidney, heart and lungs.
3. To examine the intracellular localisation of NP-Gal, NP-DNA-40^{LO} and NP-DNA-40^{HI} in the brain, kidney, liver, and spleen by light and electron microscopy.

5.1 Introduction

The previous chapter examined the uptake of different DNA density nanoparticles (low and high) NP-DNA-40 in a 3D co-culture model of the human BBB *in vitro*. However, the situation *in vivo* may be very different. In this chapter, I explain how route of administration as well as size of gold nanoparticles can affect their tissue distribution.

However, different density NP-DNA-40 have not been administered in rats before and assessed for tissue distribution and intracellular localisation by electron microscopy. Therefore, we investigated whether these different ratios 40nt DNA-nanoparticles enter the brain in vivo and whether we can locate them within the cells of the brain and other organs, making a better correlation with the results observed in vitro.

5.1.1 Route of administration of gold nanoparticles affects tissue distribution

Route of administration can significantly affect bioavailability of nanoparticles by changing the number of biological barriers the nanoparticles face. Currently, there are number of administration routes such as Intra-peritoneal injection which directs nanoparticles into the blood stream following the infusion at the site of administration (Prades et al. 2012; Lasagna-Reeves et al. 2010), orally (Hillyer & Albrecht 2001) as well as esophageally (i.e. by gavage) (Schleh et al. 2012), which result in rather low bioavailability of drug into the brain. Furthermore, routes of administration can affect the tissue distribution profile within an organ. For example, Hirn et al. 2011 demonstrated in his research that 18 nm nanoparticles accumulated in the brain after gavage administration in large quantities in comparison to other sized nanoparticles (1.4 – 200 nm) but when administered via a tail vein injection, these nanoparticles did not show this pattern. Therefore, for delivery to the brain, it is important to choose the correct route of administration in order to increase the maximum bioavailability of DNA-nanoparticles. Previously, gold nanoparticles have been found to enter the brain (Sonavane et al. 2008; De Jong et al. 2008; Sousa et al. 2010; Lasagna-Reeves et al. 2010; Hirn et al. 2011) but in lower quantities in comparison with other organs. Therefore, in this study, two different administration routes were selected to inject nanoparticles to increase the number of nanoparticles entering the brain. Intracarotid injection and intravenous injection were selected to administer 40nt DNA-nanoparticles in rats for the following reasons;

Previously, gold nanoparticles have been found to enter the brain (Sonavane et al. 2008; De Jong et al. 2008; Sousa et al. 2010; Lee et al. 2014; Lasagna-Reeves et al. 2010; Hirn et al. 2011). In our study we compared two different administration routes in an attempt to optimise the chances of nanoparticles entering the brain. Intracarotid injection and intravenous injection were examined for the following reasons;

- **Intracarotid injection (IC)** as a route of administration was mainly selected to replicate the study of Gromnicova et al. 2014 with the addition of 40nt DNA molecules attached to gold nanoparticles. Gromnicova et al. 2014 assessed the uptake of sugar-coated gold nanoparticles (similar to NP-Gal) in the brain and overall tissue distribution. Since our nanoparticles were very similar, we used the same dose, concentration, time of infusion and perfusion/fixation to her methodology.

Intracarotid injection is a promising approach to direct the majority of nanoparticles to the brain (Walczak et al. 2008). It has been shown to provide a rapid and virtually instantaneous high drug concentration in brain vasculature at a fraction of the total systemic dose (Joshi et al. 2008). The full dose enters the brain first before being distributed throughout the body and diluted in blood. As a result, the IC injection can be used as the primary method of drug delivery, increasing the effectiveness of methods for brain selective drug delivery (Joshi et al. 2007). Currently, IC-administered drugs are being used for the treatment of intractable cerebral vasospasm, intracranial malignancies, and ischemic strokes, as well as localizing neurological functions in the brain (Joshi et al. 2017). The disadvantage of administering nanoparticles through IC injection is that a skilled surgical procedure is involved and IC injections may lead to an inconsistent distribution of the drug in the brain (Saris et al. 1988).

- **Intravenous injection (IV)** is one of the most commonly used administration routes for nanoparticle administration directly into the bloodstream (Wiley et al. 2013; Sousa et al. 2010). IV injections are minimally invasive, the response is very rapid, with easily controlled dosage, and veins are insensitive to irritation by irritant drugs at higher concentration. Saxen M, 2016 found that drugs delivered through IV injection circulate directly to the brain within 20 to 40 seconds.

5.1.2 How gold nanoparticle size and charge affect tissue distribution

Gold nanoparticles with different sizes have been widely assessed for tissue distribution. It has been found that small nanoparticles (under 4 nm) are more likely to penetrate cells and tissues (Skotland et al. 2010). For example, Hillyer & Albrecht (2001) showed that orally fed 4 nm gold nanoparticles accumulated in all organs of mice in high amounts, in contrast to 10 nm and 28 nm nanoparticles. Moreover, Schleh et al. (2012) demonstrated that after gavage administration, 1.4 nm gold nanoparticles accumulated in all examined organs of rats in high amounts in comparison to 2.8 nm, 18 nm or 200 nm nanoparticles. This was confirmed by Hirn et al. (2011) who demonstrated correlation of size and retention of gold nanoparticles in tissues after IV administration of gold nanoparticles in rats. In their study, nanoparticles of 1.4 nm had higher tissue accumulation compared to 5 nm nanoparticles.

Therefore, both studies concluded that the smaller the gold nanoparticles, the higher the tissue accumulation.

In addition to the size-dependence properties of nanoparticles, the charge has also been found to influence tissue accumulation of the nanoparticles. Schleh et al. 2014 found that 2.8 nm negatively charged nanoparticles accumulated more in organs than positively-charged ones of the same size. They explained that perhaps negatively charged nanoparticles attract and bind onto positively charged proteins found in plasma, making them more likely to enter tissues. Moreover, 15 nm nanoparticles (Lee et al. 2014) administered intravenously into rats, when charged (carboxyl or amine group giving it a negative or positive charge, respectively) penetrated and accumulated in tissues faster than neutral PEG-ylated nanoparticles.

5.1.3 Function of liver, kidney and spleen

While the focus of this thesis was mainly assessing the gold nanoparticles localisation in brain, it was also important to assess the intracellular localisation of gold nanoparticles in liver, spleen and kidney. Liver and kidney plays important role in removing/clearing foreign material from body meanwhile phagocytic cells in spleen can initiate immune response towards the nanoparticles in order to filter the blood. In order to analyse and understand results of these organs, it's helpful to understand the structure and function of each organ. Functions of liver, kidney and spleen are detailed below.

Liver has many functions in the body, including making proteins, bile production, glycogen synthesis, manufacturing triglycerides and cholesterols, blood-clotting factors, and far most crucial function breaks down and detoxifies substances in the body. Liver helps to break down drugs and medication, including alcohol, and is responsible of breaking down hormones and insulin in the body.

Liver mainly consists of hepatocytes and phagocytic Kupffer cells. Hepatocytes aid the detoxification of blood; as the blood passes through the hepatic portal circulation, the hepatocytes of the liver remove foreign material and many potentially toxic substances from the blood before they can reach the rest of the body. Liver hepatocytes contain

enzymes that can metabolize many of these toxins, such as alcohol and drugs, into their inactive metabolites. The fixed macrophage Kupffer cells in the liver help to maintain the immune system by capturing and digesting bacteria, fungi, parasites, worn-out blood cells, and cellular debris. The Kupffer cells can clean a large volume of blood passing through the hepatic portal system very quickly.

The basic function of the spleen is to initiate immune reactions to blood-borne antigens and to cleanse the blood of foreign material and old or damaged red blood cells. For this purpose, the spleen consists of 2 main compartments, the white and red pulp with an open blood circulation system. The white and red pulps are very different in their architecture, vascular, cellular composition, and organization (summarised below and illustrated in figure 5.1). Also, the spleen is surrounded by a capsule composed of dense irregular fibrous tissue, smooth muscle, and elastic fibres. The fibroelastic tissue of the capsule contains contractile cells called myofibroblasts. These myofibroblasts cells produce weak contractions of the capsule, which helps to discharge the blood stored within the spleen into the circulation. Moreover, the capsule allows the spleen to significantly increase in size when needed and discharge a large amount of blood into circulation for tissues oxygenation (i.e., during physical exercise) (Cesta, M. F, (2006).

Red Pulp

- **Structure** - The red pulp is made up of sinusoids and reticular tissues. The sinusoids are leaky with large irregular venous spaces surrounded by thin endothelial cells. The endothelial cells have no basal lamina. The direct attachment of endothelial cells to the reticular fibers helps to open intercellular gaps making it easier for red and white cells to enter and exit. The reticular tissue in the red pulp comprises many macrophages, lymphocytes, platelets, and polymorphs.
- **Function** - The function of the red pulp (comprising about 80% of splenic tissue) is to filter blood and remove foreign material and damaged erythrocytes. Red pulp also is a storage site for erythrocytes, iron, and platelets.

White pulp

- **Structure - White pulp** contains lymphoid aggregations, mostly lymphocytes, and macrophages which are arranged around the arteries. The lymphocytes are both T (mainly T-helper) and B-cells.
- **Function –** White pulp comprises about 20% of spleen tissue and plays a role in opsonisation of extracellular pathogens.

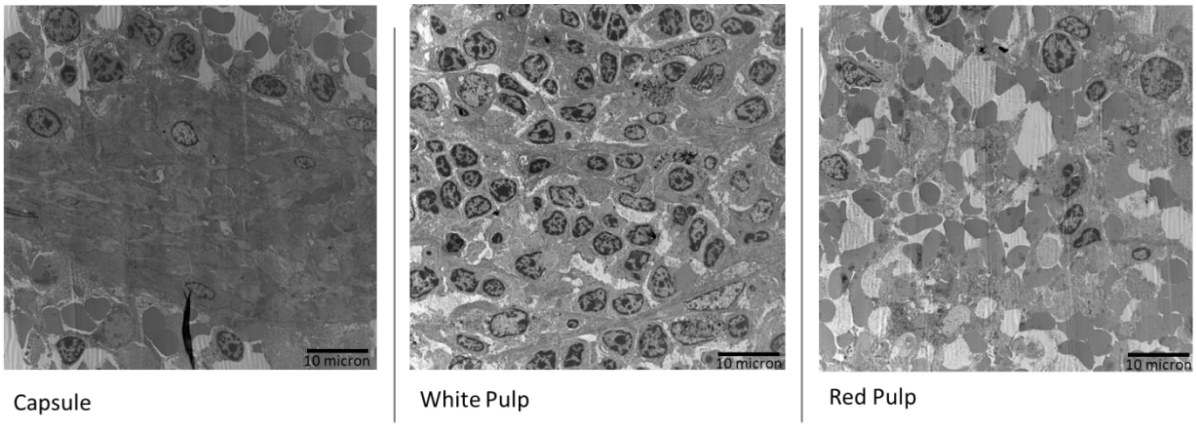

Figure 5.1 *Spleen ultrastructure, elucidating red pulp, white pulp and capsule.*

The function of the kidney is to filter blood and excrete waste products. Renal corpuscles perform the filtration at the end of each kidney nephron; each corpuscle is made up of Bowman's capsule and glomerulus. The glomerulus is surrounded by endothelial cells, basal lamina, and an epithelium layer that consists of podocytes with filtration slits between them. These filtration slits between podocytes have a thin diaphragm that acts as a final filtration barrier before the fluid enters glomerular space (illustrated in figure 5.2). Blood that is about to be filtered enters a glomerulus. The large molecules and waste products are filtered out of the glomerulus, passing from the Bowman's capsule through in turn, the proximal convoluted tubule, the loop of Henle, the distal convoluted tubule, and a series of collecting ducts to form urine.

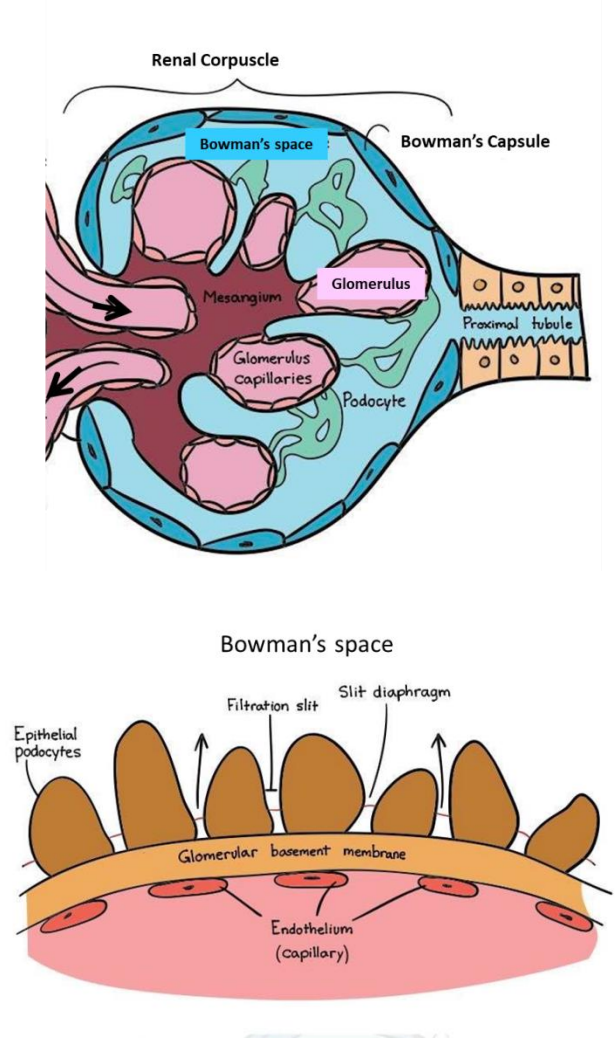

Figure 5.2 *Renal capsule composed of Bowman's capsule and glomerulus (top). Bowmans capsule (bottom). Image obtained from (Khan academy).*

5.2 Results

Our nanoparticles, despite having the same-size gold core (~2 nm), had a various overall size between~2nm to 7.5 nm due to the amount of DNA attached. This might have also affected the overall charge – since we would expect that the more DNA attached the more negative charge. Hence, our hypothesis was that NP-DNA-40^{LO} and NP-DNA-40^{HI} may have different ability to accumulate in different organs, due to the different number of DNA molecules attached to nanoparticles and due to the difference in charge (as previously shown by Hirn et al. 2011; Schleh et al. 2012; Lee et al. 2014). Furthermore, Gromnicova et al, (2014) showed that small gold nanoparticles <5 nm accumulated in kidney. We also set out to analyse gold content in organs such as kidney, liver and spleen.

5.2.1 Intracarotid versus intra-venous administration

The experiments were performed in collaboration with Koc University (Istanbul) by Mehmet Kaya and his colleagues. We used five groups of Wistar Albino male rats, age approx. 3 months (weighing 220-340g); three rats per group were injected.

As it was our first attempt to use intra-venous injection to administer sugar-coated gold nanoparticles with DNA attached, we decided to use minimum number of animals for the IV injection group to reduce cost and limit numbers of animals. Hence, for this study, we decided to not use NP-DNA-40^{LO} for intra-venous injection and compared NP-Gal to NP-DNA-40^{HI} only (summarised in table 5.1).

Table 5.1 Summary of different groups and number of rats used per group.

	Intracarotid injection	Intravenous injection
NP-Gal	3	3
NP-DNA-40^{LO}	3	-
NP-DNA-40^{HI}	3	3

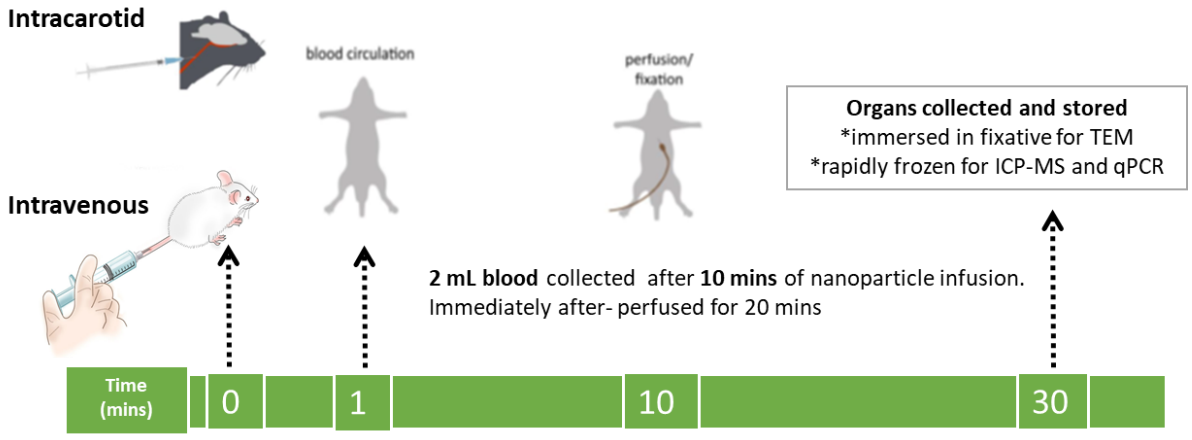

Figure 5.3 *Timeline of the in vivo experiment.*

We administered 200µg /per kg rat body weight of NP-Gal, NP-DNA-40^{LO} and NP-DNA-40^{HI} (gold concentration) over 1 min into the left carotid artery (for IC injection) and the

penile vein (for IV injection). The nanoparticles were left to circulate for 10 min in the blood (Figure 5.3).

5.2.2 The amount of gold in the organs analysed by ICP-MS

We investigated by ICP-MS the gold concentration in the brain, cerebellum, kidney, liver, spleen, heart, lung and blood for animals administered NP-Gal, NP-DNA-40^{LO} and NP-DNA-40^{HI} 10 min after IC and IV injection.

The control NP-Gal had accumulated predominantly in kidney within 10 mins of both IC and IV injections (figure 5.4 & 5.5), which is consistent with observations for <5 nm-sized nanoparticles (Skotland et al. 2010, Hillyer & Albrecht 2001) as they are cleared via this organ through the fenestrated endothelium of glomerular capillaries. Compared to kidney (4329ng/g), the amount of NP-Gal was much smaller in the brain (91ng/g), liver (50ng/g), spleen (132ng/g), and other organs, while some remained in the blood (657ng/g). For both, NP-DNA-40^{LO} and NP-DNA-40^{HI}, the nanoparticles accumulated at a high level in the liver and spleen for both IC and IV injections (figure 5.4 and 5.5). The quantity of gold with DNA observed was much less in kidney (IC-LO:250, HI:112ng/g) and all other organs compared to the liver (IC-LO:1748, HI:1839 ng/g) and spleen (IC-LO:1705, HI:1878 ng/g).

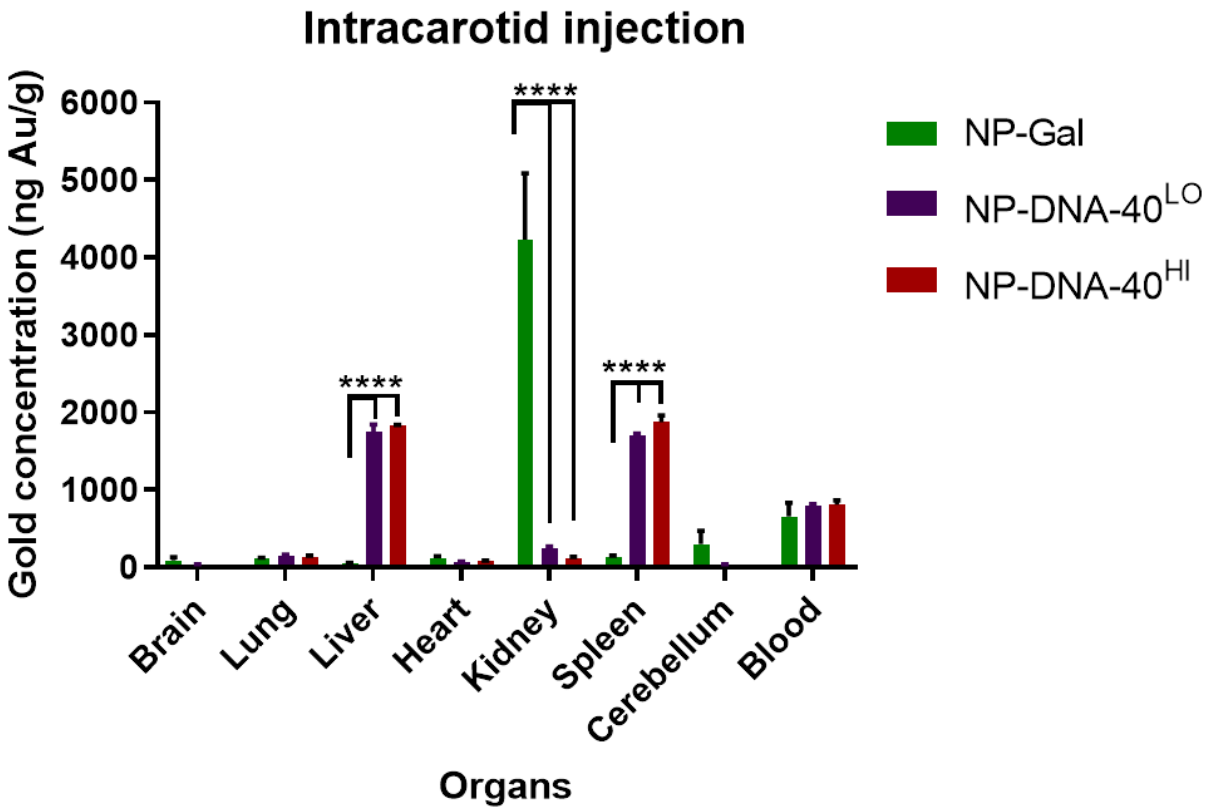

Figure 5.4 *The amount of gold (per gram of tissue) in different organs determined by ICP-MS after 10 mins of nanoparticle infusion in rats with IC injection. The gold concentration in tissue (ng Au/ml tissue) was compensated for variations in the dose administered (200µg Au/kg animal). Three animals in each group. Dunnett's multiple comparisons test was performed using Graphpad. Significant difference was detected between the NP-Gal compared to NP-DNA-40^{LO} and NP-DNA-40^{HI} for kidney, liver and spleen (****= <0.0001). Data shown as mean ±SEM.*

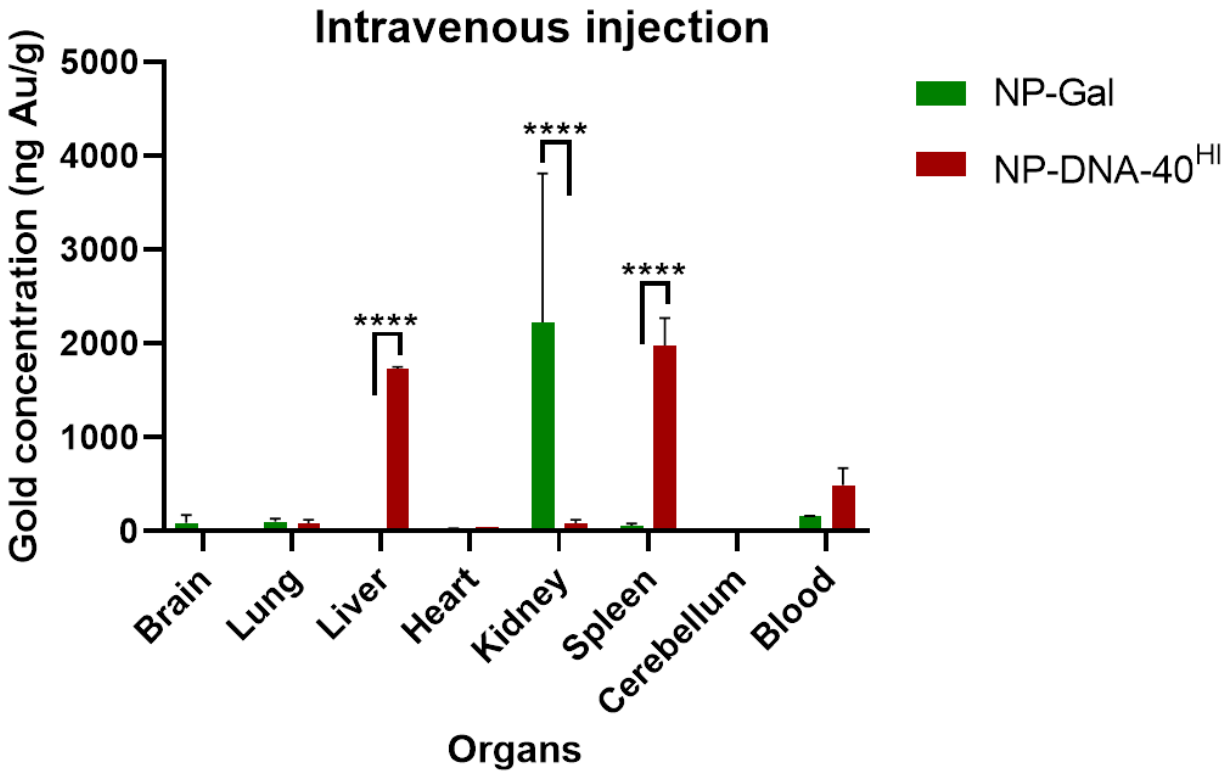

Figure 5.5 *The amount of gold (per gram of tissue) in different organs after 10 mins of nanoparticles infusion with IV- injection analysed by ICP-MS. The gold concentration in tissue (ng Au/ml tissue) was compensated for variations in the dose administered (200µg Au/kg animal). Three animals in each group. Dunnett's multiple comparisons test was performed using Graphpad. Significant difference was detected between the NP-Gal compared to NP-DNA-40^{LO} and NP-DNA-40^{HI} with for kidney, liver and spleen (****= <0.0001). Data shown as mean ±SEM.*

5.2.2.1 Gold In brain

As observed in figure 5.6 and 5.7, the amount of gold accumulated in the brain and cerebellum was undetectable. The detection signal of gold by ICP-MS in the brain was weak/low in comparison to gold concentration in other organs, and hence negative values were produced by ICP-MS analysis

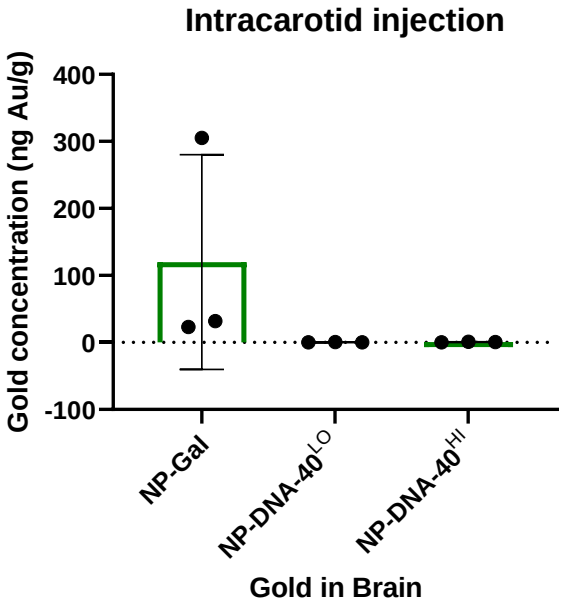

Figure 5.6 *The gold content in the brain after 10 mins following IC- injection analysed by ICP-MS. The data is insignificant as there was no detection signal for NP-DNA-40^{LO} and NP-DNA-40^{HI}*

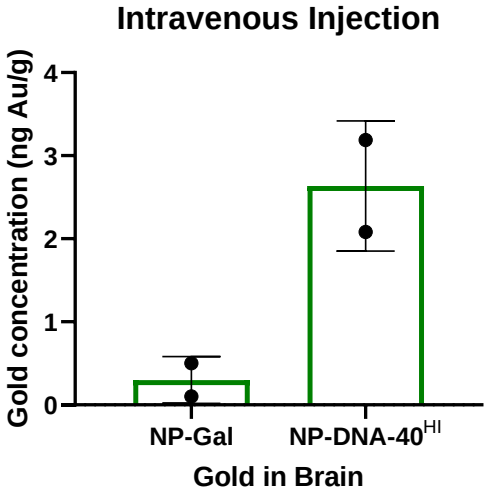

Figure 5.7 *The gold content in the brain after 10 mins following IV-injection analysed by ICP-MS. . The data is insignificant as there was weak detection signal for NP-Gal.*

5.2.3 Localisation of nanoparticles in tissues as analysed by light microscopy and TEM

The main focus of the TEM evaluation was on the brain, kidney, liver, and spleen. Silver enhancement staining at light microscopy level indicates overall presence of nanoparticles in the tissue samples. Darker staining within the tissue indicates the regions within which more nanoparticles were present. All data obtained from light microscopy is non-quantitative and only gives detail of overall tissue localisation.

The results from light microscopy and TEM analysis summarised for each organ as follow;

5.2.3.1 Nanoparticles localised in brain

Light microscopy showed light staining of whole-brain tissue sections, as the sections turned slightly brown from unstained white when we incubated the sections with silver enhancement (illustrated in figure 5.8 and 5.10). NP-Gal had the most substantial staining compared to the NP-DNA-40^{LO} and NP-DNA-40^{HI}. Overall, dark patches of brown staining were mostly observed in the region of cortex and median eminence (refer to figure 5.9) for illustrations of different brain regions) for all three nanoparticles formulations. Heavier staining patches were observed on the ipsilateral side (injected side), but light staining was also observed on the contralateral side.

Furthermore, from the results in figure 5.8 we found that within each group (i.e., NP-DNA-40^{LO}) of treated animals, there were differences in localisation and amount of brown staining. For example, with NP-DNA-40^{LO} group, there was one animal with heavier brown staining in the cortex, median eminence, choroid plexus, and striatum whereas the other two animals showed less or no staining in those regions. Saris et al, 1988 explains a possible explanation for variance in staining in the same group, that IC injections can provide irregular distribution of administered substance within the brain. There is intravascular streaming, which means nanoparticles are based in the part of the brain where the stream of blood will flow and hence, carry nanoparticles in that direction. Therefore, this can result in a random distribution of the nanoparticles into brain regions, showing a disparity in regional distribution between the same group animals.

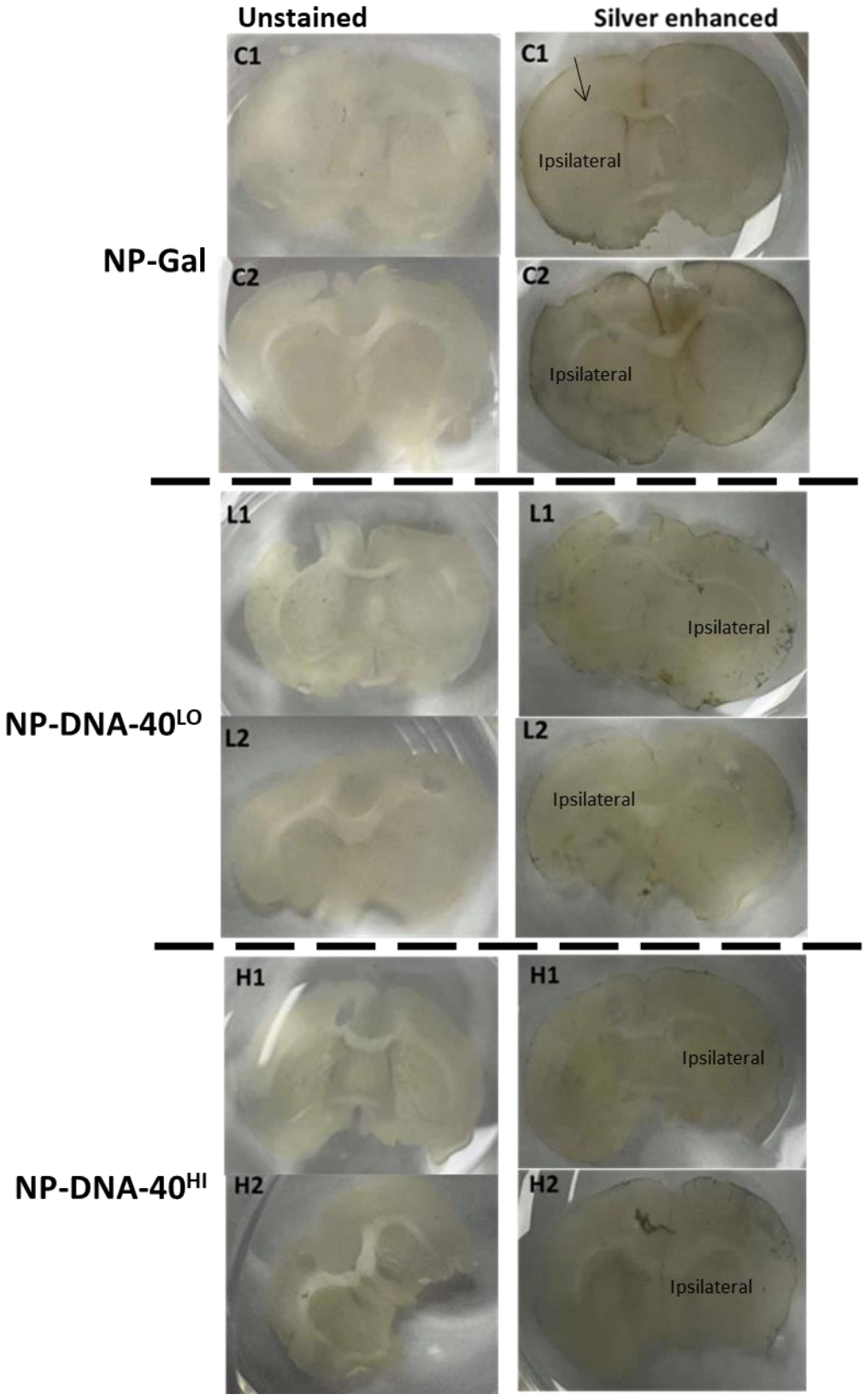

Figure 5.8 *Brain sections stained with LM silver enhancement to localise gold nanoparticles in regions of rat brain of the three intracarotid injected groups;. NP-Gal, NP-DNA-40^{LO} and NP-DNA-40^{HI}. 3 animals per group were stained.*

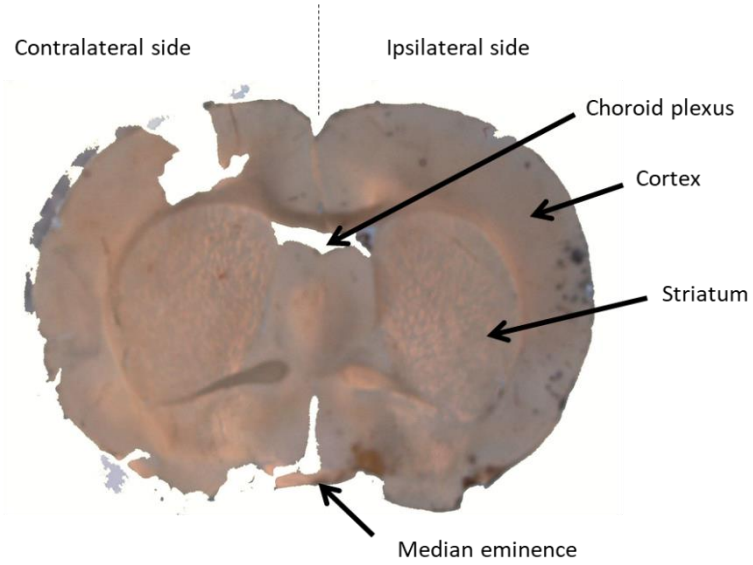

Figure 5.9 *Representative regions of the brain as described in this study. Brown/dark staining in the section corresponds to the presence of gold nanoparticles. The injected side is noted as ipsilateral, opposite to injected side is contralateral side.*

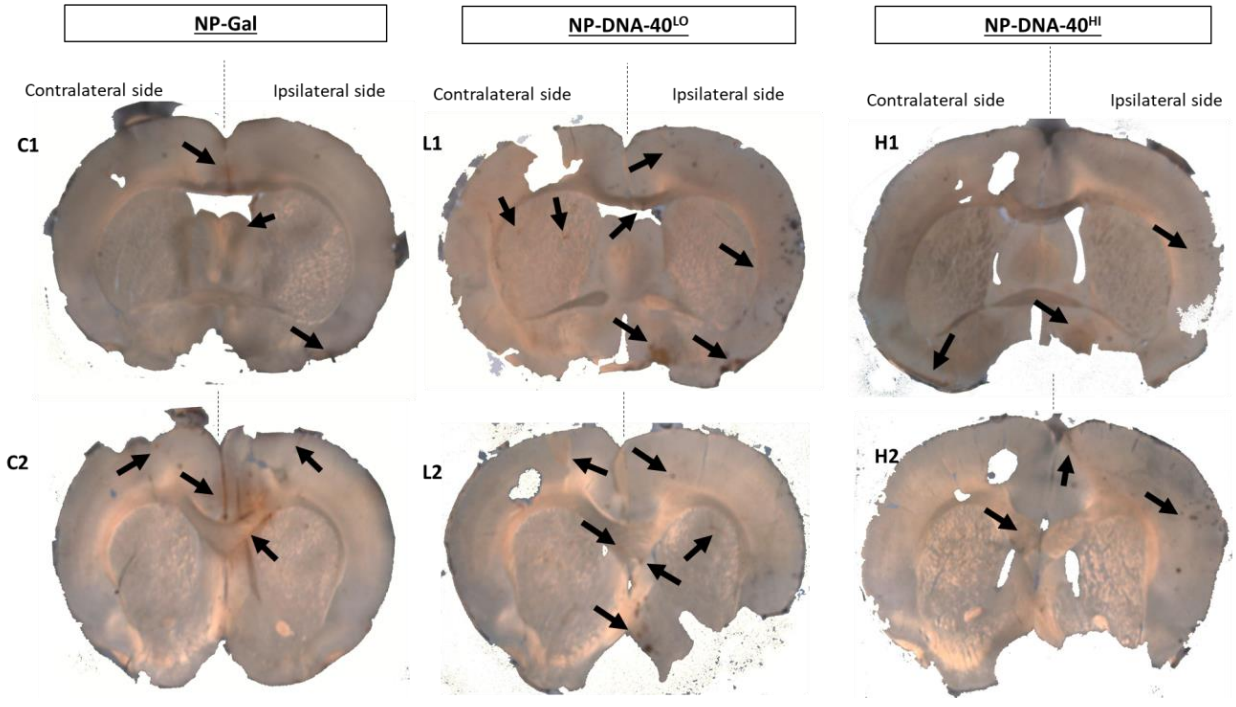

Figure 5.10 *Brain sections stained with silver enhancement to point out regional localisation of gold nanoparticles. Brown/dark staining in the sections corresponds to the presence of gold nanoparticles (NP-Gal, NP-DNA-40^{LO} and NP-DNA-40^{HI}) in the tissue. The IC injected side is noted as ipsilateral, opposite to injected as contralateral side. All images were taken after 2 hours of silver enhancement. Magnification is x1.*

When analysed by TEM, NP-Gal, *NP-DNA-40^{LO} and NP-DNA-40^{HI}* were seen to have penetrated the brain endothelium and entered the brain parenchyma (illustrated in figure 5.11, 5.12 and 5.13).

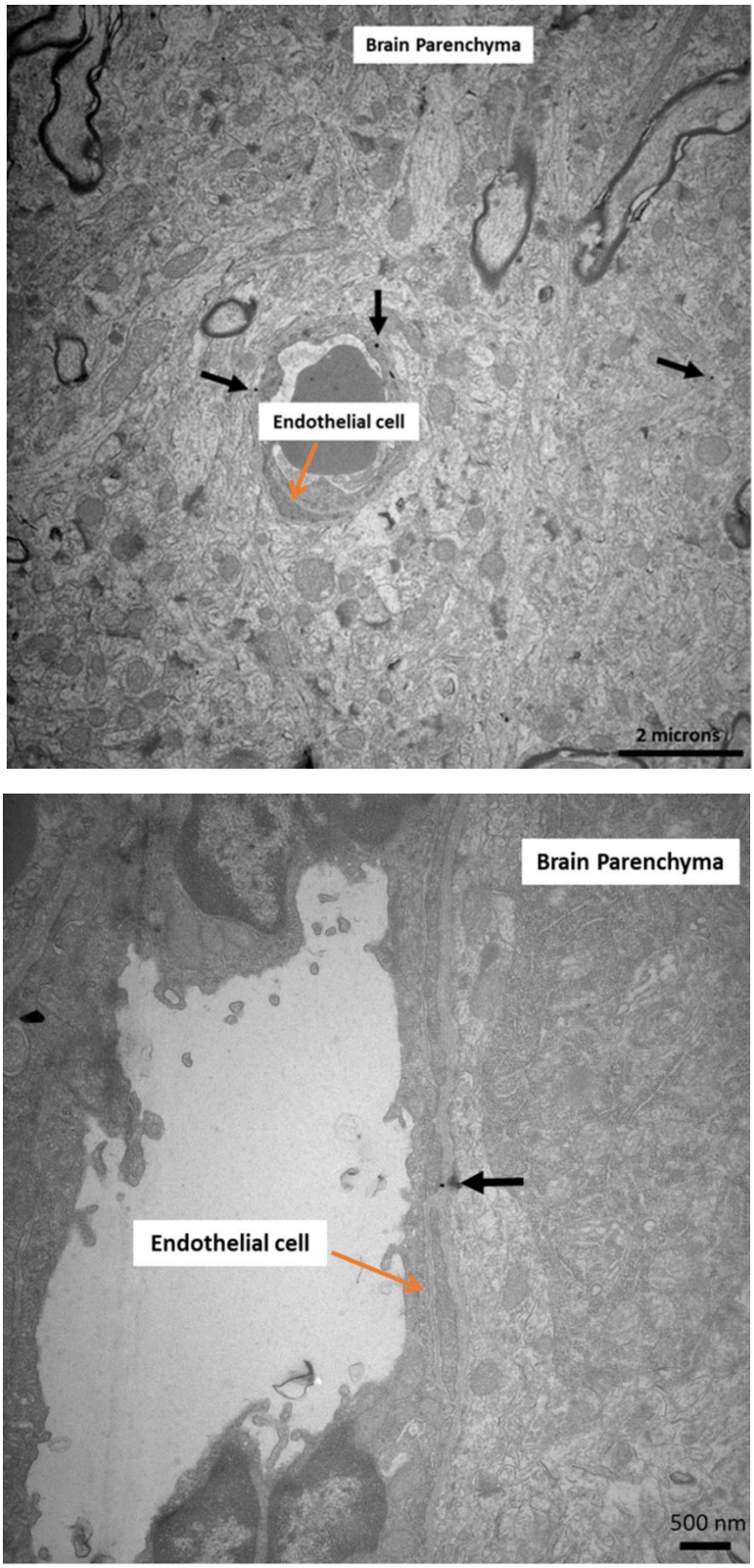

Figure 5.11 *TEM images of brain cortex of IC injected rat with NP-Gal. Silver-enhanced gold nanoparticles found in parenchyma and brain endothelium are identified with black arrows.*

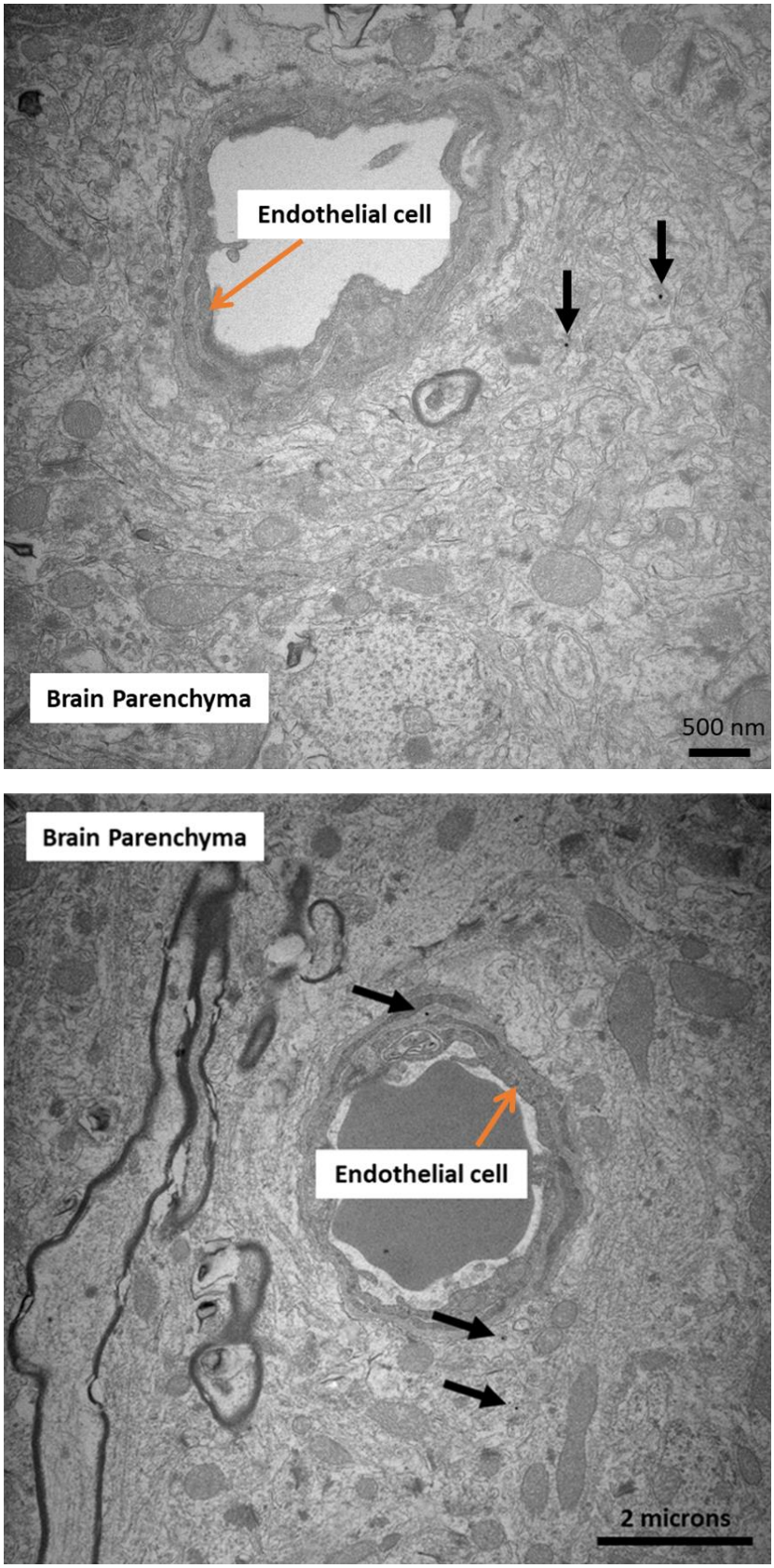

Figure 5.12 *TEM images of brain cortex of IC injected rat with NP-DNA-40^{LO}. Silver-enhanced gold nanoparticles found in parenchyma and brain endothelium are identified with black arrows.*

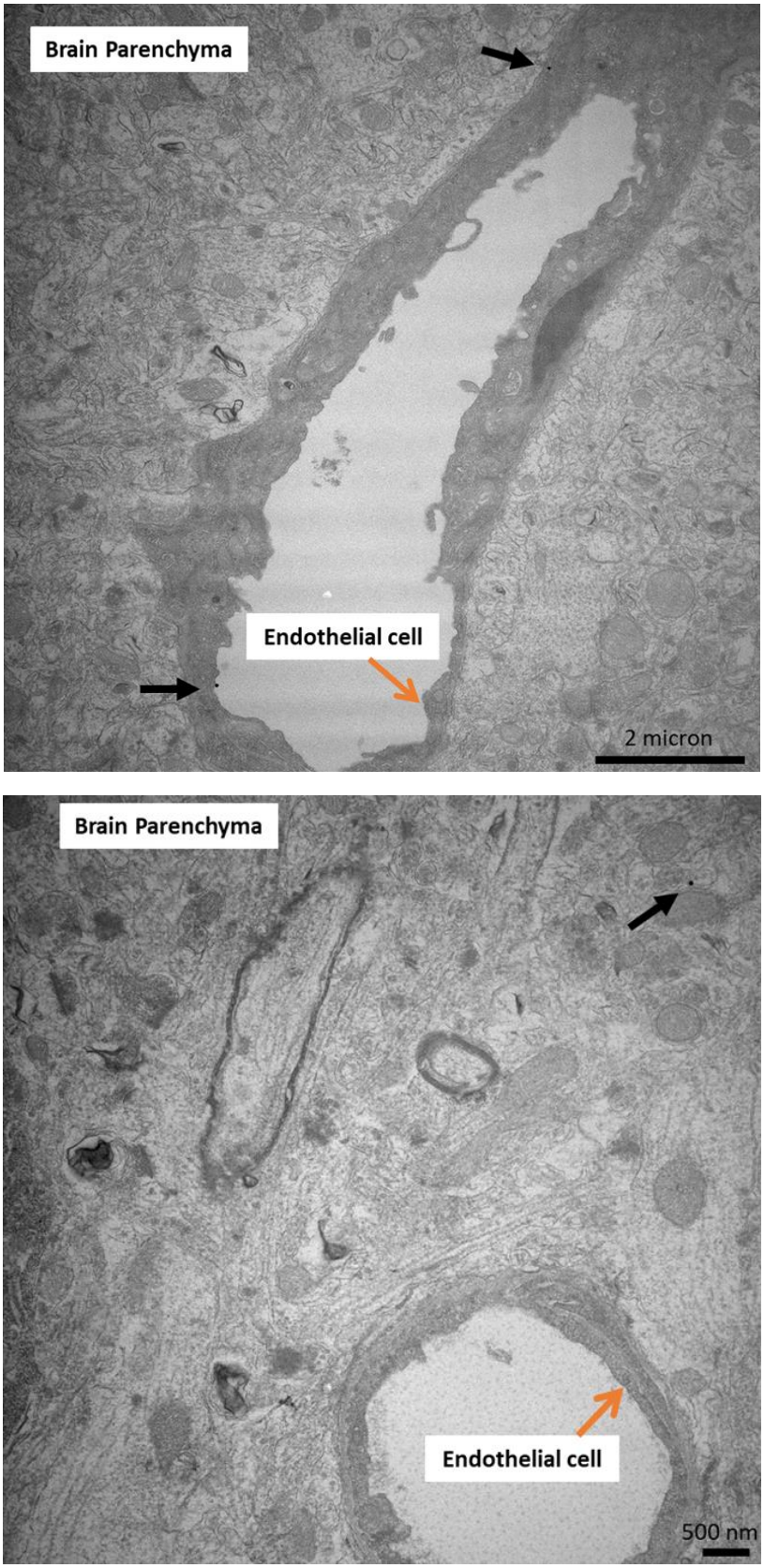

Figure 5.13 *TEM images of a brain cortex of IC injected rat with NP-DNA-40^{HI}. Silver-enhanced gold nanoparticles found in parenchyma and brain endothelium are identified with black arrows. Nanoparticles marked with black arrows.*

5.2.3.2 Nanoparticles localised in liver

Results obtained with ICP-MS showed a low amount of gold in the liver of animals treated with NP-Gal. On the other hand, high amount of nanoparticles were observed in the liver for rats treated with NP-DNA-40^{LO} and NP-DNA-40^{HI}.

Correspondingly, light microscopy silver enhancement staining showed lighter staining of the liver tissue section for the animals treated with NP-Gal. Darker staining indicating more nanoparticles was observed for liver tissue sections of animals treated with both NP-DNA-40^{LO} and NP-DNA-40^{HI} (figure 5.14).

Next, we looked for localisation of nanoparticles within tissues and cells via TEM. We observed few nanoparticles for all three formulations in liver hepatocytes, mostly in their cytosol. No nanoparticles were observed in all other liver cells. Liver hepatocytes of animals treated with NP-DNA-40^{LO} and NP-DNA-40^{HI} contained more nanoparticles than those treated with NP-Gal. Examples of nanoparticles in the liver hepatocytes for animals treated with NP-Gal, NP-DNA-40^{LO} and NP-DNA-40^{HI} are presented in Figure 5.15, 5.16 and 5.17.

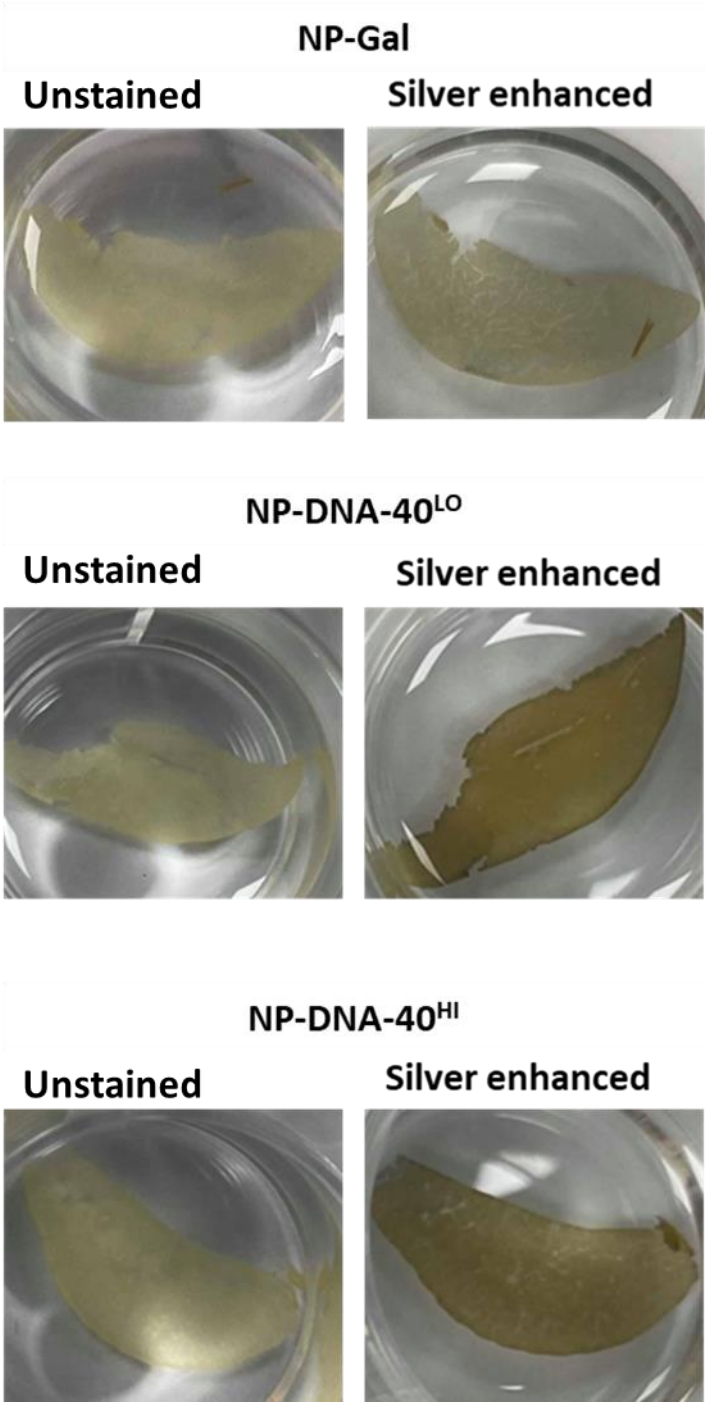

Figure 5.14 *Liver tissue sections stained with LM silver enhancement to point out regions of liver where gold nanoparticles were present. Three IC injected treated groups; NP-Gal, NP-DNA-40^{LO} and NP-DNA-40^{HI} were analysed. 3 animals per group were stained.*

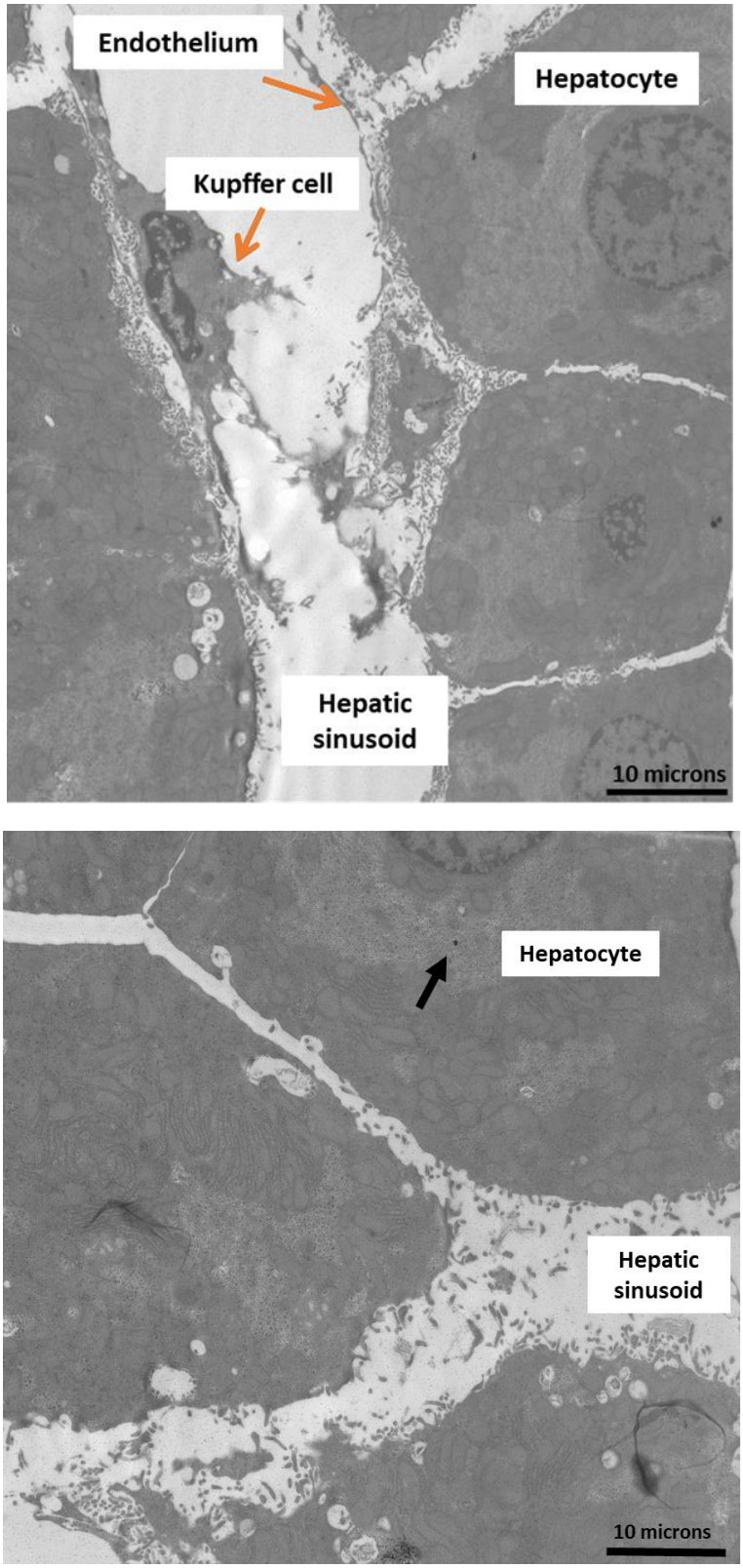

Figure 5.15 *TEM image of a liver tissue section IC injected with NP-Gal. Silver-enhanced gold nanoparticles were found in liver hepatocytes but not in Kupffer cells. Nanoparticles are marked with black arrows.*

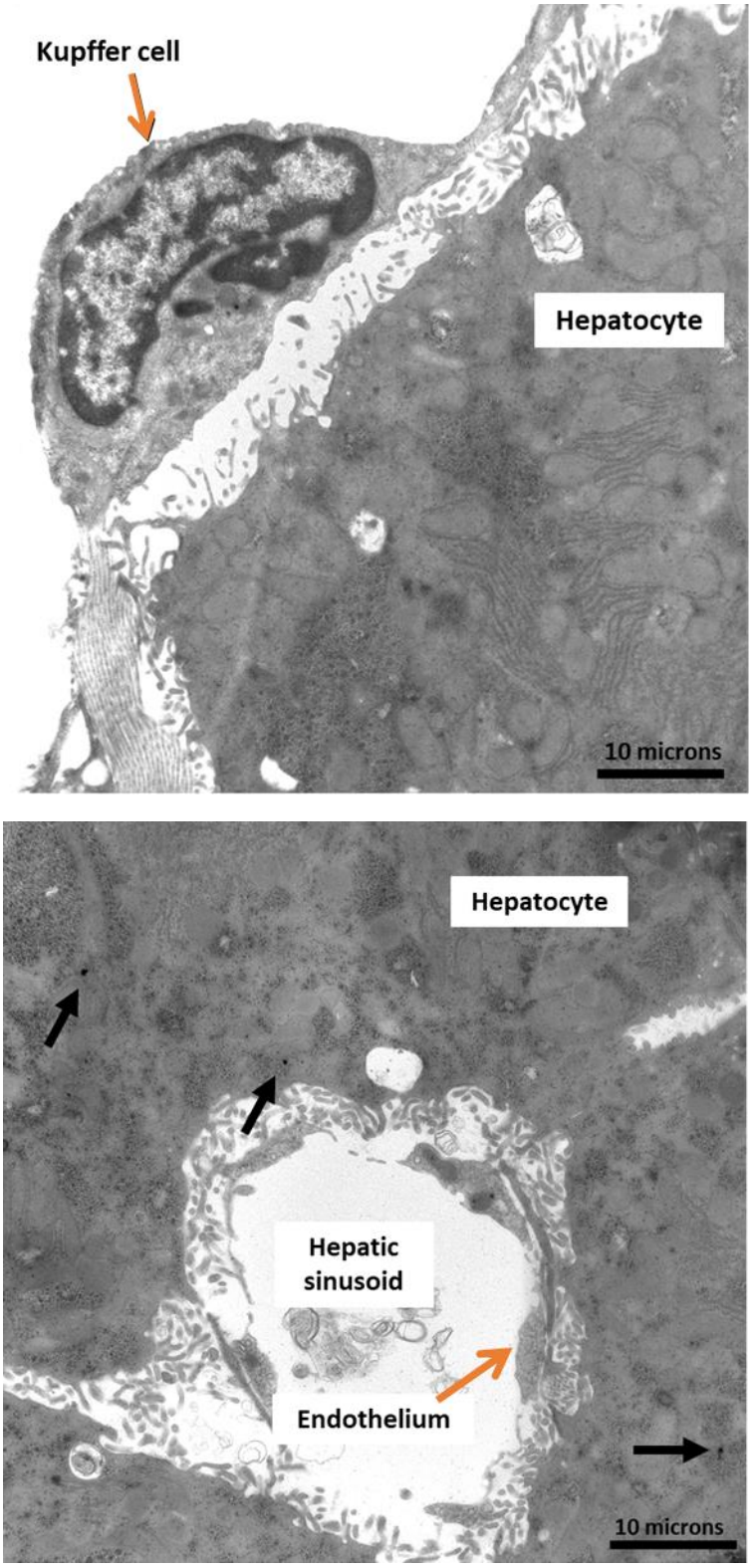

Figure 5.16 *TEM images of liver tissue sections IC injected with NP-DNA-40^{LO}. Silver-enhanced gold nanoparticles were found in hepatocytes but not in Kupffer cells. Nanoparticles are marked with black arrows.*

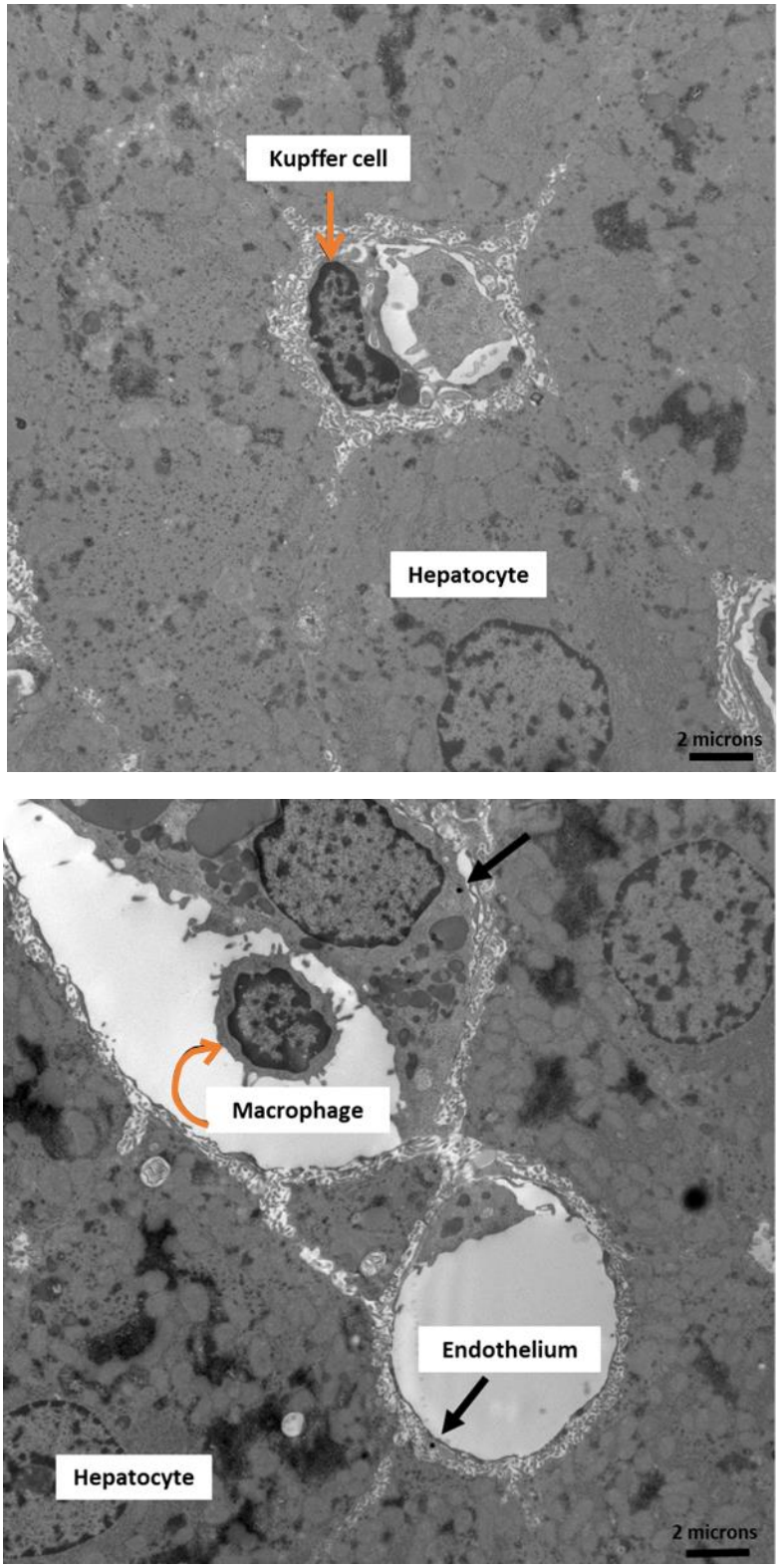

Figure 5.17 *TEM images of liver tissue sections IC injected with NP-DNA-40^{HI}. Silver-enhanced gold nanoparticles were found in liver hepatocytes but not in Kupffer cells. Nanoparticles are marked with black arrows.*

5.2.3.3 Nanoparticles localised in spleen

As previously shown, ICP-MS showed a low level of gold in spleens of animals treated with NP-Gal, whereas high amounts were observed in spleens of animals treated with NP-DNA-40^{LO} and NP-DNA-40^{HI}. However, since spleen tissue sections were darker than all other organ sections, it was hard to distinguish any difference when we stained them with silver enhancement and observed via light microscopy (figure 5.18).

Cellular and subcellular localisation via TEM showed very few nanoparticles in red pulp of the spleen of animals treated with NP-Gal. Interestingly, no nanoparticles were observed in the white pulp and the capsule of the spleen in these animals (figure 5.19).

Animals treated with NP-DNA-40^{LO} and NP-DNA-40^{HI} had many nanoparticles in macrophages of red pulp in the spleen. As with NP-Gal, no nanoparticles were observed in the white pulp, but, in contrast to the NP-Gal controls, nanoparticles were observed in the capsule of the spleen for both treated groups (figure 5.20 and 5.21).

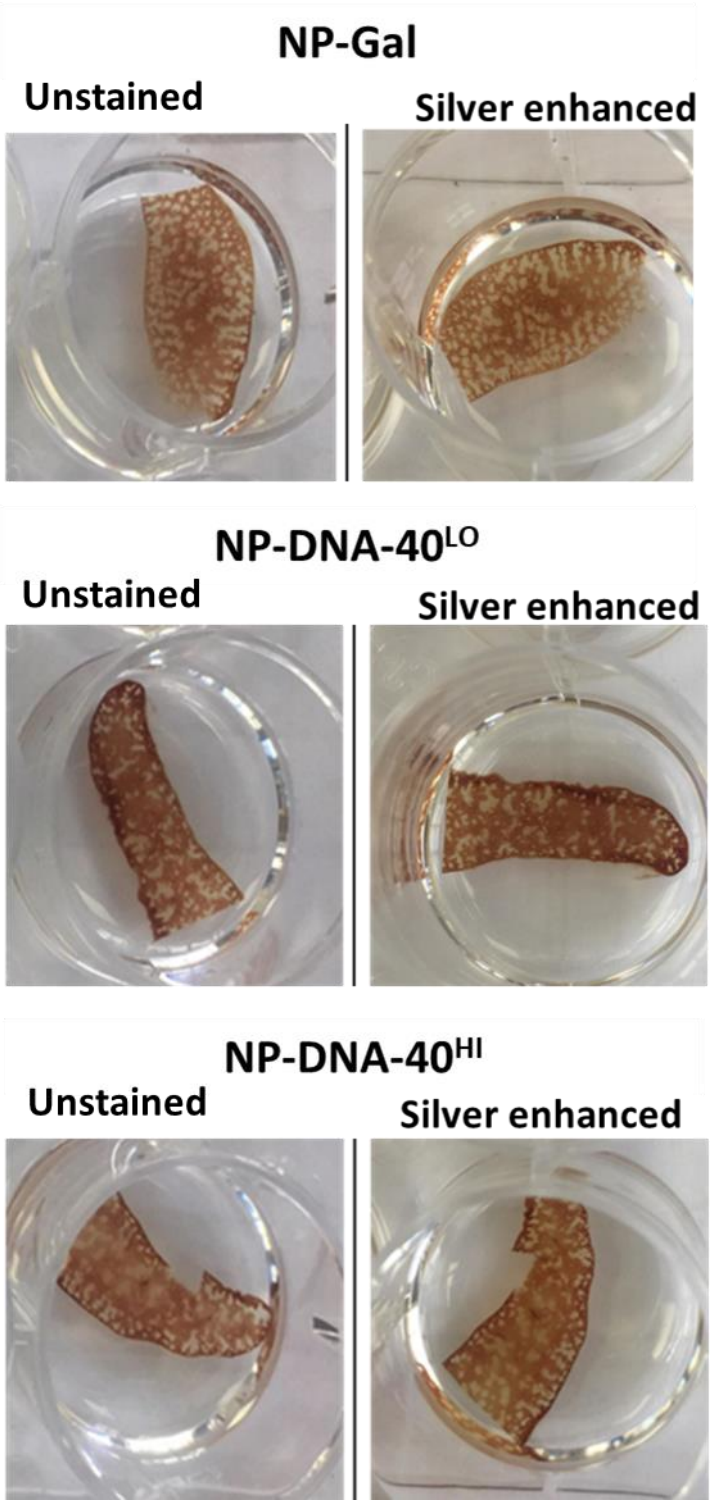

Figure 5.18 *Spleen tissue sections stained with silver enhancement to point out regions of spleen tissue where gold nanoparticles were present. Three IC injected treated groups; NP-Gal, NP-DNA-40^{LO} and NP-DNA-40^{HI} were analysed. 3 animals per group were stained.*

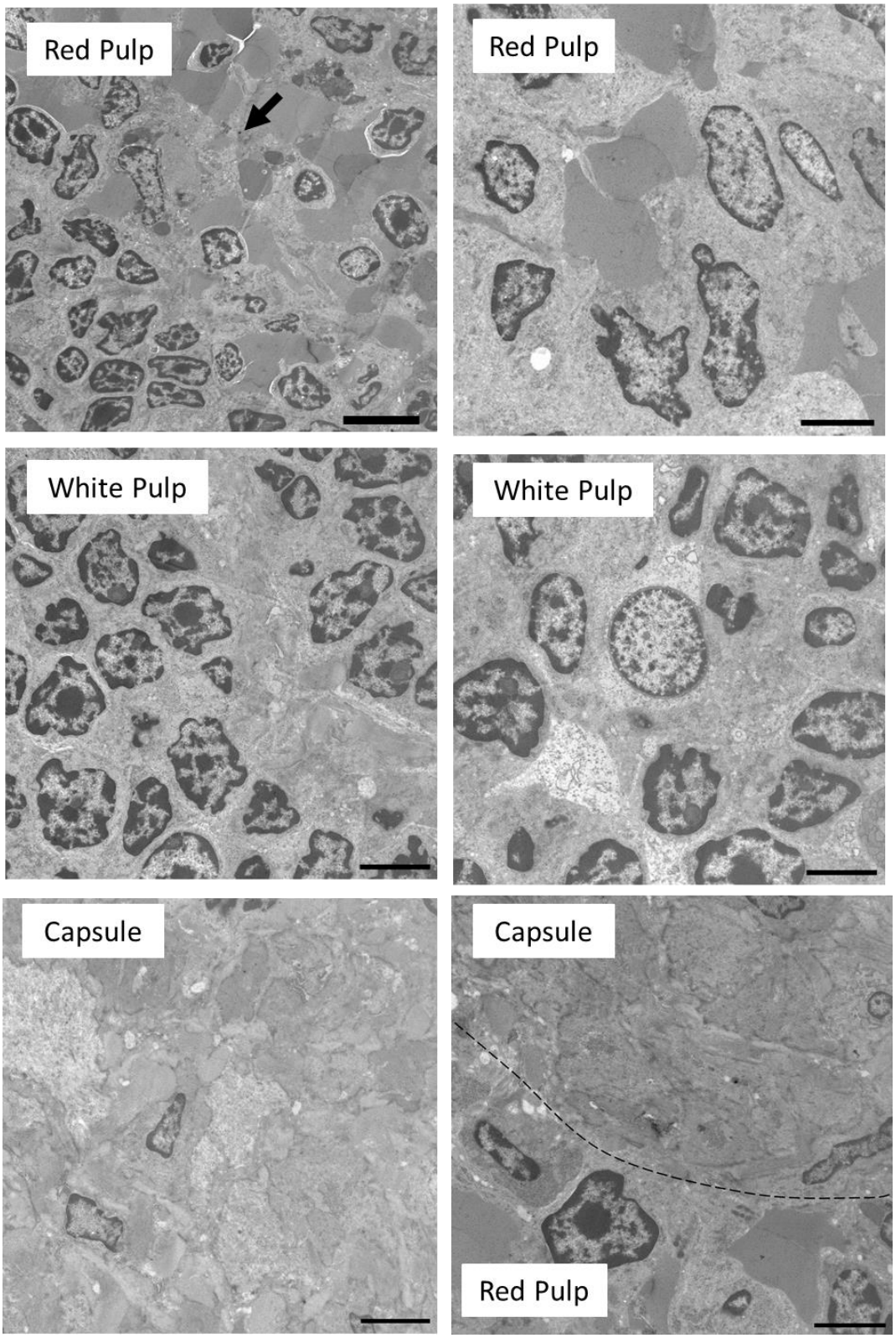

Figure 5.19 *TEM images of spleen tissue sections IC injected with NP-Gal. Few silver-enhanced gold nanoparticles were found in red pulp only but not in white pulp and capsule. Nanoparticles marked with arrows. Scale bar = 10 microns. The dashed line in capsule shows separation of capsule and red pulp.*

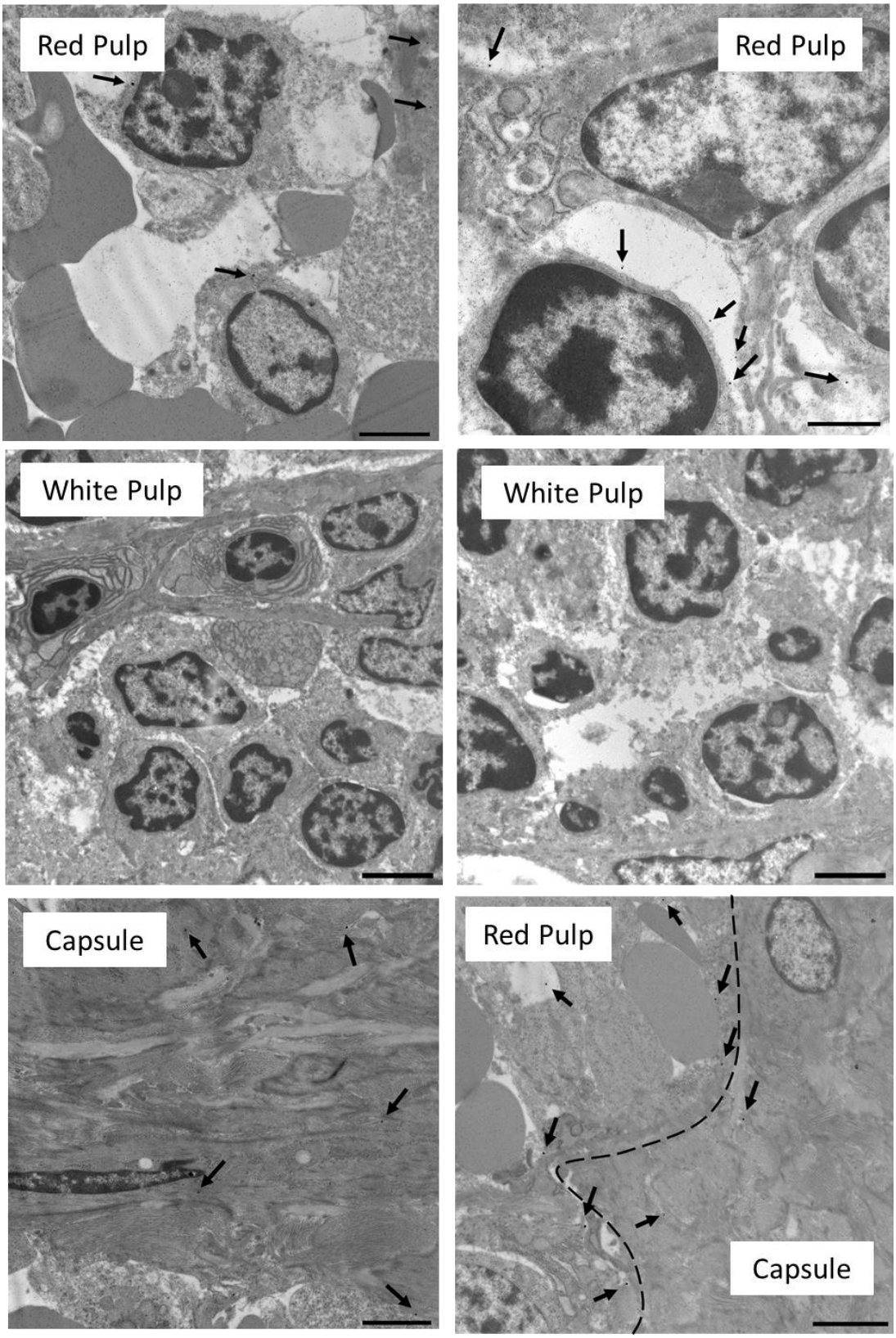

Figure 5.20 *TEM images of spleen tissue sections IC injected with NP-DNA-40^{LO}. Many silver-enhanced gold nanoparticles were found in red pulp and white pulp but not in the capsule. Nanoparticles marked with arrows. Scale bar = 10 microns. The dashed line in capsule shows separation of capsule and red pulp.*

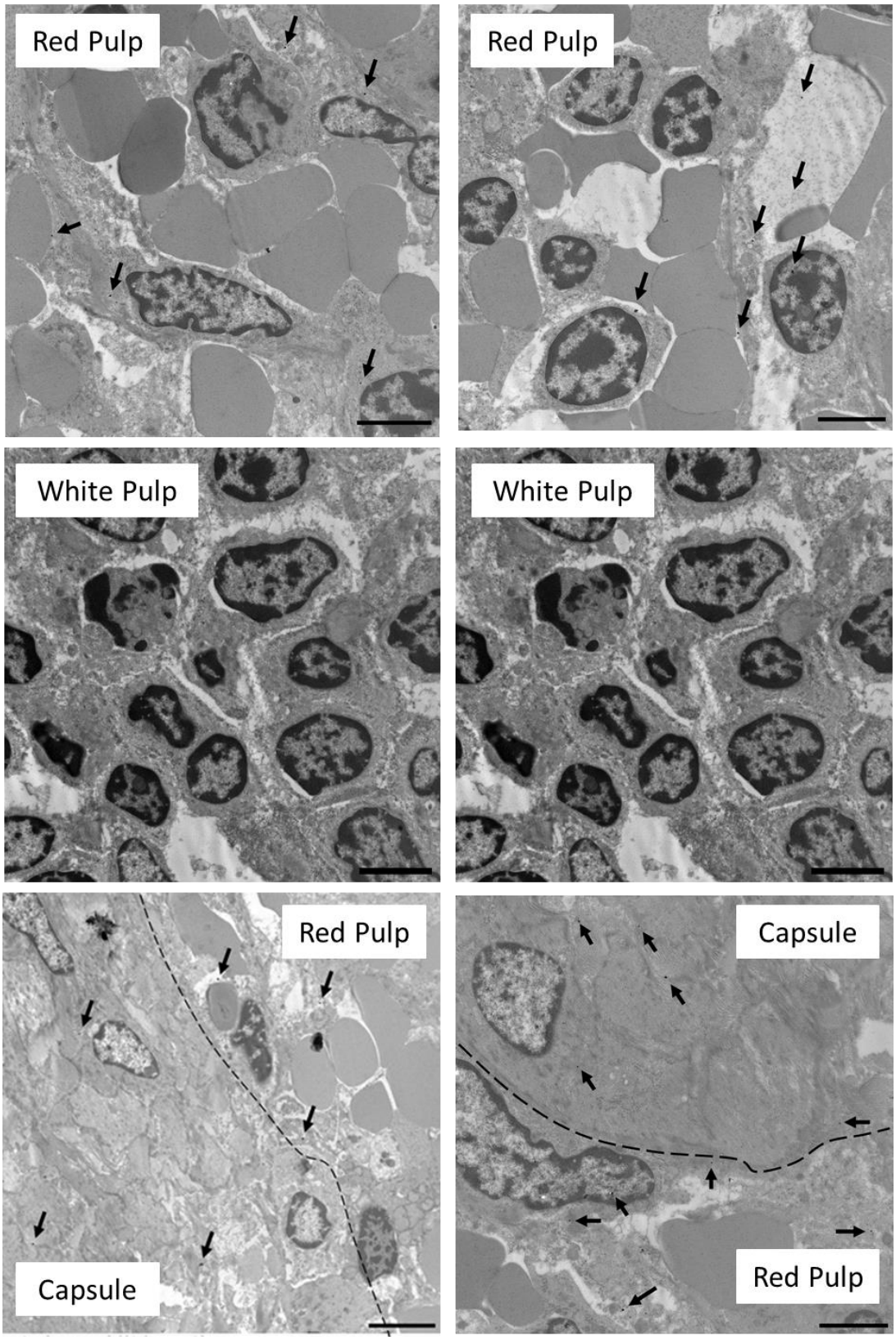

Figure 5.21 *TEM images of spleen tissue sections IC injected with NP-DNA-40^{HI}. Many silver-enhanced gold nanoparticles were found in red pulp and white pulp but not in the capsule. Nanoparticles marked with arrows. Scale bar = 10 microns. The dashed line in capsule shows separation of capsule and red pulp.*

5.2.3.4 Nanoparticles localised in kidney

ICP-MS showed a relatively high level of gold present in the kidney for animals treated with NP-Gal, but low levels in the kidneys of animals treated with NP-DNA-40^{LO} and NP-DNA-40^{HI}.

When we performed silver enhancement of kidney sections, we found stained regions all over for animals treated with NP-Gal. In contrast, few stained regions were observed on the outer cortex of kidney tissue for an animal treated with NP-DNA-40^{LO}. No staining was observed for an animal treated with NP-DNA-40^{HI} (figure 5.22).

Localization study using TEM showed many NP-Gal nanoparticles in the cytoplasm of the proximal tubule epithelium and in the brush borders for kidney tissue (figure 5.23). Meanwhile, only a few nanoparticles were observed in the proximal tubule epithelium and brush border of animals treated with NP-DNA-40^{LO} and NP-DNA-40^{HI} (figure 5.24 and 5.25). The distinctive characteristic of the proximal tubule is its luminal brush border, which facilitates re-absorption. The re-absorptive function is to remove water and solute from the tubular fluid (pre-urine).

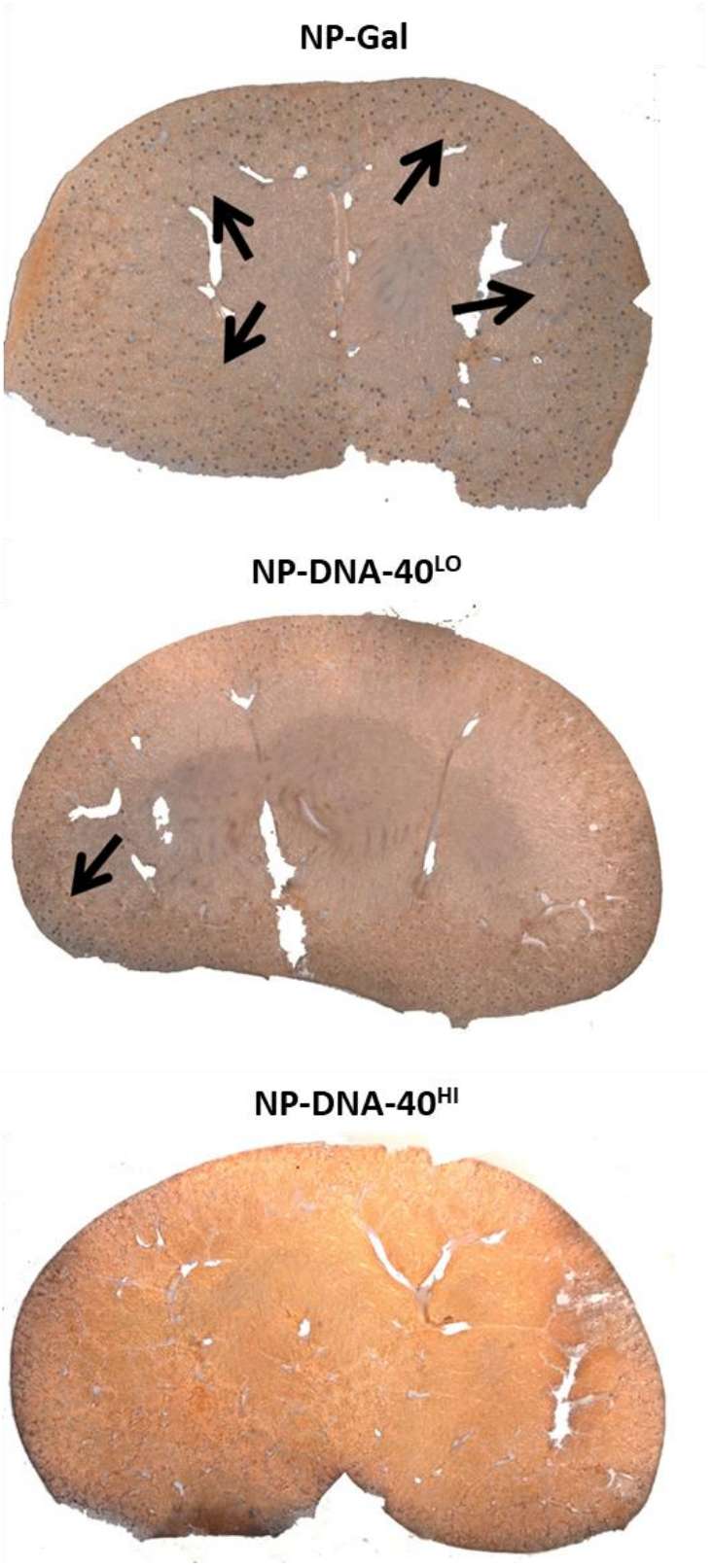

Figure 5.22 *Silver enhanced kidney tissue sections showing regions where NP-Gal, NP-DNA-40^{LO} and NP-DNA-40^{HI} localized inside kidney. Magnification 1x. 3 animals per group were stained.*

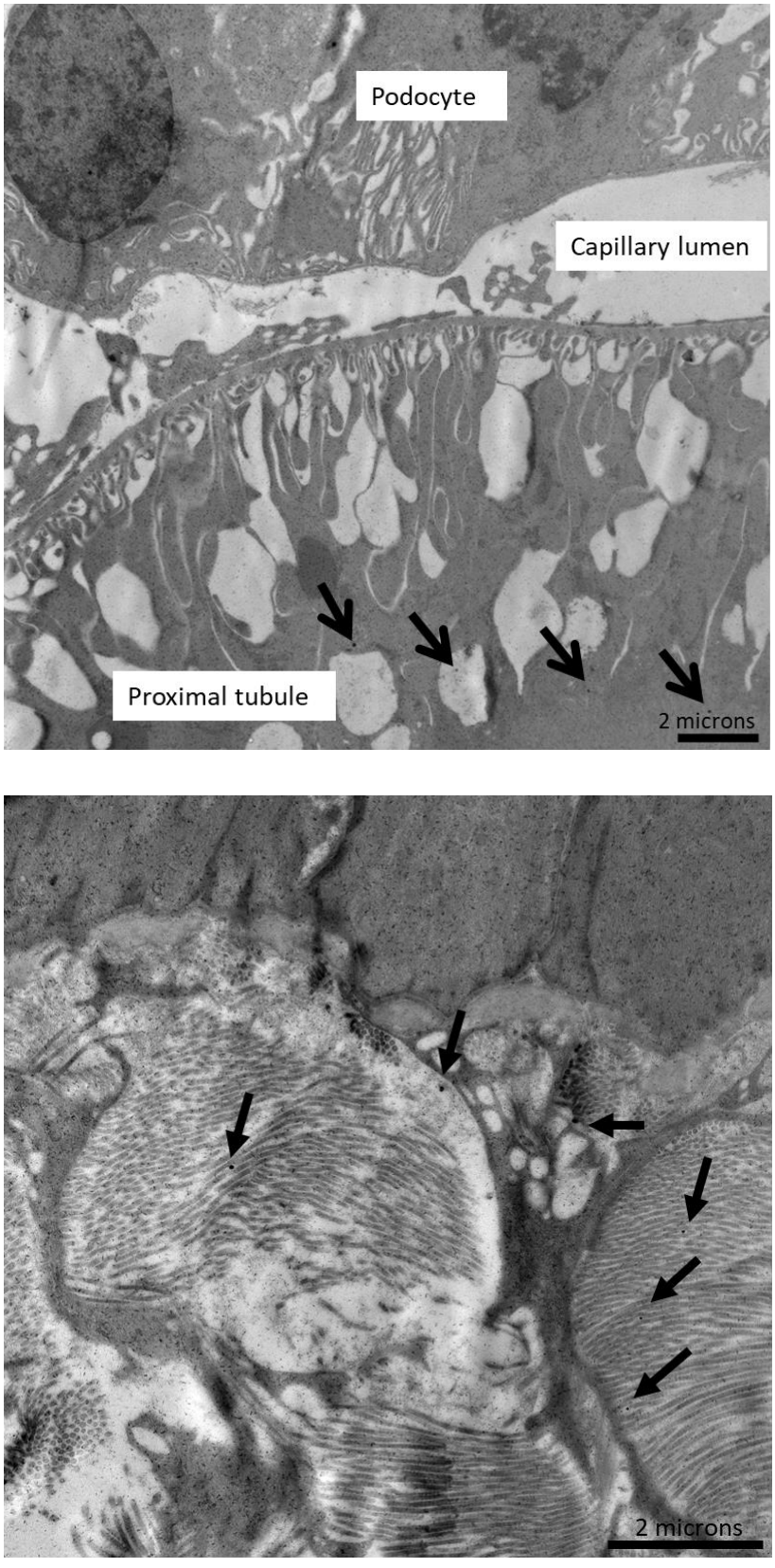

Figure 5.23 *TEM images of kidney tissue section IC injected with NP-Gal. Silver-enhanced gold nanoparticles were found in proximal tubule and brush border, marked with black arrows.*

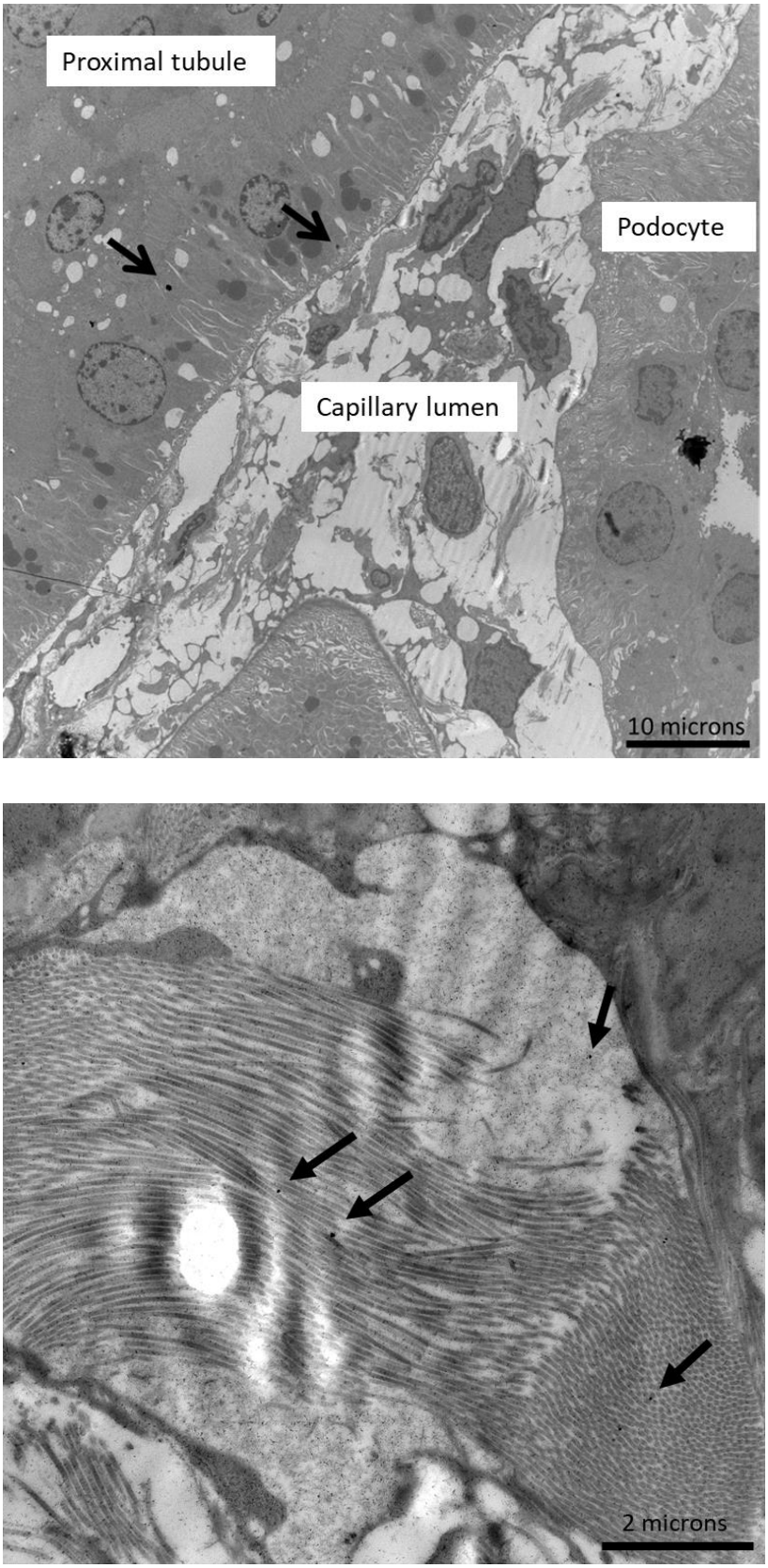

Figure 5.24 *TEM images of kidney tissue section IC injected with NP-DNA-40^{LO}. Silver-enhanced gold nanoparticles were found in proximal tubule and brush border, marked with black arrows.*

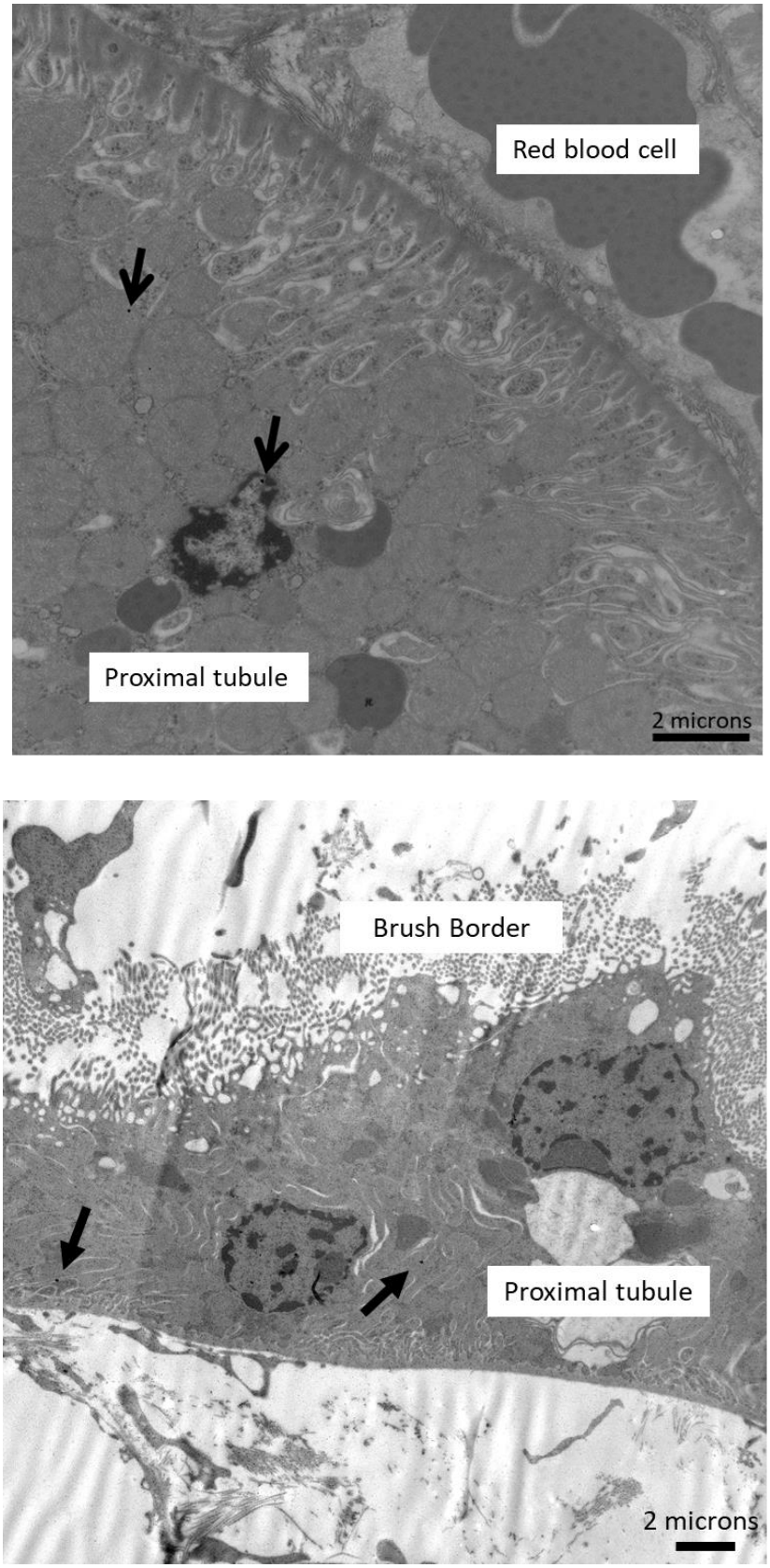

Figure 5.25 *TEM images of kidney tissue section IC injected with NP-DNA-40^{HI}. Silver-enhanced gold nanoparticles found in proximal tubule and brush border, marked with black arrows.*

5.3 Discussion and summary

In this chapter, we investigated the distribution and intracellular localisation of NP-Gal, NP-DNA-40^{LO} and NP-DNA-40^{HI} in the organs of rat following administration by two different routes; IC injection and IV injection. ICP-MS to quantify gold in tissue samples showed that tissue distribution of control nanoparticles NP-Gal was quite different to DNA-coated ones of NP-DNA-40^{LO} and NP-DNA-40^{HI}. NP-Gal localised primarily in kidney within 10 mins of both IC and IV injections. This is a typical observation for <5 nm-sized nanoparticles (Skotland et al. 2010, Hillyer & Albrecht 2001) as they are cleared through the fenestrated endothelium of glomerular capillaries in kidney. On the other hand, both DNA-coated nanoparticles (NP-DNA-40^{LO} and NP-DNA-40^{HI}) primarily accumulated in the liver, in particular we found them in cytoplasm of hepatocytes. No nanoparticles were observed in all other liver cells. Liver hepatocytes of animals treated with NP-DNA-40^{LO} and NP-DNA-40^{HI} contained more nanoparticles than those treated with NP-Gal. Moreover, DNA-coated nanoparticles were observed in macrophages of the red pulp in the spleen for both IC and IV injections. Our results contrast to those reported by Sadauskas, et al, 2007 who found that Kupffer cells/phagocytic cells of liver accumulated gold nanoparticles. We did not observe any nanoparticles in Kupffer cells/phagocytic cells, maybe because our nanoparticles were much smaller in size compared to their 40nm gold nanoparticles. Our nanoparticles were mostly observed in hepatocytes which detoxify blood and remove foreign material. Perhaps hepatocytes in liver and red pulp cells in spleen were removing NP-DNA-40^{LO} and NP-DNA-40^{HI} from the blood. If the distribution of gold nanoparticles is size- or charge-dependent, perhaps the negative charge on 40nt DNA-nanoparticles may have attracted (positively charged) proteins in the blood, facilitating nanoparticle penetration into liver and spleen. The low levels of 40nt DNA-gold nanoparticles observed in kidney may be linked to that the fact that NP-DNA-40^{LO} and NP-DNA-40^{HI} are larger - 15 nm than NP-Gal (3.6 nm). Since the pores in kidney capillary endothelium are 5.5 nm, nanoparticles smaller than the 5.5 nm diameter can enter easily (Joshi et al. 2007).

In comparison to other organs, the level of gold as detected by ICP-MS was lowest in the brain, suggesting that gold nanoparticles cannot cross over the BBB within 10 mins of IC and IV injection. This result is quite different from the previous study of Gromnicova et al. 2016, which claimed that NP-Gal could pass through the BBB and into the brain *in vivo*. Although we observed all three nanoparticle formulations in the brain by TEM localised in endothelial and glial cells of the cortex. The difference of our observations in ICP-MS

versus TEM might be because we used only anterior half (frozen tissue) for ICP-MS analysis, whereas, posterior half was used fixed for TEM analysis. As the nanoparticle accumulation can differ depending on the region of the brain (nanoparticles have a tendency to accumulate in specific brain regions, where they can access the neural cells, including neurons, astrocytes, and microglia) (Caudle, W. M, 2017) and depending on the administration route, we may have omitted the gold nanoparticles that were located in the posterior half of the brain when doing ICP-MS. Therefore, full brain might need to be analysed by ICP-MS.

There are also several ways to improve BBB targeting drug delivery of gold nanoparticles, such as receptor-mediated transcytosis. Receptor-mediated transcytosis may be used to facilitate brain targeting drug delivery, by using brain endothelial cells' receptors, e.g. transferrin receptor (Wiley et al. 2013; Prades et al. 2012), or insulin receptor (Shilo et al. 2014)) to initiate receptor-mediated endocytosis. However, the disadvantage of this approach is that targeted receptors (i.e. transferrin receptor or insulin receptor) found on brain endothelium for receptor-mediated transcytosis are not only found on the brain endothelium but also found on the liver and bone marrow (Simionescu et al. 2002). Another way to improve brain selectivity is to use peptides that are not localised in any other organs but solely found in the brain. A phage display library has identified peptides that are only brain tissue-specific (Pasqualini & Ruoslahti 1996; Rajotte et al. 1998). It would be interesting to bind targeting peptides along with the therapeutic oligonucleotides (as there is space for 40 ligand spaces on each nanoparticle) and investigate the targeting efficiency of such peptides to increase the uptake of therapeutic nanoparticles in the brain.

An important limitation of our study was that only 1 time point was selected for analysis – 10 minutes after the injection. In future studies, long term (with different time points) accumulation of nanoparticles in each organ might show fuller picture of how nanoparticles are cleared from the body. Additionally, during our in vivo experiments, we were encountered with problems in tissue sample delivery from Istanbul, Turkey to UK. The fixed (in glutaraldehyde) tissue samples arrived at our lab on dry ice (fully frozen), which affected the preservation of the tissue samples and as well as majority of samples received were poorly perfused making micro-sectioning of tissue samples incredibly harder for electron microscope analysis. Hence, for future studies, it is important to note that tissue samples must be perfused well and freezing of fixed samples is avoided.

6 ASSESSMENT OF TRANSPORT AND DELIVERY OF DNA VIA NP-DNA-40 IN BRAIN ENDOTHELIAL CELLS.

Aim:

1. To quantify by qPCR how much DNA has been transported across the brain endothelial cells.
2. To determine how the density of DNA on the NPs affects the transport rate of the DNA.

Previously, we found that DNA-coated gold nanoparticles entered and possibly crossed brain endothelial cells as detected using TEM. However, it is not clear by TEM whether DNA from the nanoparticles remained attached and crossed the cells. Since DNA is attached covalently to the nanoparticles, it may detach during exposure to reducing conditions found in cells. Hence, we decided to assess whether and how much DNA attached onto the nanoparticles entered and crossed the endothelial cells. This would help us to understand the effectiveness of our gold nanocarriers for transporting oligonucleotides into the brain for future therapeutic purposes.

6.1 Introduction

Quantitative PCR (qPCR) technique is regarded as a standard method currently available for DNA quantification. It works in a similar way to a standard PCR but uses real-time fluorescence to rapidly measure the quantity of DNA present at each cycle during a PCR. It is characterized by high accuracy, time effectiveness, and reproducibility. It is the most common molecular technique used for nucleic acid quantification (Huggett and Bustin, 2011). Therefore, it was chosen to detect the amount of DNA entering and crossing the brain endothelial cells.

6.2 Results

The first step in this study was designing primers to detect the 40nt DNA template used to attach to gold nanoparticles using these criteria:

- The primers were complementary to a sequence of nucleotides of the 40nt DNA template. While designing the primers, primers matched a sequence within the 40nt DNA sequence.
- The primers did not contain complementary regions within themselves, to prevent folding over and binding onto themselves to form a hairpin or to prevent forming a primer dimer. As the reverse and forward primer sequence was only small between 20 and 23 nucleotide base pair (bp) in length, the issue of forming hairpin and starting off PCR late to miss a portion of DNA sequences was avoided.

The sequences for primers used;

5′-AATATCGCGGACAGAAGACG-3′ **Forward primer for 40nt**

5′-AAAAGCTCTGCCTTGGTTTC-3′ **Reverse primer for 40nt**

6.2.1 Testing effectiveness of selected primers by PCR

A. Test of primers on 40nt DNA without nanoparticles present

Once the sequence of primers was selected, we examined if these primers work by amplifying the 40nt DNA template (without gold nanoparticles at this stage) by PCR followed by acrylamide-gel electrophoresis to check amplicon size.

Figure 6.1 shows a single band at 40bp and light bands of excess primers at the bottom of the gel (20 bases) at annealing temperatures of 42 °C and 50 °C. The negative control (MM only-no DNA template) showed no bands at the 40bp and only primers at the bottom of the gel.

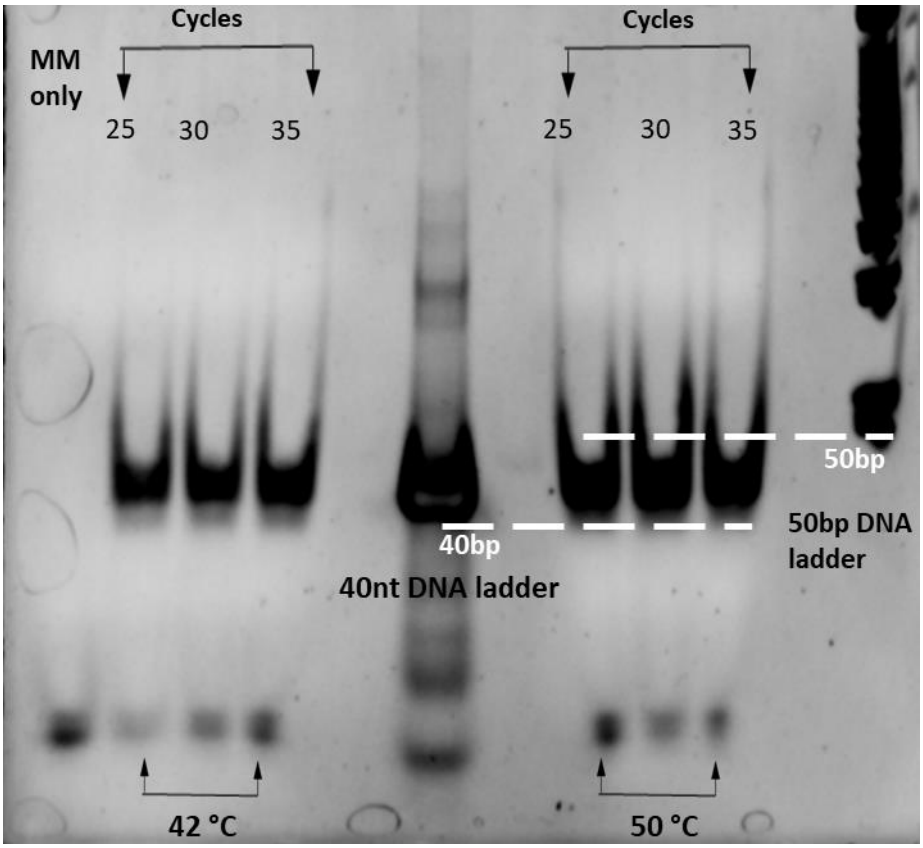

Figure 6.1 *6% acrylamide gel showing effective PCR amplification of 40nt DNA template with 20base reverse and forward primers. The column with MM (Master Mix only- no 40nt DNA template) is a negative control.*

B. Test of primers on 40nt DNA attached onto nanoparticles

Next, we tested if the 40nt DNA attached with gold nanoparticles can be detected with the primers effectively. A batch of NP-DNA-40 were separated on 5% acrylamide gel, transferred onto a nylon membrane and then each band cut into a small strip to place it in the PCR reaction for amplification (as illustrated in figure 6.2a). A plain area, where there was no band (no NP-DNA-40) was cut as a negative control and 40nt DNA without gold nanoparticles was used as the positive control.

After we amplified NP-DNA-40 bands cut from the nylon membrane by PCR and ran them on a gel, we found a successful amplification of NP-DNA-40 by the 20bp reverse and forward primers at an annealing temperature of 50 ºC (figure 6.2b). Band 1 (NP-DNA-40^{HI}), which had more 40nt DNA molecules attached to each nanoparticle, showed darker band density, confirming that more 40nt DNA molecules were present in band 1 compared to band 2. Band 2 (NP-DNA-40^{LO}) showed slightly lighter band density than band 1, confirming less 40nt DNA material compared to band 1. The negative control showed no

amplification and hence no band, confirming there was no NP-DNA present. Overall, the result confirmed that DNA attached to the NPs can still act as a template for detection by PCR.

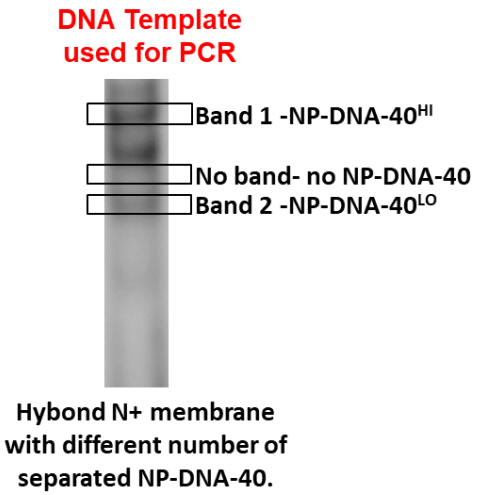

Figure 6.2 ***a)*** *NP-DNA-40 bands on nylon membrane used to separate distinctive bands from excess 40nt DNA. Each band strip was used as a template in PCR at an annealing temperature of 50 °C with 12, 30 and 35 cycles each.*

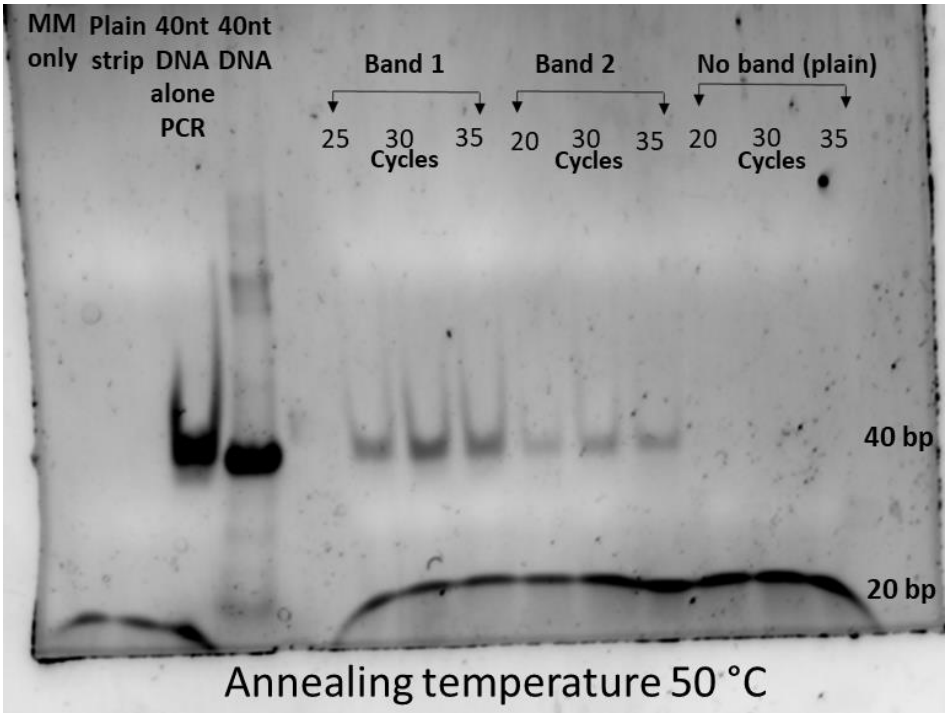

Figure 6.2 *b) Effective PCR amplification of separated NP-DNA-40 cut from a nylon membrane, as run on a polyacrylamide gel (Figure 6.2a). Band 1 – NP-DNA-40^{HI}, Band 2 –* NP-DNA-40^{LO}, No band – no DNA-40-related material, MM only – Master Mix with no 40nt DNA template.

6.2.1.1 Extension of primers to distinguish an amplified product from a primer dimer by-product

Both reverse and forward 20bp primers were detecting our 40nt DNA template with or without gold nanoparticles attached. However, since 20bp primers can form the same length (40bp) primer dimer as the amplified 40nt DNA template, it was difficult to distinguish between the amplified product and the primer dimer. Therefore, we extended the primers sequence by adding a few extra bases to make the final amplified product longer. This made the amplified product 48bp long (illustrated in figure 6.3) and easier to separate on the gel from the primer dimer by-product.

Extended sequence to make longer amplicons;

5'**CCCG**AATATCGCGGACAGAAGACGGAAACCAAGGCAGAGCTTTT**GCTC**'3

Extended forward primer for 40nt
5'CCCGAATATCGCGGACAGAAGACG'3

Extended reverse primer for 40nt
5'**GAGC**AAAAGCTCTGCCTTGGTTTC'3

Figure 6.3 *An illustration of using 24bp extended primers to amplify 40nt DNA template to create a product of 48bp.*

We tested the extended primers for their effectiveness in amplification of the target sequence (figure 6.4), and observed that it was similar at both annealing temperatures of 46 °C and 50 °C. The main concern was that a double band was observed when the extended reverse and extended forward primers were used to reaction to amplify 40nt DNA. We

observed two bands; one at 40bp, and another one at 48/50bp. This may indicate that the extended primers were less efficient in the amplification reaction of 40nt DNA, or that one of the primers might not have worked properly.

Therefore, we used the un-extended primers with the extended ones, in the following combinations: reverse primer (20bp) with an extended forward primer (24bp), and un-extended forward primer (20bp) with extended reverse primer (24bp). This created a final DNA product of 44bp. Figure 6.5 shows that the combination of un-extended reverse primer (20bp) + extended forward one (24bp) had 2 bands. This was similar to what we observed with previous combination of both un-extended primers – perhaps the reverse primer worked effectively in reaction of amplifying the DNA, but the extended forward primer (24bp) did not work as well.

Finally, the combination of un-extended forward primer (20bp) with extended reverse primer (24bp) showed one band, higher than the 40nt marker, indicating that the extended forward primer (24bp) amplified the DNA product to the expected length of 44bp.

.

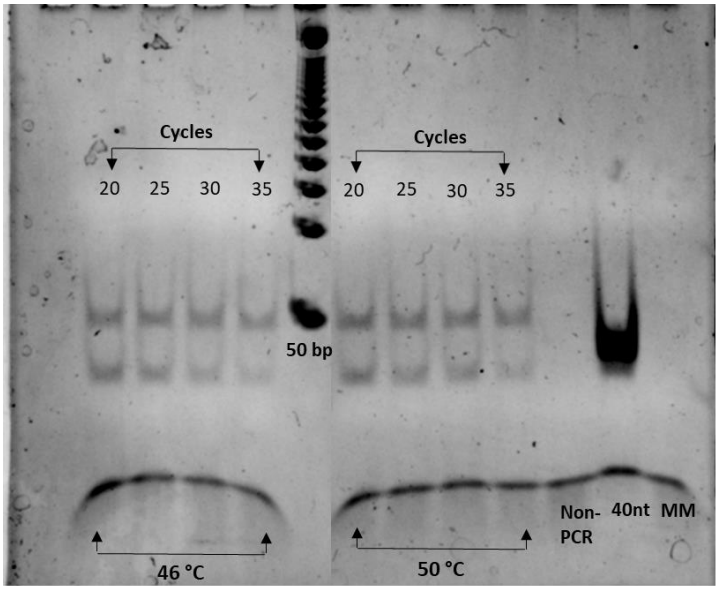

Figure 6.4 *6% acrylamide gel showing amplification by PCR of 40nt DNA by extended primers to make a final amplicon of 48bp. Acronyms; MM- master-mix only (without DNA template), non-PCR- sample not amplified and 40nt is the 40bp marker).*

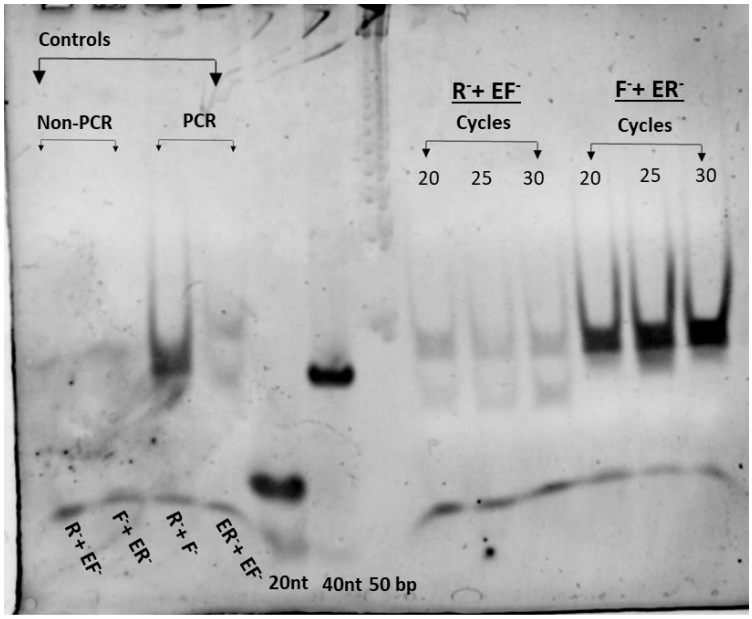

Figure 6.5 *6% acrylamide gel showing amplification by PCR of 40nt DNA using a reverse primer with the extended forward primer and forward primer with extended reverse primer. 20nt, 40nt and 50bp are the base pairs ladder/marker. Acronyms; R- -Reverse primer (20bp), F- - Forward primer (20bp), ER- -Extended reverse primer (24bp), EF-Extended forward primer (24bp).*

6.2.2 Assessment of DNA from DNA-coated nanoparticles crossing the brain endothelial cells.

Brain endothelial cells (hCMEC/D3) were used for DNA-coated nanoparticle transport assay and subsequent DNA quantification by qPCR. The uptake and crossing of cells with NP-DNA-40^{LO} and DNA-40^{HI} (refer to chapter 2.2.1 for 2D assay and 2.2.2 for 3D assay) was assessed. For qPCR analysis, the cells were rapidly frozen.

Our initial plan was to use co-cultures of brain endothelial cells and astrocytes in 3D collagen gel to assess the localization of DNA cargo from NP-DNA-40^{LO} and NP-DNA-40^{HI}. However, the astrocyte co-cultured gel contracted during several attempts (see example in Figure 6.6). The contracted co-cultures made it unusable for transfer studies since nanoparticles could pass around the monolayer of brain endothelial cells and enter the gel without crossing the endothelium first. Therefore, we had to use monolayers of hCMEC/D3 grown on trans-well inserts (in a 2D setting), without co-cultured astrocytes.

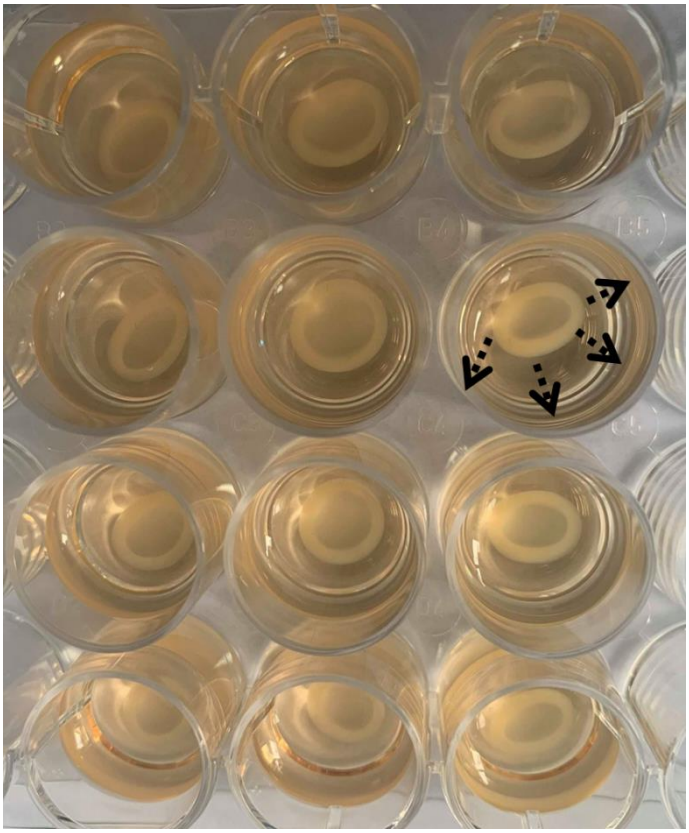

Figure 6.6 *Collagen gels embedded with astrocytes showing contraction (gels pulled away from the edge of wells-arrows). Due to this monolayer of D3 cells could not form and the 3D co-cultures could not be established*.

6.2.2.1 qPCR preparation and standard curve to determine DNA levels in different compartments

For qPCR quantification purposes, 4 treatment groups were selected; 40nt dsDNA alone, NP-Gal, NP-DNA-40^{LO}, NP-DNA-40^{HI}. 8µg/mL of nanoparticles for each group were applied to brain endothelial cells grown on trans-well inserts and incubated for 3 hours. Then, medium was collected from the top (apical side) and bottom (basal side) of the transwell. The hCMEC/D3 cells were lysed with 1% triton and frozen immediately at -20 ºC (figure 6.7). Media collected from top and bottom of trans-well was immediately frozen as well.

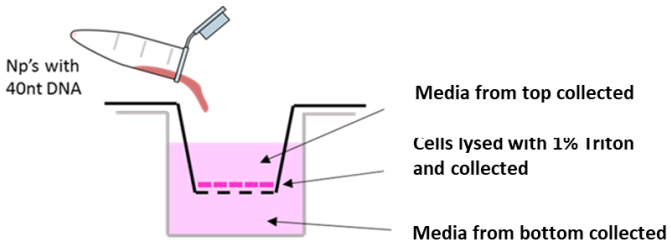

Treated group
NP-Gal
NP-DNA-40^{LO}
NP-DNA-40^{HI}
Free 40nt dsDNA

Figure 6.7 *2D transfer assay performed with four different groups to collect samples for qPCR quantification of 40nt DNA.*

The lysed cells, top and base media samples were used for DNA quantification. qPCR using SYBR Green (x2) Master Mix was performed to quantitate the 40nt DNA in this study. For all qPCR reactions, 20bp forward primers with 24bp (extended) reverse primer were used to amplify the final DNA product to 44bp. We tested a number of different primer concentrations ranging between 0.25 µM to 1 µM; all worked well, but 0.5 µM was selected as recommended by the manufacturer.

After the amplification, the qPCR readout of DNA measurement is given out in Cycles to Threshold (Ct) of PCR, a relative value that represents the cycle number at which the amount of amplified DNA reaches the threshold level. A high Ct value represents a low level of DNA, while higher expression of DNA in the sample will have low Ct value. In order to normalise Ct value in the quantitative measure (µg/mL), a standard curve was used.

To prepare a qPCR standard curve, qPCR reactions were set up to amplify different amounts of known concentration of the same 40nt DNA sample with and without nanoparticles.

For this study, 3 different 40nt DNA sample standard curves were prepared;

- Free 40nt DNA
- NP-DNA-40^{LO}
- NP-DNA-40^{HI}

Each of the three above DNA sample standard curve was prepared using 13 serial dilutions of DNA with a dilution factor of 1:10 in water. The diluted amounts were;

- 1 $x10^{-3}$µg, 1 $x10^{-4}$µg, 1 x 10^{-5}µg, 1x 10^{-6}µg, 1x 10^{-7}µg, 1x 10^{-8}µg, 1x 10^{-9}µg, 1x 10^{-10}µg, 1x 10^{-11}µg, 1x 10^{-12}µg and 1x 10^{-13}µg.

The reaction with no DNA template-negative control (SYBR green Master Mix and primers only) gave Ct value of 22.3. Hence, the DNA template was diluted to a concentration which will give Ct value similar to 22 cycles. The Ct values (x-axis) of qPCR from all known serial dilutions (y-axis) were used to make a linear regression curve slope and used to calculate the amplification efficiency for the transfer assay experiment. Figure 6.8 illustrates an example of a qPCR standard curve.

Example of how the Ct value was converted to the absolute value of DNA:

The standard curve gave us straight line equation y= -14347x + 15.931

The y is known Ct value given by the qPCR and we work out unknown, x, which will be the amount of DNA. For example;

<u>The negative control had Ct cycle of 22.3;</u>

x = (22.3 -15.931)/-14347

x = - 4 $x10^{-4}$µg= **(negative value means there is no DNA)**

<u>The positive control (free 40nt dsDNA) gave a Ct value of 14.3;</u>

x = (14.8 – 15.931)/-14347

x = 7.8 $x10^{-5}$ µg (the sample was diluted 1µl in 10,000)

Hence, x = 0.78 µg

0.78µg DNA

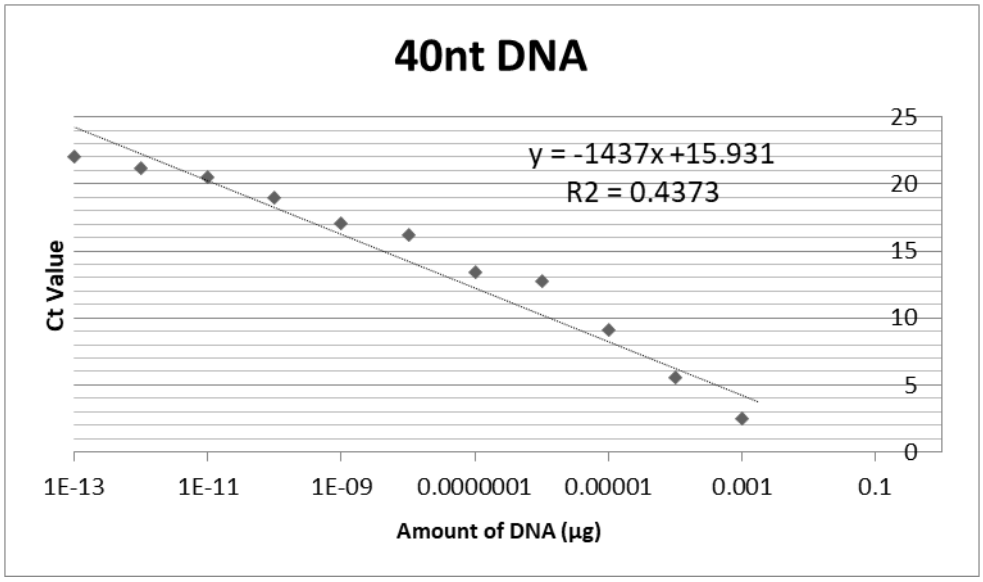

Figure 6.8 *A representative qPCR standard curve for 40nt DNA attached onto nanoparticles (NP-DNA-40). The dotted line is the straight line.*

The results from the quantification of DNA in the 2D BBB transfer assay is summarised in figure 6.9. A comparison was performed for 4 treated groups: NP- Gal (negative control), DNA without nanoparticles, NP-DNA-40^{LO} AND NP-DNA-40^{HI}. The Ct values determined by qPCR for each sample were normalised using a standard curve. The negative control with primers and SYBR Green Master mix (no DNA template) had Ct value of 23; therefore, all values over 23 cycles were negative and considered zero. The qPCR results showed higher than 23 Ct cycles for the top media, in cells and in the base media for the cellular trans-wells treated with NP-Gal, which we expected from the NP-Gal as this was our negative control. Endothelial cells treated with NP-DNA-40^{LO} showed the highest transfer of DNA across the cells and into the base media compared with NP-DNA-40^{HI} and DNA alone. The cells treated with NP-DNA-40^{HI} had higher transfer of DNA across and into the basal chamber of the trans-well than those treated with DNA alone. About half of the DNA found in top media (~0.9µg) for NP-DNA-40^{LO} was found in the base media (0.4 µg) which shows that NP-DNA-40^{LO} were enhancing the uptake of DNA across the brain endothelium compared to the NP-DNA-40^{HI} and DNA alone. Lastly, we found no free 40nt dsDNA at the basal chamber of the insert and cells.

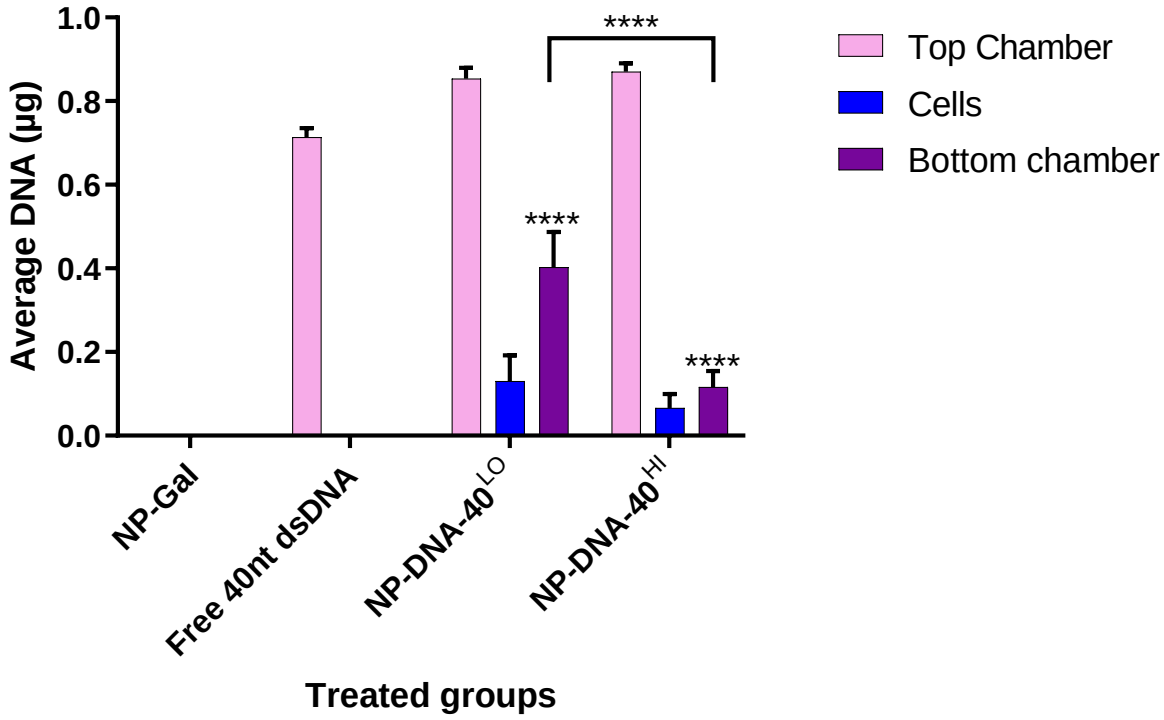

Figure 6.9 *qPCR quantification of 40nt DNA measured in each sample of NP-Gal, free 40nt dsDNA, NP-DNA-40^{LO} and NP-DNA-40^{HI} collected from 2D transfer assay (values normalised using relative standard curve), n=3. Tukey's multiple comparisons test was performed using GraphPad. There is a significant difference for NP-DNA-40^{LO} and NP-DNA-40^{HI} bottom chamber compared to NP-Gal (p-value: ****<0.0001).*

6.3 Summary and discussion

In this chapter, we tested the transport efficiency of 40nt DNA cargo using glyconanoparticles coated with DNA across the brain endothelial cells. There are three most common methods for DNA or RNA quantitation: spectrophotometry, fluorescence and real-time PCR. Real-time PCR as method of DNA quantification was selected in our study because it offers the most sensitive detection, as low as picogram quantities of nucleic acid (since we were working with small amount of DNA in the trans-well experiments, it was rational to use such sensitive technique). Additionally, real-time PCR also proved accurate quantification of nucleic acids of interest, even in the presence of common contaminants, other nucleic acids, primers and free nucleotides (because of the sequence-specific target PCR primers). Although, reagents used for real-time PCR are

costly and require advanced instrumentation. UV Spectrophotometry provides quick and simple alternative to real-time PCR as it does not require any reagents, however the technique would be unfeasible for our experiment as it would not identify our specific DNA sequence (as opposed to all the DNA in the cells) and also has limited low-end sensitivity. Lastly, DNA quantification by fluorescence technique also could not be used for our study. This is because gold nanoparticles are able to quench fluorescence, especially if they are less than 40 nm in diameter (Swierczewska et al. 2011). Quenching happens when a gold nanoparticle is at a certain distance from a fluorophore (Dulkeith et al. 2005); the nanoparticle's surface plasmon resonance may change the excitation/emission property of the fluorophore, preventing it from emitting light (Kang et al. 2011).

We measured the amount of DNA transported across via the following nanoparticle formulations: NP- Gal (negative control), free 40nt dsDNA, NP-DNA-40^{LO} and NP-DNA-40^{HI}. The primers were tested for the 40nt DNA with nanoparticles using standard semi-quantitative PCR followed by polyacrylamide gel. We amplified the 40nt DNA-gold nanoparticles into a 44bp long DNA using reverse and forward primers, so that the amplified product could be distinguished from the 40nt DNA template and from concatenated primer-dimers. We found that NP-DNA-40^{LO} and NP-DNA-40^{HI} were able to transport 40nt DNA cargo across the brain endothelium. NP-DNA-40^{LO} appeared to be most efficient in transporting DNA across brain endothelium. The material applied (top chamber) was roughly between 0.8-0.9 µg and about 0.3 -0.4 µg was transported across with the NP-DNA-40^{LO}. These findings also are consistent with our earlier studies using TEM where we observed higher uptake of NP-DNA-40^{LO} nanoparticles across brain endothelium than NP-DNA-40^{HI}.

Since brain endothelial cells hCMEC/D3 are a cell line and therefore might not form tight junctions as primary cells or in vivo, we tested movement of free 40nt dsDNA across the trans-well system with monolayer of brain endothelium. We found no free 40nt dsDNA at the basal chamber of the insert therefore, we were confident in the result since we did not observe unspecific penetration of our trans-well system (with cell monolayer) by free 40nt dsDNA. Furthermore, DNA was also found in cells in a small amount for NP-DNA-40^{LO} and NP-DNA-40^{HI}, and hence future studies could be performed with longer incubation times (longer than 3 hours) to test if more NP-DNA-40 may be transported across.

Correspondingly, for future studies it will be beneficial to analyse gold content (applied in the top chamber) along with the DNA content by the qPCR versus the bottom chamber to

see what percentage of gold nanoparticles are still holding onto the DNA or whether some have already lost the DNA in cells. As from the qPCR DNA quantification alone we cannot tell whether the DNA in the bottom chamber is attached to the gold nanoparticles or is freely floating there without nanoparticles. Gold concentration can be measured by spectrophotometric gold assay using the gold standard (AAS 1000 mg/ml, Sigma).

7 CONCLUSIONS

Oligonucleotide-based therapeutics are becoming the third major drug development platform. They are mainly focused on CRISPR (Gene editing), RNA interference (RNAi, to reduce gene expression) as well as using antisense oligonucleotides (to silence a gene). The development relies on the fact that oligonucleotides based therapeutics can delay the disease onset or halt the disease progression through target gene knockdown, knockout or splicing modulation (Evers et al, 2015). In 2018, Spinraza®, an antisense oligonucleotide drug was approved as a splicing modulator for the survival of motor neuron gene for the treatment of spinal muscular atrophy by the US Food and Drug Administration (Stein et al. 2017). However, such antisense oligonucleotide drugs require administration via highly invasive routes, e.g., intrathecal administration, because the accessibility of the antisense oligonucleotide drugs to the CNS through the bloodstream is very low as the BBB effectively prevents their entry into the brain. The BBB prevents free permeation of molecules larger than 400 Da, including oligonucleotide therapeutics (~6,600 Da or larger), between the bloodstream and the brain parenchyma (Crawford et al, 2016). Therefore, systemic oligonucleotides based therapeutics delivery to the brain remains challenging. Here, with the aim of tackling this issue, we developed small gold glyconanoparticles covalently attached with DNA capable of crossing the BBB. Gold glyconanoparticles were coated using place-exchange reaction with different length and density of oligonucleotides and assessed for their efficiency in crossing the BBB *in vitro* and *in vivo*.

In chapter 3, we showed how these nanocarrier formulations were prepared and characterised. The experimental approach used a thiol-attached DNA oligonucleotide covalently attached onto galactose-coated gold nanoparticles. EMSA was used to separate nanoparticles with different numbers of DNA molecules attached. Six different bands were observed on EMSA, perhaps demonstrating that up to 6 DNA can bind onto a single nanoparticle. Next, formulations of NP-DNA-20^{ss}, NP-DNA-20^{ds} and NP-DNA-40^{ds} were prepared and assessed for their transport rate across the brain endothelial cell line hCMEC/D3. We found that despite their net negative charge, DNA coated nanoparticles had higher cellular uptake than their uncoated equivalent, galactose-coated gold nanoparticles (NP-Gal). This investigation highlighted the possibility that attaching more DNA onto each nanoparticle may increase their uptake efficiency. However, the

nanoparticle formulations contained a mixture of free DNA and unreacted NP-Gal, so it was not possible to determine whether the detected nanoparticles entering the cells were unreacted NP-Gal or indeed NP-DNA. Since the nanoparticle mixture also contained free excess unreacted DNA, this might have affected cell membrane permeability. Therefore, we needed to remove the unreacted material from the nanoparticle mixture.

In chapter 4, we used FPLC to remove unreacted material and isolate only NP-DNA-40^{ds}. We were able to isolate different density of 40nt DNA-coated nanoparticles also using FPLC. Two fractionated formulations (NP-DNA-40^{LO} and NP-DNA-40^{HI}) were then investigated for their uptake efficiency into and across brain endothelial cells and astrocytes using an *in vitro* 3D co-culture model of the BBB. Both NP-DNA-40^{LO} and NP-DNA-40^{HI} were more effective in crossing the brain endothelial cells and entering astrocytes compared to control uncoated NP-Gal. Therefore, attaching 40nt long DNA molecule did not hinder the transport of the nanoparticles across brain endothelial cells. We also assessed cytotoxicity of DNA-coated nanoparticles on human brain endothelium (hCMEC/D3) and found none of the formulations to be cytotoxic up to 3x higher nanoparticles concentrations than those used in transport studies, and more than 8x longer nanoparticle incubation times. Hence, nanoparticles are safe to use on brain endothelial cells and may be safe for other cell types and cell lines due to their low toxicity.

In chapter 5, we investigated tissue distribution of DNA-coated nanoparticles in vivo**.** Rats were dosed with the nanoparticles via two different administration routes: intracarotid injection (an approach that has never been used in the application of DNA-gold nanoparticles before) and intravenous injection (a more accessible route). The nanoparticles circulated in the body for 10 minutes to capture the first encounter of gold nanoparticles in the brain. We found nanoparticles of all three formulations (NP-Gal, NP-DNA-40^{LO} and NP-DNA-40^{HI}) in the brain endothelial cell and glial cells of the rat cortex using TEM. We observed typical clearance of NP-Gal via the kidney. The more negatively charged nanoparticles coated with DNA were localised in liver and were observed in the cytoplasm of hepatocytes in the liver, and macrophages of the red pulp in the spleen.

In Chapter 6, we quantified whether and how much DNA cargo is transported via DNA-coated nanoparticles across brain endothelial cells. qPCR results demonstrated that NP-DNA-40^{LO} and NP-DNA-40^{HI} successfully transported 40nt DNA cargo across the brain endothelium. Out of the two nanoparticle-DNA formulations, there was higher transport of DNA across brain endothelium using NP-DNA-40^{LO} than NP-DNA-40^{HI} (~0.9µg of the nanoparticles found on the apical side (top cell culture media) and ~0. 4µg of DNA was

found on the basal side media). We were confident in this result since we did not observe unspecific penetration of our trans-well system (with cell monolayer) by free DNA. Overall, from the amount of DNA observed crossing the endothelial cells in our studies, it suggests that we may be able to treat disorders that require single gene editing or where one time immediate treatment is required (in cases of acute brain disorder), whereas delivery of therapeutic DNAs for disorders that require continuous treatment needs further investigation (discussed in detail later on in this chapter).

In conclusion, the results in our project demonstrated the possibility to deliver 40nt DNA oligonucleotide across the BBB on ~ 2nm gold glyconanoparticles. Therefore, this system may be useful to deliver DNA oligonucleotides into the brain. The NP-Gal covalently-attached with 40nt thiol DNA have not been prepared before and /or tested for their uptake efficiency on in vitro and in vivo models.

Uptake and transport of nanoparticles by endothelial cells in vitro

In 2D cell uptake assays, the nanoparticles with more DNA attached were more effective in crossing the brain endothelial cells using the vesicular pathway. NP-DNA-40^{ds} had significantly higher uptake efficiency in both cytosolic and vesicular transport across brain endothelial cells and showed a significantly higher number of nanoparticles crossing the cell from the apical side (blood) and onto the basal (brain side) compared with NP-DNA-20^{ds} and NP-Gal.

When we co-cultured our brain endothelial cells with astrocytes embedded in 3D collagen gel, NP-DNA-40^{HI} had higher transport of nanoparticles across the brain endothelial cells and into the astrocytes than did NP-DNA-40^{LO} and NP-Gal. Additionally, it was observed that the possibly larger nanoparticles (with more DNA molecules) had a tendency to use the active vesicular pathway rather than the passive cytosolic pathway to enter cells. Perhaps size may be a key to determine the uptake pathway of the nanoparticles. The phenomenon of nanoparticle size and its effect on the trans-cellular pathway has been extensively investigated on many different cell lines by Chithrani et al, 2006. They found that 40nm gold nanoparticles were taken up preferentially via active vesicular pathway whereas 2nm nanoparticles were taken up via passive cytosolic pathway.

Lastly, the DNA quantification by qPCR showed DNA material crossing to the basal side (brain side) for NP-DNA-40^{LO} and NP-DNA-40^{HI} within 3 hours. NP-DNA-40^{LO} appeared to be most efficient in transporting DNA across brain endothelium. The material applied

(top chamber) was roughly between 0.8-0.9 µg and about 0.3 -0.4 µg was transported across with the NP-DNA-$40^{LO.}$ This shows effective DNA delivery across the brain endothelial cells using gold nanoparticles. Hence, attaching longer and more DNA molecules on NP-Gal did not hinder the transport of the nanoparticles across the brain endothelial cells. In fact, the opposite was observed as the transport across brain endothelium was enhanced with the DNA bound nanoparticles compared to NP-Gal.

Distribution of nanoparticles *in vivo*

Different density 40nt DNA attached gold nanoparticles have not been administered into rats before and assessed for bodily distribution and intracellular localisation by electron microscopy. Markedly different tissue distributions were observed for NP-Gal compared to NP-DNA-40^{LO} and NP-DNA-40^{HI}. The smaller NP-Gal had moved to the kidney within 10 mins of both intravenous and intracarotid injections which is consistent with reports of <5 nm-sized nanoparticles being released into the urine as a result of simple filtration through the renal glomeruli (Skotland et al. 2010, Hillyer & Albrecht 2001). In contrast, both the NP-DNA-40^{LO} and NP-DNA-40^{HI} accumulated preferentially in the liver and spleen following both intravenous and intracarotid injections.

In our in vivo study, the results differed from previous studies in terms of which cells the nanoparticles were taken up by/localised in the liver. Sadauskas et al. (2007) explained that the bigger size (size-dependent) nanoparticles are most likely to be taken up by the phagocytic cells in liver, whereas results in our study demonstrated that nanoparticles were mostly observed in cytoplasm of hepatocytes rather than the Kupffer cells/phagocytic cells of liver, although, the nanoparticles used in the Sadauskas study (2007) were 40nm (much larger than our nanoparticles).

With regard to the to the brain, our studies found very low levels of gold concentration detected by ICP/MS in the brain for all three nanoparticle formulations (in vivo), suggesting that gold nanoparticles cannot cross over the BBB at 10 mins after intracarotid and intravenous injection. Nonetheless, gold nanoparticles were observed in the brain endothelial cells and glial cells of the cortex of the brain in the same study for all three nanoparticle formulations when analysed by TEM. Perhaps, low gold concentration detected by ICP-MS may be due to the fact that only the anterior half sample was used for gold quantification rather than the whole brain. Previously, Gromnicova et al, 2016, demonstrated the same formulation of NP-Gal (used in this project) crossed through the

BBB and accumulated in the brain in vivo. Hence, this strongly needs to be repeated and a whole brain should be used when measuring the gold concentration by ICP-MS.

7.1 Consequences of therapy using gold nanoparticles

When considering drug delivery of nucleic acids using gold nanoparticles, three aspects need to be considered:

a) Acute conditions, immediate and fast treatment are needed;

b) Chronic conditions, treatment needs to be given over a long period.

c) Correction of genetic disorders, single dose that permanently corrects the defective gene

In an acute condition such as traumatic brain injury, the action of nanoparticle drug therapy needs to be immediate (rapid penetration of nanoparticles in the brain and release of therapeutic agent), to facilitate neuronal self-repair or control the expression of a gene that leads to neuronal cell death. For this treatment, the speed of complete clearance of gold nanoparticle carrier from the body may not be relevant. Our study showed (in chapter 5) electron microscope images of the brain tissue, where, within a small amount of time (10 mins) the NP-DNA-40 has already accessed the brain parenchyma. Hence, NP-DNA-40^{LO} may be useful in treatment of brain disorders that require single immediate therapy

Meanwhile, for chronic brain conditions such as Alzheimer's disease, Parkinson's disease or amyotrophic lateral sclerosis (ALS), the application of a treatment needs to be long-term (i.e., siRNA or antisense oligonucleotide therapy requires repeated administration for long-term down-regulation of an abnormal gene expression to control the disease growth. For such treatments, it is necessary to know the time of complete bodily clearance of therapeutic gold nanoparticles. In chapter 5, we showed that NP-DNA-40 accumulate in liver and spleen mostly, however, the long term accumulation of NP-DNA-40 within each organ and body clearance has not been studied yet. Therefore, the cumulative effect of long-term administration of NP-DNA-40^{LO} and NP-DNA-40^{HI} in organs over a long period of time would need to be investigated in animal studies before considering the current nanoparticle therapy for chronic brain diseases.

As for single gene defect disorders like Huntington's disease, using CRISPR/Cas9 gene therapy could achieve the benefits through a single dose that permanently inactivates the defective gene. Whereas, if it involves antisense oligonucleotides then it may require long-term, repeated administration to provide sustained benefits, which as mentioned earlier requires more investigation of long term clearance from the body.

7.2 Clinical use

Gold glyconanoparticles have a potential to be used in the clinic, since they have already been approved for use in clinical trials for treating prostate cancer (Libutti et al. 2010) and clinical drugs have been attached to nanoparticles for treatment of heart diseases (Zhang et al, 2018). Our industrial partner Midatech has already had one of their formulations of gold nanoparticles coated with PEG-amine/galactose/insulin in a clinical trial. These formulations of nanoparticles are deemed safe by the FDA (Midatech Pharma, personal communication).

In terms of what happens to nanoparticles when they enter the brain, it has been demonstrated by Midatech that small 2nm nanoparticles are substantially removed from the brain and other organs after 24 hours (Midatech Pharma, personal communication). A study by Sela et al. (2015) also showed rapid initial accumulation in the brain of 1.3 +/- 0.3nm size gold nanoparticles, reaching a maximum level in brain after 6–16 h, followed by a fast decline until it levels out after about 24hr and then slowly decreases to a negligible level.

Our NP-Gal might start to clear out from the body after 24hrs. As for NP-DNA-40, they are not excessively larger in size (~8nm) compared to NP-Gal but do have a high negative charge which might cause opsonisation and may cause the NP-DNA-40 to clear out from body earlier than NP-Gal or via a different route. Once nanoparticles enter the body, opsonin proteins might attach to aid their clearance via the mononuclear phagocytic system (MPS) (Owens et al, 2006).

7.3 Concluding remarks

Overall, despite the early stages in the development, our studies have shown improvement in the bioavailability of oligonucleotides in the brain carried by nanoparticles, due to the rapid penetration in a short time. Hence, it may be a useful agent to treat acute brain disorders or disorders that require editing of single gene using CRISPR/Cas9 by administration of intracarotid or intravenous injection. The chronic brain conditions need further investigation into the long term (with different time points) accumulation of nanoparticles in each organ and clearance from the body. While gene delivery represents an important aspect of gold nanoparticles, diagnostics, as well as imaging techniques can also benefit enormously (most notably bioimaging) as gold nanoparticles can be visualised by MRI , making them potentially an important tool in the diagnosis of brain disorders. Although this is a broad area of research it has enormous potential.

7.4 Future studies

For future *in vitro* studies; the detailed BBB-crossing mechanism of negatively charged-DNA coated nanoparticles, along with interaction mechanism of negative charge with endothelial surface protein needs further investigation. Also, for future studies it will be beneficial to analyse gold content (applied in the top chamber) along with the DNA content by the qPCR versus the bottom chamber to see what percentage of gold nanoparticles are still holding onto the DNA or whether some have already lost the DNA in cells. From the qPCR DNA quantification alone we cannot tell whether the DNA in the bottom chamber is attached to the gold nanoparticles or is freely floating there without nanoparticles. Gold concentration and characterisation can be measured by spectrophotometric gold assay using the gold standard (AAS 1000 mg/ml, Sigma) or by mass spectrometry.

There is also a strong need to repeat the *in vivo* study with administration of 40nt DNA-nanoparticles using a whole brain when measuring the gold concentration by ICP-MS and having different time measures to assess the long term accumulation of 40nt DNA-nanoparticles within each organ and the cumulative effect of long-term administration of NP-DNA-40^{LO} and NP-DNA-40^{HI} in organs before considering nanoparticle therapy for chronic brain diseases. Moreover, we still have to explore attachment of Cas9 protein with our 40nt DNA-nanoparticles and assess the transport of 40nt DNA-nanoparticles with Cas9 protein across the brain endothelium.

8 REFERENCES

- Abbott, N. J. (2013). Blood – brain barrier structure and function and the challenges for CNS drug delivery. 437–449. https://doi.org/10.1007/s10545-013-9608-0

- Abbott, N. J., Patabendige, A. A. K., Dolman, D. E. M., Yusof, S. R., & Begley, D. J. (2010). Structure and function of the blood–brain barrier. Neurobiology of Disease, 37(1), 13–25. https://doi.org/https://doi.org/10.1016/j.nbd.2009.07.030

- Ackerson, C.J., Jadzinsky, P.D. & Kornberg, R.D. (2005). Thiolate ligands for synthesis of watersoluble gold clusters. Journal of the American Chemical Society, 127(18), pp.6550–1. Available at: http://www.ncbi.nlm.nih.gov/pubmed/15869273

- Agrawal, M., Saraf, S., Saraf, S., Antimisiaris, S. G., Chougule, M. B., Shoyele, S. A., & Alexander, A. (2018). Nose-to-brain drug delivery: An update on clinical challenges and progress towards approval of anti-Alzheimer drugs. In Journal of Controlled Release (Vol. 281, pp. 139–177). Elsevier B.V. https://doi.org/10.1016/j.jconrel.2018.05.011

- Alkilany, A. M., & Murphy, C. J. (2010). Toxicity and cellular uptake of gold nanoparticles: What we have learned so far? Journal of Nanoparticle Research, 12(7), 2313–2333. https://doi.org/10.1007/s11051-010-9911-8

- Anselmo A.C., Samir M. (2016). Nanoparticles in the clinic. Bioeng. Transl. Med. 1:10–29. doi: 10.1002/btm2.10003

- Axelsen, T. M., & Woldbye, D. P. D. (2018). Gene therapy for Parkinson's disease, an update. In Journal of Parkinson's disease (Vol. 8, Issue 2, pp. 195–215). IOS Press. https://doi.org/10.3233/JPD-181331

- Ballabh, P., Braun, A., & Nedergaard, M. (2004). The blood – brain barrier : an overview Structure, regulation, and clinical implications. 16, 1–13. https://doi.org/10.1016/j.nbd.2003.12.016

- Banks, W. A. (2009). Characteristics of compounds that cross the blood-brain barrier. BMC Neurology, 9(Suppl 1), S3. https://doi.org/10.1186/1471-2377-9-S1-S3

- Bartczak, D., Nitti, S., Millar, T. M., & Kanaras, A. G. (2012). Exocytosis of peptide functionalized gold nanoparticles in endothelial cells. Nanoscale, 4(15), 4470–4472. https://doi.org/10.1039/c2nr31064c

- Behzadi, S., Serpooshan, V., Tao, W., Hamaly, M. A., Alkawareek, M. Y., Dreaden, E. C., Brown, D., Alkilany, A. M., Farokhzad, O. C., & Mahmoudi, M. (2017). Cellular uptake of nanoparticles: Journey inside the cell. In Chemical Society Reviews (Vol. 46, Issue 14, pp. 4218–4244). Royal Society of Chemistry. https://doi.org/10.1039/c6cs00636a

- Bodor, N., & Buchwald, P. (2010.). Retrometabolism-based drug design and targeting.

- Bozzuto, G. & Molinari, A. (2015). Liposomes as nanomedical devices. International journal of nanomedicine, 10, pp.975–99. Available at: http://www.ncbi.nlm.nih.gov/pubmed/25678787.

- Brust, M. et al. (1994). Synthesis of thiol-derivatised gold nanoparticles in a two-phase liquidliquid system. J. Chem. Soc., Chem. Commun.,, (7), pp.801–802.

- Caudle, W. M. (2017). Occupational Metal Exposure and Parkinsonism. In Advances in Neurobiology (Vol. 18, pp. 143–158). Springer New York LLC. https://doi.org/10.1007/978-3-319-60189-2_7

- Cardoso, F. L., Brites, D., & Brito, M. A. (2010a). Looking at the blood – brain barrier : Molecular anatomy and possible investigation approaches. Brain Research Reviews, 64(2), 328–363. https://doi.org/10.1016/j.brainresrev.2010.05.003

- Cesta, M. F. (2006). Normal Structure, Function, and Histology of the Spleen. Toxicologic Pathology, 34(5), 455–465. https://doi.org/10.1080/01926230600867743

- Cervellera, V., Raich, L., Akola, J., & Rovira, C. (2017). The molecular mechanism of the ligand exchange reaction of an antibody against a glutathione-coated gold cluster. Nanoscale, 9(9), 3121–3127. https://doi.org/10.1039/c6nr08498b

- Chithrani, B. D., Ghazani, A. A., & Chan, W. C. W. (2006). Determining the size and shape dependence of gold nanoparticle uptake into mammalian cells. Nano Letters, 6(4), 662–668. https://doi.org/10.1021/nl052396o

- Cho, C. F., Wolfe, J. M., Fadzen, C. M., Calligaris, D., Hornburg, K., Chiocca, E. A., Agar, N. Y. R., Pentelute, B. L., & Lawler, S. E. (2017). Blood-brain-barrier spheroids as an in vitro screening platform for brain-penetrating agents. Nature Communications, 8. https://doi.org/10.1038/ncomms15623

- Choung, S., Kim, Y. J., Kim, S., Park, H. O., & Choi, Y. C. (2006). Chemical modification of siRNAs to improve serum stability without loss of efficacy. Biochemical and Biophysical Research Communications, 342(3), 919–927. https://doi.org/10.1016/j.bbrc.2006.02.049

- Crawford, L., Rosch, J., & Putnam, D. (2016). Concepts, technologies, and practices for drug delivery past the blood–brain barrier to the central nervous system. Journal of Controlled Release, 240, 251–266. https://doi.org/10.1016/j.jconrel.2015.12.041

- Cong, L., Ran, F. A., Cox, D., Lin, S., Barretto, R., Habib, N., Hsu, P. D., Wu, X., Jiang, W., Marraffini, L. A., & Zhang, F. (2013). Multiplex genome engineering using CRISPR/Cas systems. Science, 339(6121), 819–823. https://doi.org/10.1126/science.1231143

- Connor, E., Mwamuka, J., Gole, A., Murphy, C. J., Wyatt, M., D. (2005). Gold nanoparticles are taken up by human cells but do not cause acute cytotoxicity. Small. 1:325–327. doi: 10.1002/smll.200400093.

- Cucullo, L., Couraud, P. O., Weksler, B., Romero, I. A., Hossain, M., Rapp, E., & Janigro, D. (2008). Immortalized human brain endothelial cells and flow-based vascular modeling: A marriage of convenience for rational neurovascular studies. Journal of Cerebral Blood Flow and Metabolism, 28(2), 312–328. https://doi.org/10.1038/sj.jcbfm.9600525

- Cucullo, L., Hossain, M., Puvenna, V., Marchi, N., & Janigro, D. (2011). The role of shear stress in Blood-Brain Barrier endothelial physiology. BMC Neuroscience, 12. https://doi.org/10.1186/1471-2202-12-40

- Daraee, H., Eatemadi, A., Abbasi, E., Aval, S. F., Kouhi, M., & Akbarzadeh, A. (2016). Application of gold nanoparticles in biomedical and drug delivery. In Artificial Cells, Nanomedicine and Biotechnology (Vol. 44, Issue 1, pp. 410–422). Taylor and Francis Ltd. https://doi.org/10.3109/21691401.2014.955107

- Daniel, M.-C. & Astruc, D. (2004). Gold nanoparticles: assembly, supramolecular chemistry, quantum-size-related properties, and applications toward biology, catalysis, and nanotechnology. Chemical reviews, 104(1), pp.293–346. Available at: http://www.ncbi.nlm.nih.gov/pubmed/14719978

- de Boer, A. G., & Breimer, D. D. (1998). Chapter 20 Cytokines and blood-brain barrier permeability. In H. S. Sharma & J. Westman (Eds.), Brain Function in Hot Environment (Vol. 115, pp. 425–451). Elsevier. https://doi.org/https://doi.org/10.1016/S0079-6123(08)62045-2

- de Jong, W. H., & Borm, P. J. a. (2008). Drug delivery and nanoparticles:applications and hazards. International Journal of Nanomedicine, 3(2), 133–149. https://doi.org/10.2147/IJN.S596

- DeWitt, M. A., Corn, J. E., & Carroll, D. (2017). Genome editing via delivery of Cas9 ribonucleoprotein. Methods, 121–122, 9–15. https://doi.org/10.1016/j.ymeth.2017.04.003

- Dias, N., & Stein, C. A. (2002). Minireview Antisense Oligonucleotides : Basic Concepts and Mechanisms. 1(March), 347–355.

- Ding, Y., Jiang, Z., Saha, K., Kim, C. S., Kim, S. T., Landis, R. F., & Rotello, V. M. (2014). Gold nanoparticles for nucleic acid delivery. Molecular Therapy : The Journal of the American Society of Gene Therapy, 22(6), 1075–1083. https://doi.org/10.1038/mt.2014.30.

- Dulkeith, E. et al. (2005). Gold nanoparticles quench fluorescence by phase induced radiative rate suppression. Nano letters, 5(4), pp.585–9. Available at: http://www.ncbi.nlm.nih.gov/pubmed/15826091

- Dykman, L. & Khlebtsov, N. (2012). Gold nanoparticles in biomedical applications: recent advances and perspectives. Chemical Society reviews, 41(6), pp.2256–82. Available at: http://www.ncbi.nlm.nih.gov/pubmed/22130549

- Evers, M. M., Toonen, L. J. A., & van Roon-Mom, W. M. C. (2015). Antisense oligonucleotides in therapy for neurodegenerative disorders. In Advanced Drug Delivery Reviews (Vol. 87, pp. 90–103). Elsevier B.V. https://doi.org/10.1016/j.addr.2015.03.008

- Feigin, V. L., Nichols, E., Alam, T., Bannick, M. S., Beghi, E., Blake, N., Culpepper, W. J., Dorsey, E. R., Elbaz, A., Ellenbogen, R. G., Fisher, J. L., Fitzmaurice, C., Giussani, G., Glennie, L., James, S. L., Johnson, C. O., Kassebaum, N. J., Logroscino, G., Marin, B., … Vos, T. (2019). Global, regional, and national burden of neurological disorders, 1990–2016: a systematic analysis for the Global Burden of Disease Study 2016. The Lancet Neurology, 18(5), 459–480. https://doi.org/10.1016/S1474-4422(18)30499-X

- Fischbeck, K. H., & Wexler, N. S. (2019). Oligonucleotide treatment for Huntington's disease. In New England Journal of Medicine (Vol. 380, Issue 24, pp. 2373–2374). Massachussetts Medical Society. https://doi.org/10.1056/NEJMe1904861

- Fraga, S. et al. (2013). Influence of the surface coating on the cytotoxicity, genotoxicity and uptake of gold nanoparticles in human HepG2 cells. Journal of applied toxicology : JAT, 33(10), pp.1111–9. Available at: http://www.ncbi.nlm.nih.gov/pubmed/23529830.

- Fratoddi, I., Venditti, I., Cametti, C., & Russo, M. V. (2015). How toxic are gold nanoparticles? The state-of-the-art. Nano Research, 8(6), 1771–1799. https://doi.org/10.1007/s12274-014-0697-3

- Freese, C., Unger, R. E., Deller, R. C., Gibson, M. I., Brochhausen, C., Klok, H. A., & Kirkpatrick, C. J. (2013). Uptake of poly(2-hydroxypropylmethacrylamide)-coated gold nanoparticles in microvascular endothelial cells and transport across the blood-brain barrier. Biomaterials Science, 1(8), 824–833. https://doi.org/10.1039/c3bm60050e

- Gao, Q., Dong, X., Xu, Q., Zhu, L., Wang, F., Hou, Y., & Chao, C. chi. (2019). Therapeutic potential of CRISPR/Cas9 gene editing in engineered T-cell therapy. In Cancer Medicine (Vol. 8, Issue 9, pp. 4254–4264). Blackwell Publishing Ltd. https://doi.org/10.1002/cam4.2257

- Gastfriend, B. D., Palecek, S. P., & Shusta, E. v. (2018). Modeling the blood–brain barrier: Beyond the endothelial cells. In Current Opinion in Biomedical Engineering (Vol. 5, pp. 6–12). Elsevier B.V. https://doi.org/10.1016/j.cobme.2017.11.002

- Gonçalves, G. A. R., & Paiva, R. de M. A. (2017). Gene therapy: advances, challenges and perspectives. In Einstein (Sao Paulo, Brazil) (Vol. 15, Issue 3, pp. 369–375). https://doi.org/10.1590/S1679-45082017RB4024

- Goodman C. M., McCusker C. D., Yilmaz T., Rotello V. M. (2004).Toxicity of gold nanoparticles functionalized with cationic and anionic side chains. Bioconjug Chem. 15:897–900. doi: 10.1021/bc049951i.

- Gromnicova, R. (2016). Gold nanoparticles as a delivery system of oligonucleotides into the brain Radka Gromnicova , BSc. October.

- Gromnicova, R., Davies, H. A., Sreekanthreddy, P., Romero, I. A., Lund, T., Roitt, I. M., Phillips, J. B., & Male, D. K. (2013). Glucose-coated gold nanoparticles transfer across human brain endothelium and enter astrocytes in vitro. PLoS ONE, 8(12). https://doi.org/10.1371/journal.pone.0081043

- Gu, Y.-J. et al. (2009). Nuclear penetration of surface functionalized gold nanoparticles. Toxicology and applied pharmacology, 237(2), pp.196–204. Available at: http://www.ncbi.nlm.nih.gov/pubmed/19328820

- Guerrero, S. et al. (2010). Improving the brain delivery of gold nanoparticles by conjugation with an amphipathic peptide. Nanomedicine (London, England), 6(5), pp.897–913

- He, H. et al. (2013). Carbon nanotubes: applications in pharmacy and medicine. BioMed research international, 2013, p.578290. Available at: http://www.ncbi.nlm.nih.gov/pubmed/24195076

- Heidenreich, M., & Zhang, F. (2016). Applications of CRISPR-Cas systems in neuroscience. In Nature Reviews Neuroscience (Vol. 17, Issue 1, pp. 36–44). Nature Publishing Group. https://doi.org/10.1038/nrn.2015.2

- Helms, H. C., Abbott, N. J., Burek, M., Cecchelli, R., Couraud, P. O., Deli, M. A., Förster, C., Galla, H. J., Romero, I. A., Shusta, E. v., Stebbins, M. J., Vandenhaute, E., Weksler, B., & Brodin, B. (2015). In vitro models of the blood-brain barrier: An overview of commonly used brain endothelial cell culture models and guidelines for their use. In Journal of Cerebral Blood Flow and Metabolism (Vol. 36, Issue 5, pp. 862–890). Nature Publishing Group. https://doi.org/10.1177/0271678X16630991

- Hersh, D. S., Wadajkar, A. S., Roberts, N. B., Perez, J. G., Connolly, N. P., Frenkel, V., Winkles, J. A., Woodworth, G. F., & Kim, A. J. (2016). Evolving Drug Delivery Strategies to Overcome the Blood Brain Barrier. 1177–1193.

- Hersh, D. S., Wadajkar, A. S., Roberts, N. B., Perez, J. G., Connolly, N. P., Frenkel, V., Winkles, J. A., Woodworth, G. F., & Kim, A. J. (2016). Send Orders for Reprints to reprints@benthamscience.ae Evolving Drug Delivery Strategies to Overcome the Blood Brain Barrier. In Current Pharmaceutical Design (Vol. 22).

- Hillyer, J.F. & Albrecht, R.M. (2001). Gastrointestinal persorption and tissue distribution of differently sized colloidal gold nanoparticles. Journal of pharmaceutical sciences, 90(12), pp.1927–36. Available at: http://www.ncbi.nlm.nih.gov/pubmed/11745751.

- Hirn, S. et al. (2011). Particle size-dependent and surface charge-dependent biodistribution of gold nanoparticles after intravenous administration. European journal of pharmaceutics and biopharmaceutics : official journal of Arbeitsgemeinschaft für Pharmazeutische Verfahrenstechnik e.V, 77(3), pp.407–16. Available at: http://www.sciencedirect.com/science/article/pii/S093964111000370X

- Hostetler, M.J. et al. (1998). Alkanethiolate Gold Cluster Molecules with Core Diameters from 1.5 to 5.2 nm: Core and Monolayer Properties as a Function of Core Size. Langmuir, 14(1), pp.17–30.

- Hsu, P. D., Lander, E. S., & Zhang, F. (2014). Development and applications of CRISPR-Cas9 for genome engineering. In Cell (Vol. 157, Issue 6, pp. 1262–1278). Cell Press. https://doi.org/10.1016/j.cell.2014.05.010

- Huang, X. et al. (2007). Gold nanoparticles: interesting optical properties and recent applications in cancer diagnostics and therapy. Nanomedicine (London, England), 2(5), pp.681–93. Available at: http://www.ncbi.nlm.nih.gov/pubmed/17976030

- Huggett, J., & Bustin, S. A. (2011). Standardisation and reporting for nucleic acid quantification. In Accreditation and Quality Assurance (Vol. 16, Issue 8, pp. 399–405). https://doi.org/10.1007/s00769-011-0769-y

- Hühn, D., Kantner, K., Geidel, C., Brandholt, S., de Cock, I., Soenen, S. J. H., Riveragil, P., Montenegro, J. M., Braeckmans, K., Müllen, K., Nienhaus, G. U., Klapper, M., & Parak, W. J. (2013). Polymer-coated nanoparticles interacting with proteins and cells: Focusing on the sign of the net charge. ACS Nano, 7(4), 3253–3263. https://doi.org/10.1021/nn3059295

- ISIS Pharmaceuticals. (2014). Isis Pharmaceuticals Achieves Milestone In Amgen Antisense Drug Discovery Collaboration, https://ir.ionispharma.com/news-releases/news-release-details/isis-pharmaceuticals-achieves-milestone-amgen-antisense-drug: .

- Joshi, S., Emala, C. W., & Pile-Spellman, J. (2007). Intra-arterial Drug Delivery A Concise Review.

- Joshi, S., Meyers, P. M., & Ornstein, E. (2008). Intracarotid delivery of drugs: The potential and the pitfalls. In Anesthesiology (Vol. 109, Issue 3, pp. 543–564). Lippincott Williams and Wilkins. https://doi.org/10.1097/ALN.0b013e318182c81b

- Joshi, S., Ornstein, E., & Bruce, J. N. (2007). Targeting the Brain: Rationalizing the novel methods of drug delivery to the central nervous system. In Neurocritical Care (Vol. 6, Issue 3, pp. 200–212). https://doi.org/10.1007/s12028-007-0034-8

- Johansson, B. B. (2001). Blood-Brain Barrier: Role of Brain Endothelial Surface Charge and Glycocalyx.

- Juliano, R. L. (2016). The delivery of therapeutic oligonucleotides. Nucleic Acids Research, 347(6228), gkw236. https://doi.org/10.1093/nar/gkw236

- Kang, K.A. et al. (2011). Fluorescence manipulation by gold nanoparticles: from complete quenching to extensive enhancement. Journal of nanobiotechnology, 9, p.16. Available at: http://www.pubmedcentral.nih.gov/articlerender.fcgi?artid=3112388&tool=pmcentrez&re ndertype=abstract

- Kaur, C., Foulds, W. S., & Ling, E. A. (2008). Blood–retinal barrier in hypoxic ischaemic conditions: Basic concepts, clinical features and management. Progress in Retinal and Eye Research, 27(6), 622–647. https://doi.org/http://dx.doi.org/10.1016/j.preteyeres.2008.09.003

- Kim, S., Broströmer, E., Xing, D., Jin, J., Chong, S., Ge, H., Wang, S., Gu, C., Yang, L., Gao, Y. Q., Su, X. D., Sun, Y., & Xie, X. S. (2013). Probing allostery through DNA. Science, 339(6121), 816–819. https://doi.org/10.1126/science.1229223

- Kharlamov A.N., Tyurnina A. E., Veselova V. S., Kovtun O. P., Shur V. Y., Gabinsky J. L. (2015). Silica-gold nanoparticles for atheroprotective management of plaques: Results of the NANOM-FIM trial. Nanoscale. 7:8003–8015. doi: 10.1039/C5NR01050K.

- Klionsky, D., J. (2007). Autophagy: from phenomenology to molecular understanding in less than a decade. Nat Rev Mol Cell Biol, 8: 931–937. 10.1038/nrm2245.

- Kozielski, K. L., Rui, Y., & Green, J. J. (2016). Non-viral nucleic acid containing nanoparticles as cancer therapeutics. In Expert Opinion on Drug Delivery (Vol. 13, Issue 10, pp. 1475–1487). Taylor and Francis Ltd. https://doi.org/10.1080/17425247.2016.1190707

- Lasagna-Reeves, C. et al. (2010). Bioaccumulation and toxicity of gold nanoparticles after repeated administration in mice. Biochemical and biophysical research communications, 393(4), pp.649–55. Available at: http://www.sciencedirect.com/science/article/pii/S0006291X10002573

- Leboulanger, B., Guy, R. H., & Delgado-Charro, M. B. (2004). Reverse iontophoresis for non-invasive transdermal monitoring. In Physiological Measurement (Vol. 25, Issue 3). https://doi.org/10.1088/0967-3334/25/3/R01

- Lee, J.K. et al. (2014). Organ-specific distribution of gold nanoparticles by their surface functionalization. Journal of applied toxicology, (August). Available at: http://www.ncbi.nlm.nih.gov/pubmed/25348882

- Letsinger, R.L. et al. (2000). Use of a steroid cyclic disulfide anchor in constructing gold nanoparticle-oligonucleotide conjugates. Bioconjugate Chemistry, 11(2), pp.289–291.

- Li, X., Wang, B., Zhou, S., Chen, W., Chen, H., Liang, S., Zheng, L., Yu, H., Chu, R., Wang, M., Chai, Z., & Feng, W. (2020). Surface chemistry governs the sub-organ transfer, clearance and toxicity of functional gold nanoparticles in the liver and kidney. Journal of Nanobiotechnology, 18(1). https://doi.org/10.1186/s12951-020-00599-1

- Libutti, S.K. et al. (2010). Phase I and pharmacokinetic studies of CYT-6091, a novel PEGylated colloidal gold-rhTNF nanomedicine. Clinical cancer research : an official journal of the American Association for Cancer Research, 16(24), pp.6139–49. Available at: http://www.pubmedcentral.nih.gov/articlerender.fcgi?artid=3004980&tool=pmcentrez&re ndertype=abstract

- Liu, S., Agalliu, D., Yu, C., & Fisher, M. (2012). The Role of Pericytes in Blood-Brain Barrier Function and Stroke. In Current Pharmaceutical Design (Vol. 18).

- Manke, A., Wang, L., & Rojanasakul, Y. (2013). Mechanisms of nanoparticle-induced oxidative stress and toxicity. In BioMed Research International (Vol. 2013). https://doi.org/10.1155/2013/942916

- Manuscript, A. (2011). Asthma: Clinical Expression and Molecular Mechanisms. 7(6), 753–763. https://doi.org/10.1517/17425241003777010.Gold

- Manuscript, A. (2011). integrity by a gap junction dependent mechanism. 31(26), 9456–9465. https://doi.org/10.1523/JNEUROSCI.1460-11.2011.HIV

- Masserini, M. (2013). Nanoparticles for Brain Drug Delivery. ISRN Biochemistry, 2013, 1–8. https://doi.org/http://dx.doi.org/10.1155/2013/238428

- Minn, A., Ghersi-Egea, J.-F., Perrin, R., Leininger, B., & Siest, G. (1991). Drug metabolizing enzymes in the brain and cerebral microvessels. In Bruin Research Reviews (Vol. 16).

- Monopoli, M. P., Pitek, A. S., Lynch, I., & Dawson, K. A. (2013). Nanomaterial Interfaces in Biology. Nanomaterial Interfaces in Biology: Methods and Protocols, Methods in Molecular Biology, 1025, 137155. https://doi.org/10.1007/978-1-62703-462-3

- O'brien, J., Wilson, I., Orton, T., & Ois Pognan, F. Ë. (2000). Investigation of the Alamar Blue (resazurin) fluorescent dye for the assessment of mammalian cell cytotoxicity. In Eur. J. Biochem (Vol. 267).

- Oh, N., & Park, J. H. (2014). Endocytosis and exocytosis of nanoparticles in mammalian cells. In International Journal of Nanomedicine (Vol. 9, Issue SUPPL.1, pp. 51–63). Dove Medical Press Ltd. https://doi.org/10.2147/IJN.S26592

- Okamoto, S., Amaishi, Y., Maki, I., Enoki, T., & Mineno, J. (2019). Highly efficient genome editing for single-base substitutions using optimized ssODNs with Cas9-RNPs. Scientific Reports, 9(1). https://doi.org/10.1038/s41598-019-41121-4

- Osburg, B. (2003). Drug Delivery of Oligonucleotides at the Blood-Brain Barrier : a Therapeutic Strategy for Inflammatory Diseases of the Central Nervous System.

- Owens, D. E., & Peppas, N. A. (2006). Opsonization, biodistribution, and pharmacokinetics of polymeric nanoparticles. In International Journal of Pharmaceutics (Vol. 307, Issue 1, pp. 93–102). https://doi.org/10.1016/j.ijpharm.2005.10.010

- Ostrowski A. D., Martin T., Conti J, Hurt I., Harthorn B. H. (2007). Nanotoxicology: characterizing the scientific literature. J Nanopart Res. 2009;11:251–257. doi: 10.1007/s11051-008-9579-5.

- Pan Y., Leifert A., Ruau D. et al. (2009). Gold nanoparticles of diameter 1.4 nm trigger necrosis by oxidative stress and mitochondrial damage. Small. 5(18):2067–2076. doi: 10.1002/smll.200900466.

- Pannerec-Varna, M., Ratajczak, P., Bousquet, G., Ferreira, I., Leboeuf, C., Boisgard, R., Gapihan, G., Verine, J., Palpant, B., Bossy, E., Doris, E., Poupon, J., Fort, E., & Janin, A. (2013). In vivo uptake and cellular distribution of gold nanoshells in a preclinical model of xenografted human renal cancer. Gold Bulletin, 46(4), 257–265. https://doi.org/10.1007/s13404-013-0115-8

- Papasani, M. R., Wang, G., & Hill, R. A. (2012). Gold nanoparticles: The importance of physiological principles to devise strategies for targeted drug delivery. In Nanomedicine: Nanotechnology, Biology, and Medicine (Vol. 8, Issue 6, pp. 804–814). https://doi.org/10.1016/j.nano.2012.01.008

- Pardridge, W. M. (2005). The Blood-Brain Barrier: Bottleneck in Brain Drug Development.

- Pasqualini, R. & Ruoslahti, E. (1996). Organ targeting in vivo using phage display peptide libraries. Nature, 380(6572), pp.364–366. Available at: PM:8598934.

- Patra H. K., Banerjee S., Chaudhuri U., Lahiri P., Dasgupta A. K. (2007). Cell selective response to gold nanoparticles. Nanomedicine. 3:111–119.

- Petty, M. A., & Lo, E. H. (2002). Junctional complexes of the blood–brain barrier: permeability changes in neuroinflammation. Progress in Neurobiology, 68(5), 311–323. https://doi.org/http://dx.doi.org/10.1016/S0301-0082(02)00128-4

- Prades, R. et al. (2012). Delivery of gold nanoparticles to the brain by conjugation with a peptide that recognizes the transferrin receptor. Biomaterials, 33(29), pp.7194–205. Available at: http://www.ncbi.nlm.nih.gov/pubmed/22795856

- Puche, J. E., Saiman, Y., & Friedman, S. L. (2013). Hepatic stellate cells and liver fibrosis. Comprehensive Physiology, 3(4), 1473–1492. https://doi.org/10.1002/cphy.c120035

- Rader, D. J., & Kastelein, J. J. P. (2014). Lomitapide and mipomersen: Two first-in-class drugs for reducing low-density lipoprotein cholesterol in patients with homozygous familial hypercholesterolemia. Circulation, 129(9), 1022–1032. https://doi.org/10.1161/CIRCULATIONAHA.113.001292

- Rajotte, D. et al. (1998). Molecular Heterogeneity of the Vascular Endothelium Revealed by In Vivo Phage Display. Journal of Clinical Investigations, 102(2), pp.430–437.

- Rampado, R., Crotti, S., Caliceti, P., Pucciarelli, S., & Agostini, M. (2020). Recent Advances in Understanding the Protein Corona of Nanoparticles and in the Formulation of "Stealthy" Nanomaterials. In Frontiers in Bioengineering and Biotechnology (Vol. 8). Frontiers Media S.A. https://doi.org/10.3389/fbioe.2020.00166

- Roggers, R. et al. (2014). The practicality of mesoporous silica nanoparticles as drug delivery devices and progress toward this goal. AAPS PharmSciTech, 15(5), pp.1163–71. Available at: http://www.ncbi.nlm.nih.gov/pubmed/24871552.

- Sadauskas, E. et al. (2007). Kupffer cells are central in the removal of nanoparticles from the organism. Particle and fibre toxicology, 4, p.10. Available at: http://www.pubmedcentral.nih.gov/articlerender.fcgi?artid=2146996&tool=pmcentrez&re ndertype=abstract

- Sandhu, K.K. et al. (2002). Gold nanoparticle-mediated transfection of mammalian cells. Bioconjugate Chemistry, 13(1), pp.3–6.

- Sah, D. W. Y., & Aronin, N. (2011). Oligonucleotide therapeutic approaches for Huntington disease. In Journal of Clinical Investigation (Vol. 121, Issue 2, pp. 500–507). https://doi.org/10.1172/JCI45130

- Sarah J. Hurst, Abigail K. R. Lytton-Jean†, and C. A. M., Manuscript, A., Sarah J. Hurst†, Abigail K. R. Lytton-Jean†, and C. A. M., & Manuscript, A. (2008). Maximizing DNA Loading on a Range of Gold Nanoparticle Sizes. Anal Chem., 78(24), 8313–8318. https://doi.org/10.1021/ac0613582.Maximizing

- Saraiva, C., Pra??a, C., Ferreira, R., Santos, T., Ferreira, L., & Bernardino, L. (2016). Nanoparticle-mediated brain drug delivery: Overcoming blood-brain barrier to treat neurodegenerative diseases. Journal of Controlled Release, 235, 34–47. https://doi.org/10.1016/j.jconrel.2016.05.044

- Sarin, H., Kanevsky, A. S., Wu, H., Brimacombe, K. R., Fung, S. H., Sousa, A. A., Auh, S., Wilson, C. M., Sharma, K., Aronova, M. A., Leapman, R. D., Griffiths, G. L., & Hall, M. D. (2008). Effective transvascular delivery of nanoparticles across the blood-brain tumor barrier into malignant glioma cells. Journal of Translational Medicine, 6. https://doi.org/10.1186/1479-5876-6-80

- Saris, S.C. et al. (1988). Intravascular streaming and variable delivery to brain following carotid artery infusions in the Sprague-Dawley rat. Journal of cerebral blood flow and metabolism, 8, pp.116–120.

- Sauer, I., Dunay, I.R., Weisgraber, K., Bienert, M., Dathe, M. (2005). An apolipoprotein E-derived peptide mediates uptake of sterically stabilized liposomes into brain capillary endothelial cells. Biochemistry, 44, pp. 2021-2029.

- Saxen, M. A., & McDonald. (2016). Intravenous Route Pharmacologic Management of Patient Behavior Intravenous Route. In Dentistry for the Child and Adolescent.

- Schleh, C. et al. (2012). Size and surface charge of gold nanoparticles determine absorption across intestinal barriers and accumulation in secondary target organs after oral administration. Nanotoxicology, 6(1), pp.36–46. Available at: http://www.pubmedcentral.nih.gov/articlerender.fcgi?artid=3267526&tool=pmcentrez&re ndertype=abstract

- Sela H., Cohen H., Elia P., Zach R., Karpas Z., Zeiri Y. (2015). Spontaneous penetration of gold nanoparticles through the blood brain barrier (BBB) J. Nanobiotechnol.;13:71. doi: 10.1186/s12951-015-0133-1.

- Serlin, Y., Shelef, I., Knyazer, B., Friedman, A., Biology, C., & Sciences, B. (2016). HHS Public Access. 2–6. https://doi.org/10.1016/j.semcdb.2015.01.002.Anatomy

- Shen, F., Wen, L., Yang, X., & Liu, W. (2007). The potential application of gene therapy in the treatment of traumatic brain injury. In Neurosurgical Review (Vol. 30, Issue 4, pp. 291–298). https://doi.org/10.1007/s10143-007-0094-4

- Shilo, M. et al. (2014). Transport of nanoparticles through the blood-brain barrier for imaging and therapeutic applications. Nanoscale, 6(4), pp.2146–52. Available at: http://www.ncbi.nlm.nih.gov/pubmed/24362586

- Shukla R., Bansal V., Chaudhary M., Basu A., Bhonde R. R., Sastry M. (2005). Biocompatibility of gold nanoparticles and their endocytotic fate inside the cellular compartment: a microscopic overview. Langmuir. 21:10644–10654. doi: 10.1021/la0513712.

- Simionescu, M., Simionescu, N. & Palade, G.E. (1982). Differentiated microdomains on the luminal surface of capillary endothelium: distribution of lectin receptors. The Journal of cell biology, 94(2), pp.406–13. Available at: http://www.pubmedcentral.nih.gov/articlerender.fcgi?artid=2112875&tool=pmcentrez&re ndertype=abstrac

- Skotland, T., Iversen, T.-G. & Sandvig, K. (2010). New metal-based nanoparticles for intravenous use: requirements for clinical success with focus on medical imaging. Nanomedicine : nanotechnology, biology, and medicine, 6(6), pp.730–7. Available at: http://www.ncbi.nlm.nih.gov/pubmed/20570639

- Smith KA, Jasnow D, Balazs AC. J Chem Phys. (2007) ;127:084703.

- Sonavane, G., Tomoda, K. & Makino, K. (2008). Biodistribution of colloidal gold nanoparticles after intravenous administration: effect of particle size. Colloids and surfaces. B, Biointerfaces, 66(2), pp.274–80. Available at: http://www.ncbi.nlm.nih.gov/pubmed/18722754

- Sousa, F. et al., 2010. Functionalized gold nanoparticles: a detailed in vivo multimodal microscopic brain distribution study. Nanoscale, 2(12), pp.2826–34. Available at: http://www.ncbi.nlm.nih.gov/pubmed/20949211

- Stein, C. A., & Castanotto, D. (2017). FDA-Approved Oligonucleotide Therapies in 2017. In Molecular Therapy (Vol. 25, Issue 5, pp. 1069–1075). American Society of Gene and Cell Therapy. https://doi.org/10.1016/j.ymthe.2017.03.023.

- Stern, S.,T., & Johnson, D., N. (2008). Role for nanomaterial-autophagy interaction in neurodegenerative disease. Autophagy, 4: 1097–1100.

- Swierczewska, M., Lee, S. & Chen, X., (2011). The design and application of fluorophore-gold nanoparticle activatable probes. Physical chemistry chemical physics : PCCP, 13(21), pp.9929– 41. Available at: http://www.pubmedcentral.nih.gov/articlerender.fcgi?artid=3632443&tool=pmcentrez&re ndertype=abstract.

- Taton, T. A. (2002). Preparation of gold nanoparticle-DNA conjugates. Current Protocols in Nucleic Acid Chemistry / Edited by Serge L. Beaucage ... [et Al.], Chapter 12(200 2), Unit 12.2. https://doi.org/10.1002/0471142700.nc1202s09

- Teleanu, D. M., Chircov, C., Grumezescu, A. M., Volceanov, A., & Teleanu, R. I. (2018). Blood-brain delivery methods using nanotechnology.

In Pharmaceutics (Vol. 10, Issue 4). MDPI AG. https://doi.org/10.3390/pharmaceutics10040269

- Templeton, A.C. et al., (1998). Reactivity of Monolayer-Protected Gold Cluster Molecules: Steric Effects. Journal of the American Chemical Society, 120(8), pp.1906–1911. Available at: http://pubs.acs.org/doi/abs/10.1021/ja973863%2B

- Turkevich, J., Stevenson, P.C. & Hillier, J. (1951). A study of the nucleation and growth process in the synthesis of colloidal gold. Discuss. Faraday. Soc, 11, pp.55–75

- Turner M., Golovko V. B., Vaughan O. P. H., et al. (2008). Selective oxidation with dioxygen by gold nanoparticle catalysts derived from 55-atom clusters. Nature. 454:U31–981. doi: 10.1038/454031a.

- van den Berg, B. M., Vink, H., & Spaan, J. A. E. (2003). The endothelial glycocalyx protects against myocardial edema. Circulation Research, 92(6), 592–594. https://doi.org/10.1161/01.RES.0000065917.53950.75

- Veiseh, O., Gunn, J.W. & Zhang, M., (2010). Design and fabrication of magnetic nanoparticles for targeted drug delivery and imaging. Advanced drug delivery reviews, 62(3), pp.284–304. Available at: http://www.ncbi.nlm.nih.gov/pubmed/19909778.

- Verma, A. et al. (2004). “Tunable reactivation of nanoparticle-inhibited beta-galactosidase by glutathione at intracellular concentrations”. Journal of the American Chemical Society, 126(43), pp.13987–91. Available at: http://www.ncbi.nlm.nih.gov/pubmed/15506760.

- Wagner, A. M., Knipe, J. M., Orive, G., & Peppas, N. A. (2019). Quantum dots in biomedical applications. In Acta Biomaterialia (Vol. 94, pp. 44–63). Acta Materialia Inc. https://doi.org/10.1016/j.actbio.2019.05.022

- Walczak, P., Zhang, J., Gilad, A. A., Kedziorek, D. A., Ruiz-Cabello, J., Young, R. G., Pittenger, M. F., van Zijl, P. C. M., Huang, J., & Bulte, J. W. M. (2008). Dual-modality monitoring of targeted intraarterial delivery of mesenchymal stem cells after transient ischemia. Stroke, 39(5), 1569–1574. https://doi.org/10.1161/STROKEAHA.107.502047

- Wei, G.-T., & Liu, F. K. (1999). Separation of nanometer gold particles by size exclusion chromatography. In Journal of Chromatography A (Vol. 836).

- Weksler, B., Romero, I. A., & Couraud, P. (2013). The hCMEC / D3 cell line as a model of the human blood brain barrier. Fluids and Barriers of the CNS, 10(1), 1. https://doi.org/10.1186/2045-8118-10-16

- Whitesides, G. M. (2004). Whitesides' Group: Writing a paper. Advanced Materials, 16(15 SPEC. ISS.), 1375–1377.

- Wiley, D.T., et al. (2013). Transcytosis and brain uptake of transferrin-containing nanoparticles by tuning avidity to transferrin receptor. Proceedings of the National Academy of Sciences of the United States of America, 110(21), pp.8662–7. Available at: http://www.ncbi.nlm.nih.gov/pubmed/23650374

- Wolburg, H., & Lippoldt, A. (2002). Tight junctions of the blood–brain barrier. Vascular Pharmacology, 38(6), 323–337. https://doi.org/http://dx.doi.org/10.1016/S1537-1891(02)00200-8

- Wu, M., Chen, L., Li, R., Dan, M., Liu, H., Wang, X., Wu, X., Liu, Y., Xu, L., & Xie, L. (2018). Bio-distribution and bio-availability of silver and gold in rat tissues with silver/gold nanorod administration. RSC Advances, 8(22), 12260–12268. https://doi.org/10.1039/c8ra00044a

- Wurster, C. D., & Ludolph, A. C. (2018). Antisense oligonucleotides in neurological disorders. In Therapeutic Advances in Neurological Disorders (Vol. 11). SAGE Publications Ltd. https://doi.org/10.1177/1756286418776932

- Xu Z. Q., Broza Y. Y., Ionsecu R., Tisch U., Ding L., Liu H., Song Q., Pan Y. Y., Xiong F. X., Gu, K. S. (2013). A nanomaterial-based breath test for distinguishing gastric cancer from benign gastric conditions. Br. J. Cancer. 108:941–950. doi: 10.1038/bjc.2013.44.

- Yang, P.-H. et al. (2005). Transferrin-Mediated Gold Nanoparticle Cellular Uptake. Bioconjugate Chemistry, 16(3), pp.494–496. Available at: http://dx.doi.org/10.1021/bc049775d\nhttp://pubs.acs.org/doi/pdfplus/10.1021/bc049775d.

- Zhang, Y., Zhan, X., Xiong, J., Peng, S., Huang, W., Joshi, R., Cai, Y., Liu, Y., Li, R., Yuan, K., Zhou, N., & Min, W. (2018). Temperature-dependent cell death patterns induced by functionalized gold nanoparticle photothermal therapy in melanoma cells. Scientific Reports, 8(1). https://doi.org/10.1038/s41598-018-26978-1

- Zhang, Z., Ma, Z., Zou, W., Guo, H., Liu, M., Ma, Y., & Zhang, L. (2019). The Appropriate Marker for Astrocytes: Comparing the Distribution and Expression of Three Astrocytic Markers in Different Mouse Cerebral Regions. BioMed Research International, 2019. https://doi.org/10.1155/2019/9605265

- Zimmermann JL., Nicolaus T., et al. (2010). “Thiol-based, site-specific and covalent immobilization of biomolecules for single-molecule experiments”. Nat Protoc, 5(6):975–985.